Stability and Gravitational Collapse in Extended Theories of Gravity: from Singularities to Bouncing Scenarios

Kirtika Juhi Hurgobin

A dissertation submitted in full fulfilment of the requirements for the degree of Master of Science by Research in the Department of Mathematics and Applied Mathematics

University of Cape Town

Supervised by:

Dr. Álvaro de la Cruz-Dombriz
Department of Mathematics and Applied Mathematics

February 2019

Plagiarism Declaration

I, **Kirtika Juhi Hurgobin**, hereby declare that the work on which this thesis is based is my original work (except where acknowledgements indicate otherwise) and that neither the whole work nor any part of it has been, is being, or is to be submitted for another degree in this or any other university. I authorise the University to reproduce for the purpose of research either the whole or any portion of the contents in any manner whatsoever.

Signature: Signed by candidate

Date: **11 February 2019**

If we knew what it was we were doing,
it would not be called research, would it?
- Albert Einstein

Abstract

Einstein theory of General Relativity was well adapted and accepted until limitations in the form of an unexplained form of energy, referred today as Dark Energy, were observed. For this reason, modifications to the standard Theory of General Relativity were proposed: the so-called $f(R)$ theories. In this dissertation, after a passage on the generalities of cosmology, we use the metric formalism technique to derive the field equations for the general $f(R)$ function. Thereafter we analyse and check the solutions proposed in [85] for the quadratic model in $f(R)$ gravity, for spherically symmetric and static neutron stars, using two different viable equations of state. We also check the accuracy of our code through a forward-backward integration technique, to show that in both directions, we obtain the same results. We then perform a thorough analysis in the case of $f(R) = R^{1+\epsilon}$ models. Results will show that for a negative ϵ value, we have non-Schwarzschild, but asymptotically flat solutions, for which we can use the backward integration technique to retrieve the solutions from the forward integration. However, for the case of positive ϵ values, we will show the existence of horizons, which deny us the possibility of using the backward integration technique. One of the aims of this thesis is to check, through the backward integration technique that we developed, whether the exact exterior solutions proposed in [86], are indeed realistic solutions for neutron stars. We will see that for some cases, we do have realistic profiles, while for some others, although solutions exist, they are rejected due to their disagreement with the equation of state used therein.

Acknowledgements

I would like to convey my most sincere thanks to my supervisor, Dr. Álvaro de la Cruz-Dombriz, for presenting me with the opportunity to do my Masters thesis under his guidance, as well as the UCT Cosmology and Gravity Group. This work has been possible with his financial support (NRF Grant, code: 99077, Ref No. CSUR150628121624). I am also very grateful for the immense patience, faith, kindness and support that he has offered to me in the most invaluable ways during these years. I would also like to thank Prof. Peter K. S. Dunsby, our head of department, for the great opportunities facilitated together with my supervisor, regarding the exchange program to Spain (Erasmus+), at the beginning of my first year of Masters. I am thankful to the Institute of Theoretical Physics at the Autonomous University of Madrid for the hospitality during my visit. I extend my gratitude to Miguel Aparicio Resco for his help during this project. I am also grateful to Dr. Jonathan Shock for his precious help with some of my coding. A kind thought also goes to the administrative staff of the Mathematics and Applied Mathematics Department, as well as the Disability Unit at UCT.

I would like to thank many of my friends for their continuous words of encouragement and help. Thank you Miguel Méndez Isla and Francisco Torralba for welcoming me to your office whenever I was stuck in my work and needed a new outlook. Many thanks to Sulona Kandhai for all the times I needed a bit of boost and self-confidence regarding this work. My sincere thanks goes to Jack Morrice, who also helped me out with useful discussions. And to Sheean Jolicoeur, I am eternally grateful for the pressing motivation through all the times I needed the drive, and for useful insights and cross checks up until the very end. A special thought to Jake, Kimeel and Brandon for the few fun moments, and to my office colleagues Sim, Mariam and Anele.

Aleeshah Nujjoo, you have been one of my greatest support systems ever since I came to Cape Town. Thank you for always checking up on me and for all the little adventures in quest of motivation. My most sincere thanks to Hyder Lallmamode and Irshad Caunhye for the endless motivation, laughter and fun roadtrips. Jenicca Poongavanan and Delan Loyd Hassoo, you guys have been the best Rustenburg-Mews-homies one could ask for. Deepesh Gungaram, thank you for being the amazing best friend and Zubair Lall Mahomed, for all the good times. I cannot thank you all enough for your overflowing love, motivation and patience, especially during the times I dragged you along my moody and stressful roller coaster. Tashvin Ramma, thank you for all the love and support especially during the last phases, and for believing I could make this work, and Shafy Erigadoo, thank you for simply being around. A huge thanks to my high school girls from across the globe. We share a beautiful bond. Like they say, *Loin des yeux, près du coeur.*

Last, but not least, my deepest gratitude and thanks to my parents, Robin and Sujata Hurgobin, for giving me this opportunity that they never had themselves. Hemisha Hurgobin, you are the best sister one could be blessed with. Thank you and Dad for the unconditional love, encouragement and prayers since day one. Mum, there has not been a day where you were not missed, thank you for always keeping an eye on me. From the bottom of my heart I thank my grandparents, all my family members and family-like neighbours for all their good wishes. Thank you Sangeeta, Toshina and Videsh Vanmari for each and everything since 2012 . Special thanks to Chetrvy and Yashwinee for all the times I just needed a glimpse of you to feel better. Love you all beyond words!

Contents

List of Figures

List of Tables

Notations

In this thesis, the following conventions and notations have been used. A (- + + +) convention in four dimensional spacetime is employed as the metric signature, unless otherwise stated, and thus the following definitions of the Christoffel symbol and Riemann tensor respectively are:

$$\Gamma^{\lambda}_{\mu\kappa} = \frac{1}{2} g^{\lambda\sigma}(\partial_{\mu} g_{\sigma\kappa} + \partial_{\kappa} g_{\sigma\mu} - \partial_{\sigma} g_{\mu\kappa}) \tag{0.0.1}$$

$$R^{\sigma}_{\mu\nu\kappa} = \partial_{\nu}\Gamma^{\sigma}_{\mu\kappa} - \partial_{\kappa}\Gamma^{\sigma}_{\mu\nu} + \Gamma^{\sigma}_{\nu\lambda}\Gamma^{\lambda}_{\mu\kappa} - \Gamma^{\sigma}_{\kappa\lambda}\Gamma^{\lambda}_{\mu\nu} \tag{0.0.2}$$

Contracting on the third index, we obtain the Ricci Tensor is given by:

$$R_{\mu\kappa} = R^{\sigma}_{\mu\sigma\kappa} = \partial_{\sigma}\Gamma^{\sigma}_{\mu\kappa} - \partial_{\kappa}\Gamma^{\sigma}_{\mu\sigma} + \Gamma^{\sigma}_{\sigma\lambda}\Gamma^{\lambda}_{\mu\kappa} - \Gamma^{\sigma}_{\kappa\lambda}\Gamma^{\lambda}_{\mu\sigma} \tag{0.0.3}$$

where μ, ν, κ run from 0 to 3, and Einstein summation convention is employed.

Ricci Scalar: $R \equiv g^{\mu\kappa} R_{\mu\kappa}$.

D'Alembert operator: $\Box \equiv \nabla^{\kappa}\nabla_{\kappa} = g^{\mu\kappa}\nabla_{\mu}\nabla_{\kappa}$

Covariant derivative: ∇ which satisfies the condition $\nabla_{\alpha} g_{\mu\kappa} = 0$

Determinant of the metric tensor $g_{\mu\kappa}$: g

Inverse metric: $g^{\mu\kappa}$

Geometrized units are used, in which the speed of light c and gravitational constant, G assume unitary value and for the most part $k = 8\pi G/c^4$.

Acronyms

BBT $\equiv$ Big Bang Theory

BH $\equiv$ Black Holes

BW $\equiv$ Brane World

CMBR $\equiv$ Cosmic Microwave Background Radiation

EFE $\equiv$ Einstein Field Equations

EoS $\equiv$ Equation of State

ETG $\equiv$ Extended Theories of Gravity

GR $\equiv$ General Relativity

GUT $\equiv$ Grand Unified Theories

GW $\equiv$ Gravitational Wave

HOTG $\equiv$ higher-order Theories of Gravity

$\mathcal{L}_M \equiv$ Matter Lagrangian

NS $\equiv$ Neutron Star

QFT $\equiv$ Quantum Field Theory

SDSS $\equiv$ Sloan Digital Sky Survey

SM $\equiv$ Standard Model

TOV $\equiv$ Tolman-Oppenheimer-Volkoff

Mom and Grandma, this one's for you ...♡

I know you are always watching over me

Love you tremendously

Preface

General Relativity provides a synthesis of Special Relativity and Gravitation. Being a cornerstone of Classical Physics, it enables us to understand several areas of Astrophysics and Cosmology. The latter was hardly considered as a scientific discipline initially. Eventually, the Hot Big Band cosmology was accepted as the phenomenon describing the Universe as a whole.

The Cosmic Microwave Background, on a routine basis, detected relics of times during different epochs, concluding the expansion of our Universe and the inadequacy of the Standard Model of Cosmology to explain certain limitations. We are currently in an era where we seek answers for these limitations. We are in quest of wanting to understand and study the nature of Dark Matter, which is the dominant form of matter in the Universe.

Propositions for modifying gravity came forward in an urge to try explain the issues arising from the Standard Cosmological Model. One of the methods put forward, was a modification to the Einstein-Hilbert action, and since there were no rules in imposing a linear Lagrangian, higher-order theories of gravity emerged.

Research about types of modified gravity theory has substantially grown over a few decades. One of our aims in this work, is to study such $f(R)$ theories from which more can be known about the existence of neutron stars. This thesis has four parts, which are elaborated below.

Part I of this thesis includes two chapters, 1 and 2, which introduce the foundations of Cosmology and modified gravity. An overview is given on the basic concepts and accepted theories in Cosmology, such as the Big Bang theory, which is the widely accepted model of the Universe. We then look at $f(R)$ theories of gravity, where we discuss the different functions which exist already; the Starobinsky model which explains inflation and the Hu-Sawicki model which explains the accelerated expansion.

Part II consists of only one chapter for the research work done in this thesis. We analyse static and spherically symmetric solutions in $f(R)$ models, more specifically in $f(R) = R + \alpha R^2$ and $f(R) = R^{1+\epsilon}$. A detailed derivation of $f(R)$ field equations is given. We provide the interior and exterior solutions for our models with two equations of state. Vacuum solutions of our models are compared against the exact ones proposed by [86] for $f(R) = R^{1+\epsilon}$.

Part III deals with concluding the work done in this thesis, as well as providing scopes and ideas for future work.

Part IV contains the Appendices which mostly involve the derivations of our field equations and some important mapping conditions.

Part I

Introduction

Chapter 1

1 Generalities in Standard Relativistic Cosmology

1.1 The Big Bang Theory

The origin of the Universe has always been a mystery, and its expansion has led scientists to conclude that the Universe used to be much smaller than it is today. It was believed that if we go backward in time, it would appear that all the points of the Universe would be adjacent to each other. One plausible explanation for this is the Big Bang Theory (BBT), which has been accepted as a cosmological model and which best describes our Universe right from the earliest birth stage until its eventual evolution on the large scale [1]. Precision of this theory lies in that the Universe was born 13.8 billion years ago from a dense space-time singularity [1]. Because of this singularity, certain laws of Physics fail to provide the solutions to the standard equations and therefore, we hardly understand the very first initial stages of the Universe.

Nevertheless, scientists have been able to physically describe the occurrences merely seconds after the Big Bang, right up to the epoch we are currently in. This theory, although does not explain how and why our Universe exists, it successfully elucidates its evolution with respect to different phenomena, such as in the Hubble Diagram, Light Chemical Abundances, Cosmic Microwave Background Radiation (CMBR). However, although this theory displayed these successes, like most theories, the model comes with drawbacks.

In this section, we will discuss the main ideas of the Big Bang, as well as brief about the major observations and problems related to this theory.

1.1.1 Foundations

In the very early stages of the Universe, there was a brief period of accelerated expansion known as cosmic inflation. This exponential expansion era aided in the super-cooling of the energy-content of the Universe [3]. Some time after, relativistic particles such as electrons, gluons and quarks were

formed from the decaying of the field's potential energy. This period is known as reheating and resulted in the temperature of the Universe to rise, and from which particle-antiparticle pairs were continuously formed and annihilated [2, 3].

Thereafter, baryogenesis, a physical process which occurred during the early Universe producing baryonic asymmetry, disrupted the conservation of baryon number. This led to an increase in the particle to antiparticle ratio. This ratio is what explains the excess density of matter relative to antimatter in the Universe today. However, the theory underlying this strange reaction is still mysterious and incomprehensible [1]. With the continued expansion of the Universe, in order for the sub-atomic particles to interact, combine and be created, temperature, pressure, number density and energy of the particles diminished. At around 10^{-6} seconds after the Big Bang, protons and neutrons created quarks and gluons, and the high temperature no longer aided the generation of particle-antiparticle pairs [1, 2, 4].

The resulting excess density of particles to antiparticles was then frozen, thereafter, the protons, neutrons and electrons were not relativistic anymore because they yielded sufficient energy. Consequently, photons were uppermost in energy density in the Universe. During this time, atoms nor nuclei could be formed, as this was prevented by the high energy from the photons [1, 4]. When the Universe cooled down sufficiently, after approximately three minutes, big bang nucleosynthesis started. This process, from interacting protons and neutrons, gives off light atomic nuclei, helium and deuterium [1].

The continuous loss of energy and decrease in temperature made the energy density of photon radiation dominant over the energy density of matter. After over 300 000 years, atoms began forming, thus reducing the obscurity of plasma and allowing the decoupling of radiation from matter. This radiation is what is referred to as CMB radiation and travels through space. Even though it was assumed that the Universe was initially homogeneous, the existence of different structures therein insinuates that fluctuations in the consistency of primordial plasma, from which growth of structure began [1].

The slow gravitational collapse of overdensity regions around the uniform Dark Matter density

field led to gas clouds formation, which consequently resulted in the formation of stars, galaxies and large scale structures, as in the cosmic web, in the Universe [5]. The epoch between CMB and the Big Bang is what is referred to as the cosmic Dark Ages [6]. The reason for this is because at recombination, the formation of the first hydrogen atoms and scattering of the CMB photons occurred. Due to the shift of their energy in the infrared side, the Universe became completely dark. It was after a very long time that the birth of the first stars happened, which ended the Dark Age period. These stars were the first heavy celestial bodies and sources of light which eventually formed more complex bodies like planets and galaxies. This can be seen with the cosmic timeline in Figure1.

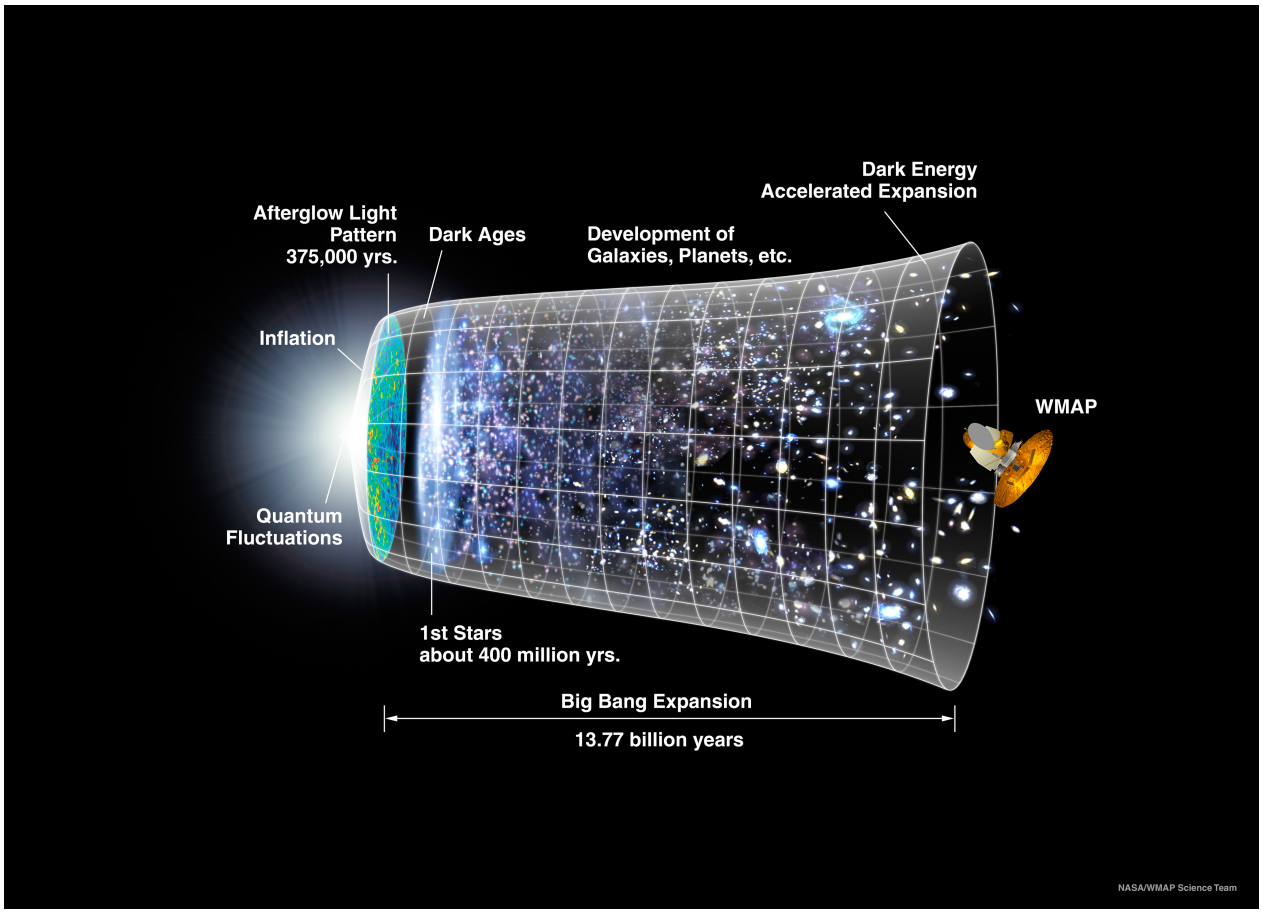

Figure 1: The Timeline of our Cosmos (taken from [7])

1.1.2 Proofs from Observations

As mentioned earlier, although the Big Bang Theory does not fully answer why the Universe exists, it succeeds in explaining different phenomena, for example, the Hubble Law, Light Chemical Abundances and the CMB. We can observe the spatial expansion from the Hubble diagram and the Big Bang Nucleosynthesis (BBN) explains the abundance of light elements.

The Hubble Diagram

The measurement of the doppler shifted spectral lines of galaxies was crucial for obtaining information on radial velocities of galaxies. Reason being that, what was known as "spiral nebulae" in the early 1900s, were a mystery. It was thus important to confirm that the motion of these spatial objects is random, to find the relationship between the Sun's motion around the Milky Way, and the vector sum of the radial velocities of the nebulae [2]. This method was invented by astronomer V. M. Slipher, in 1914, and he discovered that most galaxies that were observed, were in fact not only receding from us, but also from each other very swiftly, except for Andromeda, where a blueshift was exposed from its spectral lines. Over the years, his study of the spectra of 40 galaxies showed that, each of them displayed redshifted spectral lines instead of blue ones [1].

In 1925, Cepheid variable stars in M31 were discovered by Hubble. He also unraveled that Andromeda is in fact a galaxy outside of the Milky Way. The distances of 18 external galaxies were also measured using Cepheid variables. Using Slipher's data on redshift, Hubble standardised his own findings and showed that the recession velocity of a galaxy is actually proportional to its distance. With this useful discovery, he obtained the distances and velocities of 32 galaxies. This important finding is what gave rise to a law of the Universe [1], which eventually displayed proof for the expansion of the Universe we live in, and which plays a crucial part in the Big Bang theory.

Abundance of Light Elements

Nucleosynthesis, based on the Big Bang theory, began only a few minutes after the initial expansion and lasted for about 17 minutes. This process apparently took place through space and as a result, many species of element were obtained, which, today, form a large part of the baryonic matter content of the Universe. The following ratios for the mass abundances of the main elements

are 75% ^{1}H, 25% ^{4}He, 0.01% ^{2}He, with trace amounts of Lithium and Beryllium, but no heavy elements [2]. The predictions comply with observations of the abundances, and this fact is a very strong evidence for the Big Bang Theory [1].

Cosmic Microwave Background

The early Universe was so hot and dense that the free paths of photons were short enough to preserve a state of thermodynamic equilibrium, during which the radiation field would have a blackbody spectrum [2]. As the Universe went through expansion and cooling, the peak of this blackbody would have moved much ahead into lower energies. In 1948, according to the Big Bang theory, Herman and Alpher made a prediction that the Universe would be filled with an isotropic blackbody radiation, at a temperature of 5K, due to the hot and compact radiation that saturated the early Universe.

Using a horn reflector antenna, Penzias and Wilson, detected, in 1964, an interrupted signal coming from all directions in the sky but which, to them, had no source back then. The radiation was calculated to be 3K and coming from a blackbody. A year later, after struggling to eliminate the interference, Penzias managed to solve the puzzle after discovering Peeble's publications. There was probably a link between the blackbody radiation that the Big Bang model predicted, and the 3K radiation. In the electromagnetic spectrum, the radiation was recorded at a maximum value of $\lambda = 1.06$ mm in the microwave region. This radiation is proof for the Big Bang theory and is what is known as the CMB radiation (or also, CMBR). Today, the value for the mean temperature of the CMB, according to WMAP data sets, is 2.7255 ± 0.0006 K.

1.1.3 Shortcomings of the Theory

The Big Bang theory also comes with drawbacks, the main reason being that, for normal matter, solely the possibility of a decelerating expansion of the Universe can exist. Some of the problems are detailed below, with the two main ones being the horizon problem and the flatness problem. These two fine-tuning problems two issues arise due the Big Bang singularity for which the standard model of cosmology (founded from GR and the standard model of Particle Physics) unable to satisfactorily describe the Universe at extreme energy regimes [10].

Horizon Problem

This issue arises because of the isotropy of the CMB, which, by the Copernican principle, is also isotropic [11]. Within almost all distinct observable regions of the sky (10^{90} Plankian-size [12]), the CMB is uniform, and this shows that the radiation is totally in thermal equilibrium, but this requires interaction of particles. In the beginning, a comoving Hubble sphere of radius r_H, in different regions of the sky, were not expected to have intercommunicated due to the small comoving particle horizon between them. The greatest distance within which the particles interact randomly, exchanging information with each other at the speed of light, is the comoving particle horizon.

Therefore, two random particles would never have been able to share any kind of information prior to this time, if the comoving particle horizon was lesser than the radius of the Hubble sphere. Thus, due tot the isotropy and homogeneity of the CMB, the different regions of the sky seemed to have had ample communication time, at the moment that the CMB photons were ejected at the surface of the last scattering. A possibility to solving this issue would be to be able to devise a way to reduce the radius of the Hubble sphere in order for the particles to interchange information.

Furthermore, points in the sky with a difference of 2 degrees between them, would not possibly have been, at the time of decoupling (epoch exhibited by the CMB), in causal contact. Considering this, another problem comes up. The temperature of the CMB displays slight variations, which are considered to be structure sources in the Universe. However, there exists no theory allowing for the generation of fluctuations in a photon bath thermally regulated [2]. This implies that, the fluctuations in the early Universe probably already existed.

Flatness Problem

From observations, it was found that the total density of the Universe is almost the same as the critical density (a particular density needed for the Universe to be geometrically flat), at the present time, within one percent. However, according to the Big Bang theory, it is unlikely for the Universe to be spatially flat. This is because the total energy density of matter, radiation and Dark Energy is related to the comoving Hubble radius, r_H, through [11],

$$1 - \Omega(t) \propto r_H^2(t) \tag{1.1.1}$$

where a unitary value has been used for the speed of light c. Considering all world models with a big bang origin, near the big bang event, there exists the relationship $r_H^2 \propto t$. This highlights that $|\Omega - 1|$ should imperatively deviate with increasing time. Therefore, the critical point which imposes the condition for flatness, $\Omega = 1$, is an unstable point [23]. Additionally, the Universe was flat during the time of Big Bang nucleosynthesis [24], where $|\Omega - 1| \sim 10^{-18}$ [25]. This is based on extrapolating the CMB constraints to very early times, and is not an independent measurement. Once again, one way to solve this flatness problem is to contract r_H from an early time, so that, since the very beginning, the Universe remains flat.

Growth of Structure

Although it is an accepted fact that the Universe was born from a hot, dense homogeneous and isotropic state, as affirmed by the Big Bang theory, observation of the growth of structure cannot be explained as one needs to resort to inflationary paradigm to solve this issue; from quantum mechanics, dilutions lead to fluctuations, which need to be non-trivially shifted to classical mechanics. Thus, one of the hurdles faced by this theory lies in attesting for this evident discrepancy.

Monopole Problem

This issue arises due to the failure that the Big Bang theory faces in trying to be in agreement with certain areas of the Grand Unified Theories (GUTs). These theories, which predict the existence of magnetic monopoles, seek to model three forces arising from the Standard Model, as one single force. Although there exists favourable conditions for the production of these magnetic monopoles, they are regrettably still undetected.

One way of attempting to remedy these problems is to devise a way in which the comoving Hubble radius can be made small since the very beginning, and to make the evolution go back to the standard Big Bang model. One process which allows for such criteria to be satisfied is through the theory of cosmic Inflation.

1.2 Inflation

In the early 1980s, A. Linde, A. Guth and A. Starobinsky each brought forward propositions for a brief period of speedy accelerated expansion of the Universe arising only because of its vacuum energy, as a plausible explanation to all of the problems coming from the Big Bang theory. This is what is commonly referred to as inflation, and this proposition attempts to ameliorate the theory on the primordial Universe described by the Big Bang, while eliminating the issues arising from the latter theory.

In the case of the horizon problem, before inflation, according to theories relating to inflation, the Universe was so dense and compact that what was predicted by the Big Bang theory, that before the rapid expansion, thermalisation of the Universe was due to the fact that all points in the Universe were in causal contact. Shortly after, the Universe grew way too quick over a too small time interval, and this caused the comoving horizon to increase in size faster than the Hubble sphere, thus leading to the disconnection of the points, and eliminating the horizon issue. The flatness problem, in a brief note, can be eliminated from the fact that the accelerated expansion of the Universe causes the total density of the Universe to tend to unity.

From the CMB, the slight fluctuations which showed the formation of large scale structure, are also explained by inflation. Intrinsic quantum fluctuations were magnified in order to explain how structures in the Universe originated. As for the monopole issue, the rapid accelerated expansion of the Universe gave rise to the process of "dilution" of the particles which were anticipated by particle Physics, but which cannot be detected. This is because their densities decrease with a power of the scale factor, and in a sufficient amount of time, this process affirms that although the monopoles are created, they cannot be detected in this present time [1, 4, 13].

Different paths have been attempted to define inflation, and a more geometrical way of describing it (see Eq.(1.2.1)), is from the negative rate of change of the comoving Hubble radius, indicating the shrink that we were talking about in the previous section. The idea is that in a very short period of time, the Universe goes through a speedy accelerated expansion, such that, relative to

this expansion, the Universe is relatively small with regards to any length scale measurement.

$$\frac{\mathrm{d}r_H}{\mathrm{d}t} < 0 \tag{1.2.1}$$

The most common model of inflation, among the different proposition, is the slow-roll inflation, which we define in the next part.

1.2.1 The Slow-Roll Inflation

The slow-roll inflation assures that inflation is not a process which can go on forever. The accelerated expansion of the Universe comes to a halt when the potential energy of the scalar field is dominated by its kinetic energy [14, 19]. This can be seen from the following dynamical system of equations, which were derived by assuming the existence of a scalar field, also known as inflaton field, $\phi(t)$, with a Lagrangian of the usual form of a kinetic term minus a potential, denoted by $V(\phi)$ [16]

$$\mathcal{L} = \frac{1}{2} g^{\mu\kappa}(\partial_\mu \phi)(\partial_\kappa \phi) - V(\phi) \tag{1.2.2}$$

For an inflationary epoch, the equation of motion of the scalar field is [16]

$$\ddot{\phi} + 3H\dot{\phi} + V' = 0 \tag{1.2.3}$$

where the prime denotes the first derivative with respect to the scalar field, that is, $\mathrm{d}/\mathrm{d}\phi$. The geometry of spacetime and the scalar field ϕ interact with the potential $V(\phi)$ through the following dynamical system, governed by the Eq.(1.2.3) and

$$H^2 = \frac{1}{3}\left[\frac{1}{2}\dot{\phi}^2 + V(\phi)\right] \tag{1.2.4}$$

where inflation occurs only if

$$\dot{\phi}^2 < V(\phi) \tag{1.2.5}$$

The inflation equations described by Eq.(1.2.4) and Eq.(1.2.3) can be solved in both a numerical approach or analytical approach, depending on the choices one assumes for $V(\phi)$, but, in the *slow-roll approximation*, an analytical solution is only possible when assuming $\dot{\phi}^2 \ll V(\phi)$, the differentiation

of which has the consequence that the $\ddot{\phi}$ term can be neglected and we have [16]

$$3H\dot{\phi} = -V' \tag{1.2.6}$$

$$H^2 = \frac{1}{3}V(\phi) \tag{1.2.7}$$

Further to this, in the slow-roll approximation, the conditions can be in the form of a dimensionless quantity through [16]

$$\epsilon \equiv \frac{1}{2}\left(\frac{V'}{V}\right)^2 \ll 1 \tag{1.2.8}$$

where, by differentiation the above with respect to ϕ, we also have that [16]

$$\eta \equiv \frac{V''}{V} \ll 1 \tag{1.2.9}$$

These two conditions are useful as they need that the potential $V(\phi)$ be adequately "flat" in order to allow the scalar field ϕ to "roll" slow enough to allow the occurrence of inflation. One should note that, although these conditions solely are required, they are not sufficient for inflation, because they do not limit the form of $\dot{\phi}$, as they do for $V(\phi)$. Therefore, it is imperative to assume that Eq.(1.2.5) holds in order to respect this condition.

1.2.2 Types of Inflation Models

Inflation models, using single field models, can be categorised into three main broad types, and these are [16]

Small Field Models In these models, a maximum value for the potential $V(\phi)$, usually unstable, makes the scalar field "roll" away and we have the following condition: $\eta < 0 < \epsilon$.

Large Field Models In these models, a minimum value perturbs the scalar field by a magnitude of $\Delta\phi \approx 1$. We have the following condition: $0 < \eta < \epsilon$.

Hybrid Field Models Conditions for these models involve $V''(\phi)$ which help identify such models, and these conditions are: $V''(\phi) > 0$ as well as $0 < \epsilon < \eta$. The hassle in these models is

that, another scalar field is needed to cease inflation. Despite this, hybrid models are considered as efficient models for single fields.

Now that we have illustrated some main ideas about how the Universe originated, and how the Big Bang theory is the best accepted theory describing the origin of the Universe, together with the explanations about how inflation remedies to the shortcomings of the Big Bang theory, we now get into the part of explaining how the evolution and structure formation in the Universe relies on the parameterization of this model. As mentioned before, the paraterisation of the Big Bang model will depend on the amounts and types of the various matter forms present at that time.

As a general fact, several forms of matter exist in the Universe. Additionally to the typical baryonic matter, such as neutrons and protons, more exotic forms of matter, with elementary particles lying beyond the standard model of particle Physics, may well be contained in the Universe. Large-scale structure observations indicate that most of the matter in the Universe is in the form of non-baryonic Dark Matter that interacts electromagnetically only very weakly [16], the invisibility of which forces it to be termed "dark".

The nature of Dark Matter is unknown. This weak electromagnetic interaction is what prevents its detection. It is only through its gravitational force, that inferences can be made. Classification of Dark Matter candidates are usually done according to their energy into two kinds: Cold Dark Matter (CDM) and Hot Dark Matter (HDM). HDM involves particles which travel with relativistic speeds, while although those in CDM are slow-moving and have low energies, they more realistically explain structure formation in the Universe.

One famous and effective configuration which encompasses the desired assumptions in the Universe, is the ΛCDM model, which we introduce in the next section. But we will first go through some fundamental ideas and equations in Cosmology.

1.3 The Standard Model of Cosmology

The most important assumption in the standard model of cosmology is that the Universe assumes homogeneity and isotropy on adequately large scales, and this is what is commonly known as the Cosmological Principle. In this section, we will be looking at the equations in Cosmology and their implications, but before that, we need to introduce some basic ideas of Einstein theory of General Relativity (GR). Further to this, we then introduce the Friedmann-Robertson-Walker (FRW) Universe via a metric and the related background equations. We will then end this section with the famous ΛCDM model.

1.3.1 General Relativity

Einstein Theory of General Relativity is a generalization of Special Relativity and the laws of universal gravitation formulated by Newton. Thus, from this theory, we have a better understanding of gravity, an interaction, which is beautifully described as a warping of the fabric of space and time. Gravity is a very special fundamental interaction, more like a property, which says a lot about the geometry of spacetime. In other words, spacetime tells matter how to move; matter tells spacetime how to curve and these can be modeled with Einstein Field Equations.

1.3.2 Einstein Field Equations and Gravitational Dynamics

As introduced above, Einstein General Theory of Relativity describes gravity as a distortion of spacetime, which caused by the presence of matter and energy. A massive object, such as the Earth, generates a gravitational field by warping the geometry of the spacetime that surrounds it. It was in 1915 that Hilbert discovered that this description can be embodied by Einstein's Field Equations (EFEs), derived from the action described below, using variational techniques.

If we start with the Einstein-Hilbert (EH) action, its variation with respect to the inverse metric $g^{\mu\kappa}$ is zero according to the action principle. Starting with

$$S_{EH} = \frac{1}{2k}\int \mathrm{d}^4x\sqrt{-g}R \tag{1.3.1}$$

where, $k = 8\pi G/c^4$ and $G = c = 1$, in order to obtain the field equations, the variational

technique for this action needs to be satisfied, that is,

$$\frac{\delta S_{EH}}{\delta g^{\mu\kappa}} = 0 \tag{1.3.2}$$

From the above, we then obtain Einstein Field Equations in vacuum, described by the Einstein tensor $G_{\mu\kappa}$, where $G_{\mu\kappa} = R_{\mu\kappa} - \frac{1}{2}Rg_{\mu\kappa} = 0$ and $R_{\mu\kappa}$ is the Ricci tensor obtained from contracting the Riemann tensor, as already defined before.

$$R_{\mu\kappa} = R^{\sigma}_{\mu\sigma\kappa} = \partial_\sigma \Gamma^{\sigma}_{\mu\kappa} - \partial_\kappa \Gamma^{\sigma}_{\mu\sigma} + \Gamma^{\sigma}_{\sigma\lambda}\Gamma^{\lambda}_{\mu\kappa} - \Gamma^{\sigma}_{\kappa\lambda}\Gamma^{\lambda}_{\mu\sigma} \tag{1.3.3}$$

Our connection (Christoffel Symbol) is defined as

$$\Gamma^{\lambda}_{\mu\kappa} = \frac{1}{2}g^{\lambda\sigma}(\partial_\mu g_{\sigma\kappa} + \partial_\kappa g_{\sigma\mu} - \partial_\sigma g_{\mu\kappa}) \tag{1.3.4}$$

and, R is the Ricci Scalar, or so-called curvature tensor, defined sa

$$R = g^{\mu\kappa}R_{\mu\kappa} \tag{1.3.5}$$

Now, if we want to find the Einstein field equations in the presence of matter, we then have $S = S_{EH} + S_M$ where,

$$S_M = \int \mathrm{d}^4x\sqrt{-g}\,\mathcal{L}_M \tag{1.3.6}$$

Therefore, from the principle of action, the following applies

$$\delta S_{EH} + \delta S_M = 0 \tag{1.3.7}$$

The result for δS_{EH} is already known to be $R_{\mu\kappa} - \frac{1}{2}Rg_{\mu\kappa}$. We then have the full Einstein field equations

$$G_{\mu\kappa} = R_{\mu\kappa} - \frac{1}{2}Rg_{\mu\kappa} = kT_{\mu\kappa} \tag{1.3.8}$$

If we compare with Eq.(1.3.8), then we can define the stress energy-momentum tensor as [18]

$$T_{\mu\kappa} = -\frac{2}{\sqrt{-g}}\frac{\delta S_M}{\delta g^{\mu\kappa}} = -\frac{2}{\sqrt{-g}}\frac{\delta(\sqrt{-g}\,\mathcal{L}_M)}{\delta g^{\mu\kappa}} \tag{1.3.9}$$

The tensor described above is very important, as it describes the kind of fluid for which we are trying to solve the field equations. In our case, for simplicity, we will assume that our fluid is *perfect* and has only one kind of energy density relating pressure p, and density ρ through a barotropic fluid Equation of State (EoS) of the form $p = p(\rho)$. Therefore, our perfect fluid can be described by the following energy-momentum tensor [4, 16]

$$T_{\mu\kappa} = (\rho + p)U_\mu U_\kappa + p g_{\mu\kappa} \tag{1.3.10}$$

For a comoving observer, we have the 4-velocity, $U_\mu = (-1, \mathbf{0})$, and from the assumption that matter in our Universe is a barotropic fluid, the following relationship holds as a plausible EoS [4]

$$p = \omega\rho \tag{1.3.11}$$

where ω is referred to as the EoS parameter, and assumes different values depending on the kind of energy density. We can summarise, under three categories, some of the important values of this parameter as

1. $\omega = 0$, for pressure-free, non-relativistic matter (or so-called "dust")
2. $\omega = 1/3$, for gas of relativistic matter (or radiation)
3. $\omega = -1$, for a cosmological constant

However, due to the complexity of neutron plasma, the EoS are not that simple to deal with. We will see this in more details in Section 3 for the case of neutron stars.

We have seen that the standard Einstein gravitational equations are given by Eq.(1.3.8). As a matter of fact, it is only shortly after the proposition of these equations that Einstein came up with a newer version, that included a cosmological term as the modification, denoted by $\Lambda g_{\mu\kappa}$. The reason for this is because, Einstein thought that the Universe was static, but instead from his previously derived equations (Eq.(1.3.8)), the solutions were rather pointing towards an expanding Universe. We then have

$$R_{\mu\kappa} - \frac{1}{2}R g_{\mu\kappa} + \Lambda g_{\mu\kappa} = kT_{\mu\kappa} \tag{1.3.12}$$

Eventually, after it was found from observations that galaxies are receding from each other, as well as from us, with velocities proportional to their separation from the observation point, they explained this phenomenon through a volume expansion of the observable Universe. Thereafter, the cosmological constant was no longer included in the Einstein equations.

1.3.3 The Friedmann-Robertson-Walker Geometry

The Cosmological Principle

As we have mentioned before, the Cosmological Principle makes two very important assumptions about the Universe - being homogeneous and isotropic on sufficiently large scales(> 100 Mpc). This is due to the fact that on small scales, matter distribution is extremely erratic, but on a much larger scale, it seems more uniformly distributed. Since this principle is applied everywhere, it is imperative to constrain the geometry of spacetime. In other words, both homogeneity (constancy under translations) and isotropy (constancy under rotations) are a must.

As a motivation to this, isotropy has indeed been observed by the CMB, where, when photons were emerging from various segments of the sky, their average temperature was nearly the same [4]. Large scale structures like galaxy clusters, as well as empty parts in the sky have a random distribution in space [15]. Additionally, the cosmological redshift of distant galaxies is isotropic, and this demonstrates an even space expansion [1, 4, 15].

The Friedmann Universe

The Friedmann-Robertson-Walker (FRW) metric is the only metric known which can successfully satisfy the constraints from the Cosmological Principle and which acts as an exact solution of the Einstein Field Equations (Eq.(1.3.8)). It can be proven that these are in fact all the possibilities for a homogeneous and isotropic metric. It can be defined as [16]

$$\mathrm{d}s^2 = -\mathrm{d}t^2 + a(t)^2\left[\frac{\mathrm{d}r^2}{1-\mathcal{C}r^2} + r^2\left(\mathrm{d}\theta^2 + \sin^2\theta\mathrm{d}\phi^2\right)\right] \tag{1.3.13}$$

where t stands for the cosmic time, (r, θ, ϕ) represent the spherical coordinates of the maximally symmetric 3-space part of the metric [16], a is the cosmological scale factor describing the background expansion of the Universe, and $\mathcal{C}$ represents curvature of the space and can take the

values -1, 0, or 1. These values respectively correspond to open (or hyperbolic), flat and closed (or spherical) description of the spatial section. We briefly address these three cases below:

Positive Spatial Curvature: $\mathcal{C} = 1$

In this case, we have a singularity as $r \to 1$, thus imposing the need for introducing a new radial coordinate, χ through the transformation [16]

$$r = \sin\chi \tag{1.3.14}$$

such that $\mathrm{d}r = \cos\chi \mathrm{d}\chi = (1 - r^2)^{1/2}\mathrm{d}\chi$.

We can then rewrite the metric as

$$\mathrm{d}s^2 = -\mathrm{d}t^2 + a(t)^2\left[\mathrm{d}\chi^2 + \sin^2\chi(\mathrm{d}\theta^2 + \sin^2\theta\mathrm{d}\phi^2)\right] \tag{1.3.15}$$

Zero Spatial Curvature: $\mathcal{C} = 0$

In this case, we have a flat space which is analogous to the ordinary Euclidean space in three dimensions [16]. Letting $r = \chi$ allows us to rewrite our metric as

$$\mathrm{d}s^2 = -\mathrm{d}t^2 + a(t)^2\left[\frac{\mathrm{d}\chi^2}{1 - \mathcal{C}\chi^2} + \chi^2\big(\mathrm{d}\theta^2 + \sin^2\theta\mathrm{d}\phi^2\big)\right] \tag{1.3.16}$$

Negative Spatial Curvature: $\mathcal{C} = -1$

In this case, we conveniently introduce the radial coordinate χ with a hyperbolic transformation through [16]

$$r = \sinh\chi \tag{1.3.17}$$

such that now $\mathrm{d}r = \cosh\chi\mathrm{d}\chi = (1 + r^2)^{1/2}\mathrm{d}\chi$, thus allowing us to rewrite the metric as

$$\mathrm{d}s^2 = -\mathrm{d}t^2 + a(t)^2\left[\mathrm{d}\chi^2 + \sinh^2\chi(\mathrm{d}\theta^2 + \sin^2\theta\mathrm{d}\phi^2)\right] \tag{1.3.18}$$

In the rest of this part of this thesis, for simplicity of explanations, we assume the case of zero spatial curvature.

The Cosmological Redshift

The scale factor $a(t)$, which describes the relationship between the comoving and proper distance between two points in the Universe, holds information about time dependence. This relationship can be written down as

$$D(t) = a(t)\chi \tag{1.3.19}$$

where in our expanding Universe, $D(t)$ represents the physical distance and χ is the comoving distance. Therefore, from this we can define the comoving distance, of a incoming photon for example, through [16]

$$\int_{t_e}^{t_r} \frac{c\mathrm{d}t}{a(t)} = \int_0^{\chi_e} \mathrm{d}\chi \tag{1.3.20}$$

where t_e is the cosmic time at which the photon is emitted by a comoving observer having fixed spatial coordinates, and t_r is the time at which the photon is received by some other observer bearing fixed comoving coordinates.

The change in wavelength of the signal which is emitted, and later received, is measured by what is called, the redshift, which is denoted by z. Its relation to the scale factor is as follows:

$$1 + z = \frac{a(t_r)}{a(t_e)} \tag{1.3.21}$$

where $a(t_r)$ is the scale factor for the present time and usually assumes a unit value, so that at the present epoch, $z \sim 0$.

From the relationship between redshift and scale factor $a(t)$ given by Eq.(1.3.21), we can conclude that, if $a(t)$ goes up along the cosmic time leading to the expansion of the Universe, then photons experience a redshift by an amount z [16]. On the contrary, if we have a contraction in the Universe, photons experience a blueshift. Lastly, if the Universe remains static, then $a(t)$ is constant, displaying no shift in frequency.

The Hubble and Deceleration Parameters

If distant galaxies emit photons which are received today, at the present cosmic time, t_0, and if

the emitting galaxy is close by and emits a photon at cosmic time t, it is possible for us to define [16] $t = t_0 - \delta t$, where $\delta t \ll t_0$. We have the scale factor as $a(t)$ and if we expand it as a power series about t_0, we obtain [16]

$$\begin{aligned} a(t) &= a[t_0 - (t_0 - t)] \\ &= a(t_0) - (t_0 - t)\dot{a}(t_0) + \frac{1}{2}(t_0 - t)^2\ddot{a}(t_0) - ... \\ &= a(t_0)\big[1 - (t_0 - t)H(t_0) - \frac{1}{2}(t_0 - t)^2 q(t_0)H^2(t_0) - ...\big] \end{aligned} \tag{1.3.22}$$

where the dot represents the derivative with respect to cosmic time t and we have defined the Hubble parameter $H(t)$ as [16]

$$H(t) = \frac{\dot{a}(t)}{a(t)} \tag{1.3.23}$$

and the deceleration parameter $q(t)$ as

$$q(t) = -\frac{\ddot{a}(t)a(t)}{\dot{a}(t)^2} \tag{1.3.24}$$

With these definitions, due to a recession velocity, v of an emitting galaxy, it is possible to interpret the cosmological redshift as a Doppler shift by [16]

$$v = cz = H_0 d \tag{1.3.25}$$

which is approximately valid for small z. We have that d is the proper distance and H_0 is the present-day value of the Hubble parameter. What this means, is that galaxies seem to recede from us, with a speed which is proportional to their distance from us [16], as previously mentioned.

This is the famous Hubble's law, although Lemaître had already discovered this law and also computed H_0. It was in 1929 that Edwin Hubble made the discovery about the expanding Universe. His results, which displayed a linear recession, were measured in Cepheid variables, when he compared distances to close-by galaxies with redshifts. The implication of this finding, is that, at some finite time in that past, the Universe started off from a very high density.

The Cosmological Field Equations

After the investigation of the geometric consequence of the FRW metric, we come back to the analysis of the scale factor. In fact, the scale factor is responsible for the dynamics of the spacetime geometry. Its evolution can be analysed by solving the Einstein Field Equation in the presence of matter. We start with Eq.(1.3.12). Using the definition of the Ricci tensor and connection, we can define the following non-zero coefficients [16] for our flat Universe characterised by the metric at Eq(1.3.16)

$$\begin{aligned}
\Gamma^0_{11} &= \frac{a\dot{a}}{1-\mathcal{C}\chi^2} & \Gamma^1_{22} &= -\chi(1-\mathcal{C}\chi^2) \\
\Gamma^0_{22} &= a\dot{a}\chi^2 & \Gamma^1_{33} &= -\chi(1-\mathcal{C}\chi^2)\sin^2\theta \\
\Gamma^0_{33} &= a\dot{a}\chi^2\sin^2\theta & \Gamma^2_{33} &= -\sin\theta\cos\theta \\
\Gamma^1_{01} &= \Gamma^2_{02} = \Gamma^3_{03} = \frac{\dot{a}}{a} & \Gamma^2_{12} &= \Gamma^3_{13} = \frac{1}{\chi} \\
\Gamma^1_{11} &= \frac{\mathcal{C}\chi}{1-\mathcal{C}\chi^2} & \Gamma^3_{23} &= \cot\theta
\end{aligned} \tag{1.3.26}$$

Substituting these coefficients (Eq.(1.3.26)) into Eq.(1.3.3), we have the following non-zero entries

$$\begin{aligned}
R_{00} &= -3(\dot{H}+H^2) & R_{22} &= a^2\chi^2\Big(\dot{H}+3H^2+\frac{2\mathcal{C}}{a^2}\Big) \\
R_{11} &= \frac{a^2}{1-\mathcal{C}\chi^2}\Big(\dot{H}+3H^2+\frac{2\mathcal{C}}{a^2}\Big) & R_{33} &= R_{22}\sin^2\theta
\end{aligned} \tag{1.3.27}$$

where we have used the Hubble parameter definition $H = \frac{\dot{a}}{a}$ and once again, the dot is the differentiation with respect to cosmic time t. Manipulating the components of Eq.(1.3.27) allows us to define the Ricci scalar as

$$R = 6\Big(\dot{H}+2H^2+\frac{\mathcal{C}^2}{a^2}\Big) \tag{1.3.28}$$

Once again, we assume that our fluid is a perfect one, which can be described by the energy-momentum tensor defined by Eq.(1.3.10), such that for a comoving observer we have that

$$\begin{aligned}
T_{00} &= \rho & T_{22} &= pa^2\chi^2 \\
T_{11} &= \frac{pa^2}{1-\mathcal{C}\chi^2} & T_{33} &= T_{22}\sin^2\theta
\end{aligned} \tag{1.3.29}$$

By using Eqs.(1.3.26), (1.3.27) and (1.3.29), we arrive at the cosmological field equations de-

scribed by the following two differential equations

$$H^2 = \frac{8\pi G\rho}{3} - \frac{\mathcal{C}}{a^2} \tag{1.3.30}$$

$$H^2 + \dot{H} = -\frac{4\pi G}{3}(\rho + 3p) \tag{1.3.31}$$

The two equations above resolve the time evolution of the scale factor. Eq.(1.3.30) is commonly known as the Friedmann equation and Eq.(1.3.31), as the Raychaudhuri equation.

Just as in the case of the Einstein Field Equations from the previous section of this chapter, we can assume that matter in our Universe can take up the form of a barotropic fluid whose EoS is given by Eq.(1.3.11), wherein the same characteristic values of ω can be assumed for the different kinds of fluid domination in the Universe. The EoS allows us to rewrite the Raychaudhuri equation as

$$H^2 + \dot{H} = -\frac{4\pi G}{3}(\rho + 3\omega\rho) \tag{1.3.32}$$

Equation of motion

The cosmological field equations described by Eqs.(1.3.30-1.3.31) are adequate for analysing and calculating the scale factor $a(t)$ for any model of the Universe. Nevertheless, the following a crucial requirement for the energy-momentum tensor should be considered, that is

$$\nabla_\kappa T^{\mu\kappa} = 0 \tag{1.3.33}$$

This requirement allows us to derive the relativistic equations of motion and continuity for the cosmological fluid of the form as in Eq.(1.3.11), and thus we can write the energy conservation as [16]

$$\dot{\rho} + 3H\rho(1 + \omega) = 0 \tag{1.3.34}$$

This energy conservation equation yields solutions for our scale factor $a(t)$ for the different values which are known for the EoS parameter. The equation gives how the fluid density is diluted with the expansion. In order to obtain $a(t)$, we require Eq.(1.3.30). The energy equation can be written

as

$$\frac{d(\rho a^3)}{da} = -3\omega\rho a^2 \tag{1.3.35}$$

whose immediate solution can be written as the evolution of density ρ as a function of the scale factor $a(t)$ through [16]

$$\rho \propto a^{-3(1+\omega)} \tag{1.3.36}$$

These solutions, for a flat Universe, are summarised in the following table

	ω	$\rho(a)$	$a(t)$
Λ	-1	a^0	e^{Ht}
Matter	0	a^{-3}	$t^{\frac{2}{3}}$
Radiation	$\frac{1}{3}$	a^{-4}	$t^{\frac{1}{2}}$

Table 1: Scale factor evolution for a flat FRW Universe

where $H = \sqrt{\Lambda/3} = \text{constant}$.

Due to the fact that gravity is an attractive force, the expansion of the Universe is supposed to decelerate if we consider gravity as the sole force in our Universe. This is unfortunately not possible as studies have shown that the Universe is expanding at a fast rate, for example, studies on luminosity distances of type Ia Supernovae (SNIa) have not only shown that our Universe is expanding but that this expansion is accelerated [29]. Efforts from different surveys, for instance, the Baryon Acoustic Oscillation Spectroscopic Survey (BOSS) [40], the Sloan Digital Sky Survey (SDSS) and the Dark Energy Survey (DES), have been made in order to try explain the nature and reason of this acceleration [41].

Considering the Raychaudhuri equation defined at Eq.(1.3.32), it is only when $\omega < -1/3$ that $\ddot{a} > 0$, that is, we observe an accelerated expansion of the Universe. The only way to favourably explain this acceleration, is for the pressure to be negative, $p < (-1/3)\rho$. Matter is no longer dominating the deceleration phase due to this mysterious density of energy, which has thus been named "Dark Energy". This unknown energy currently outweighs all other energy forms in our Universe. This can be seen below from the 5-year WMAP data below [7] (we present a latest version of these visual statistics in the next chapter).

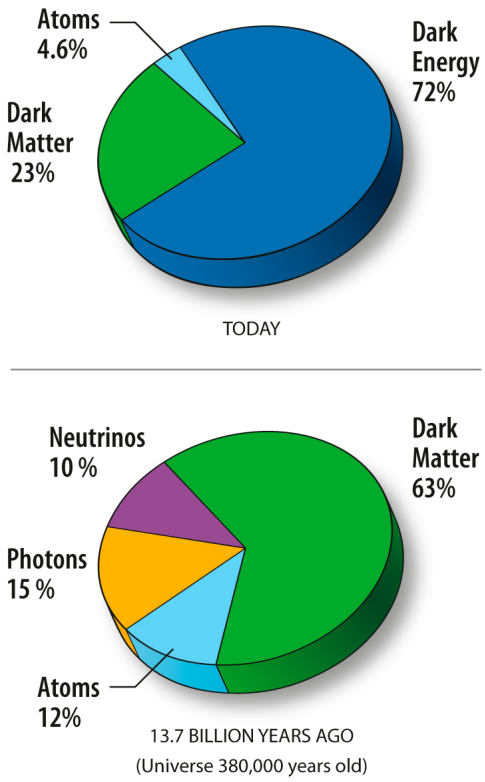

Figure 2: Content of the Universe: Today vs. 13.7 billion years ago (taken from [7])

1.3.4 The ΛCDM Model

We have seen from all the literature above, that the Universe is composed of different types of fluids, which can be described by different equations of state. Our current model which is the Lambda Cold Dark Matter (ΛCDM) model, Dark Energy is parameterised by the Λ parameter.

This Dark Energy, as can be compared in Figure 2 from 13.7 billion years ago to today (as per the 5-year WMAP data) [7], makes up 72% of the energy content of our Universe. One threatening fact about this source of energy, is that there is no known technique of observing nor analysing it. Its enigmatic nature is what termed it as Dark Energy. It is fair to say that one of the ultimate goals of cosmologists is to be able to understand its nature and predict its behaviour.

The ΛCDM model is known as the Cosmological Concordance model due to its simplicity and ease in explaining certain properties of the cosmos, such as, the existence and structure of the CMB

radiation, the large scale structures from galaxy distributions and the abundance of hydrogen, helium and lithium. Also referred to as the "cosmological constant", Λ which is treated as Dark Energy fairly explains the late expansion of our Universe at a very fast rate. This constant bears a negative pressure.

In the ΛCDM paradigm, it is generally assumed that the Universe contains both matter and radiation, and that Λ is non-zero. A modern way of interpreting this constant is in respect of the energy density of vacuum, which can also be analysed with a perfect fluid. It becomes natural to be of the view that the cosmological fluid is made up of three parts, coming from the cosmological constant, radiation and matter, each bearing a different EoS. Although matter and radiation did previously interact in the early Universe, we still make the assumption that matter, radiation and vacuum do not interact. Thus, the total equivalent mass density is simply made up of the sum of the individual parts [16]

$$\rho(t) = \rho_\Lambda(t) + \rho_r(t) + \rho_m(t) \tag{1.3.37}$$

where t is the cosmic time.

With the introduction of this cosmological constant in the Cosmological Concordance model, we can therefore rewrite the Friedmann equation as [16]

$$H^2 = \frac{8\pi G}{3}\Big(\rho_\Lambda + \rho_r + \rho_m\Big) \tag{1.3.38}$$

where ρ_Λ, ρ_r and ρ_m are the energy densities of Dark Energy, radiation and (dust) matter respectively. For convenience, we can write Eq.(1.3.38) using dimensionless density parameters [16]

$$\Omega_{(i)}(a) = \frac{8\pi G}{3H^2}\rho_{(i)}(a) \tag{1.3.39}$$

where H is the Hubble parameter and i denotes "Λ", "r" and "m" accordingly.

We can also express the Friedmann equation as

$$\Omega_\Lambda + \Omega_r + \Omega_m = 1 \tag{1.3.40}$$

or alternatively as,

$$H(a) = H_0\sqrt{\Omega_{\Lambda 0} + \Omega_{r0}a^{-4} + \Omega_{m0}a^{-3}} \tag{1.3.41}$$

where the $H_0 = 67.8$ kms^{-1}Mpc^{-1} is the Hubble constant, and $\Omega_{\Lambda 0} = 0.692$, $\Omega_{r0} = 9.24 \times 10^{-5}$ (negligible) and $\Omega_{m0} = 0.308$ are dimensionless density parameters from [21, 22].

Although the ΛCDM model bears many successes, just like several other theories, challenges are also involved. For example, at the time of decoupling, the existence of frozen relics of the early Universe, known as the Baryon Acoustic Oscillations (BAO), is a great success, just as has been the statistics of weak gravitational lensing and the polarization of CMB. However, as of today, this model has not been able to account for searches of Dark Matter particles nor the laboratory detection of Dark Energy. This is one of the reasons why alternative theories of gravity are being proposed as some kind of remedy to these limitations.

1.4 Conclusion

In this chapter, we have given insights on the Big Bang theory, which, although does not explain why, does provide a plausible theory of how the Universe was formed. Like many cosmological theories, the Big Bang theory also had drawbacks: the horizon and flatness problem, to which inflation came as a rescue. We have also seen how the FRW metric for a spatially flat Universe is our best model at encompassing the consequences of the Cosmological Principle. While Hubble's law came as the groundbreaking discovery about the accelerating expansion of the Universe, and that the ΛCDM model, parameterised from the Big Bang is the standard model of Cosmology, it unfortunately still does not help detect or provide satisfactory explanations for the ad-hoc need of both Dark Matter particles nor Dark Energy. As a direct consequence arising from these limitations, propositions of alternative theories of gravity were put forward. This is precisely what we address in the next chapter.

Chapter 2

2 Modified Gravity

As seen from the previous chapter, the ΛCDM model has had enormous successes in explaining the formation of the Universe, but due to some limitations, theoretical physicists and cosmologists have suggested changes to be brought to the model. General Relativity (GR) is a widely accepted theory of gravity, but can however not explain the phenomena of dark matter and dark energy, and due to this fact, it can no longer be considered as the only way of finding solutions for the behavior of spacetime. These limitations appeared from the failure of the conventional theory to prove the existence of strange forms of energy, that is, if General Relativity is used to build the standard cosmological model where the fluid content is modeled by standard matter and radiation, it still does not elucidate this strange form of Dark Energy.

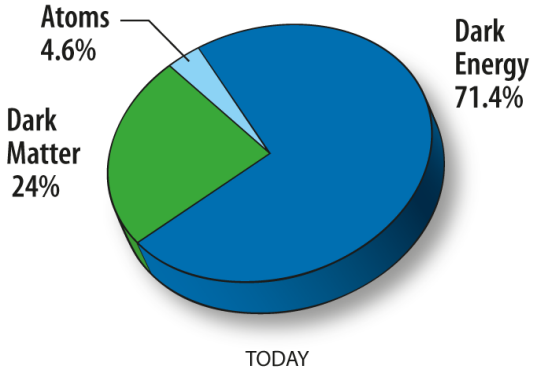

Figure 3: Universe Content Today(taken from [7])

Supportive data from different sources such as the CMB and supernovae surveys [7, 27, 28, 29, 30], indicate that, today the Universe is made up of 4.6% ordinary matter, 24% Dark Matter and 71.4% of a mysterious energy form. These strange and unknown forms of energy, referred to as Dark Energy (DE) behave in a way that has caused scientists to question their understanding of gravity. The fact that this mysterious Dark Energy does not form clusters like ordinary matter does, and its undetectable nature, are the causes of what is now so commonly known as “Dark Energy problem” .

In the cosmological environment, the 'Dark Energy problem' results in the accelerated expansion of the Universe, and ranks among one of the most perturbing theory-related problems of this century. Unfortunately GR, by itself fuelled with standard fluids only, cannot justify this accelerated expansion on adequately large scales. This theory requires the addition of a cosmological constant to explain this accelerated expansion. Moreover, a Dark Matter contribution needs to be implemented to balance data with theoretical predictions, since GR with gravitating luminous matter is incapable of agreeing with the observed galactic rotation curves. Therefore, instead of trying to adjust observations with GR by adding terms to the cosmological content, there would seem to be an alternative option [26]. Statistical research from gravitational lensing alongside alternative methods have also imposed on scientists to reconsider GR via the possibility of having Extended Theories of Gravity (ETG) to solve these puzzles.

Extended Theories of Gravity, or so commonly known as Modified Gravity theories, are a line of research which translates gravity theories in a more general way, and this has been attempted by numerous scientists over the last few decades. In this chapter, we will motivate the choice of alternative theories of gravity, as well as the viability criteria for an applicable theory. Thereon, we will derive the $f(R)$ field equations for the general modified $f(R)$ theory, and look at some known models in a similar line.

2.1 Motivation for alternative theories of gravity

Einstein theory of General Relativity has been questioned and criticised the moment it was published, in the early 20th century. It seemed to many, that GR could not be the unique theory of gravitation. Several attempts, amongst many others, have been made to modify gravity in order to challenge and compete with Einstein theory. For example, Weyl and Eddington in [31] and [32] modified the gravitational action by adding higher-order invariants, and since this was unable to be motivated theoretically and experimentally, it proved to be that the Einstein-Hilbert (EH) action could be traditionally quantised but was not UV-complete. It is widely known that GR without matter is finite at one-loop. As a matter of fact, higher-order terms need to be added to the action so that the resulting theory can be two-loop renormalizable [33, 34].

As we know, modern Physics rests on two theoretical frameworks, namely GR and Quantum Field Theory (QFT). On one side, GR deals with gravity relating to the interpretation of the Universe in regions of both high mass and large scale, for example, stars, galaxies, galaxy clusters, etc. On the other side, QFT is one theoretical framework which deals with three forces, other than gravitation, relating to the interpretation of the Universe in regions of both low mass and small scale, such as sub-atomic particles, atoms, molecules etc. QFT has had enormous success in implementing the Standard Model (SM) and unifying into a single force the interactions between the three non-gravitational forces: weak, strong and electromagnetic force, referred to as the Grand Unified Theories (GUT). Unfortunately these theories are inadequate because they exclude gravity.

The hurdle in obtaining a theory that unifies the other forces with gravity is that GR is an Effective Field Theory (EFT), much like the other interactions, and therefore excludes the uncertainty principle of quantum mechanics, while the additional partial theories are crucially based on quantum mechanics. As Hawking said in [35], a necessary first step is to be able to combine GR with the uncertainty principle, which can have some phenomenal outcomes, such as the Universe being limitless, in the sense that it is self-contained and has no boundary, as well as black holes not being black, that is, they actually glow from the radiation they emit (Hawking Radiation). However, the issue is that the uncertainty principle implies that pairs of antiparticles and virtual particles. This results in their gravitational attraction curving up the Universe to a cosmically small size.

Back to alternative theories of gravity, in more recent research, when higher-order modifications in low energy string dynamics were considered, the gravitational action which is of low energy, included higher-order curvature invariants [36, 37, 38]. These results diverted the attention in higher-order theories of gravity, which would imply modifying the higher-order curvature invariants in the EH gravitational action. The new contributions were assumed to be applicable in intense gravity regimes, such as close to the Planck scale, and thus in the early Universe or close to black hole singularities, and were not likely to affect gravitational phenomenology neither at low energy regimes nor at low curvature [26]. They were therefore thought of being of minor contribution at large scales.

Recent evidences pointing towards the unusual and urgent accelerated expansion of the Universe, have forced researches in the astrophysical and cosmological fields to query the correctness of GR, as this theory alongside radiation and ordinary matter has left them scrambling for a plausible explanation. As mentioned in the first chapter, the energy content of the Universe comprises two unusual "dark components": Dark Energy which dominates the current epoch, does not form any clusters, and has unknown properties and an apparent negative pressure, and Dark Matter, which is undetectable but forms clusters just like ordinary matter. Data from large structure formation, measurements of the CMB anisotropies from the Wilkinson Microwave Anisotropy Probe (WMAP) and type Ia supernovae (SNIa) surveys [39, 42, 43] only show that our Universe is expanding at a fast rate, thus the urgency in finding its cause.

Several explanations have been attempted, which can be summarised into three classes. The first one conjures a cosmic fluid, DE alongside an EoS in order to resolve this acceleration with GR. While DE is necessary in explaining and solving for this accelerated expansion of the Universe, DM on the other hand is needed to explain the missing mass issue that occurs in both galaxy clusters and single galaxies. As discussed in chapter 1, the EoS relating pressure to density is given by $p = \omega\rho$. Modeling DE with this EoS for $\omega < -1/3$ is the condition which explains the accelerated expansion.

For the case where $\omega = -1$, the fluid acts like the cosmological constant. An auxiliary part of the standard cosmological model which is not yet fully deciphered, is an epoch involving an early time cosmic inflation. It was put in place to explain the horizon, flatness and monopole problems, and to give rise to the origins of the large scale structure (primordial fluctuations). Still, it seems that by modeling DE through the cosmological constant Λ, we face what is called *the cosmological constant problem*, since the fitted value of Λ is much smaller than the expected magnitude of the vacuum energy of matter fields, as speculated by particle Physics [26].

Other attempts to explain this speedy evolution of the Universe, classified as the second class, involved dealing with Cartan Brans-Dicke, whereby a new scalar field is added to the dynamical DE, giving rise to what is generally called scalar-tensor theories, or in our case, the quintessence theories. Finally, the third type of explanations involved using the repercussions of new gravitational Physics [44, 46]. Modifying the EH gravitational action is an attempt which has been dealt with since a

very long time [47, 48, 50, 54, 55, 56]. Some years ago, DE proposals involved vector-tensor theories of gravity [58]. Higher or lower powers of the scalar curvature, the Ricci and the Riemann tensors or their derivatives are used in these theories [57]. Such theories involved $f(R)$ theories of gravity and Lovelock theories.

However, these were not the only attempts to explain the accelerated expansion of the Universe. Modifying gravity was also proposed through a theory attempting to unify gravity and the other forces such Kaluza-Klein. In this theory, a fifth dimension was added to the standard three space and one time, in order to obtain Einstein's gravity, Maxwell's Electromagnetism, and a new extra scalar field [59]. In order not to interfere with the laws of gravity nor to have any discernible effects on the Universe, the extra dimension is required to be small enough and the extra scalar field, modeled very carefully. Eventually since it was impossible to formulate a quantum theory of gravity with these cautionary steps, this unification was ruled out too. Lastly, string theory (and M-theory) were proposed as plausible explanations, which seem to fit our Universe, but unfortunately also fail at certain levels (considering the possibility of multiverses). Cosmologists are still in quest of this one theory, referred to as *the theory of everything*, one single unifying equation that will explain everything in the Universe.

In the next section, we will be looking at some of the properties which need to be satisfied, in order to have a viable theory for modifying gravity. One of the most crucial criteria for a theory to be tenable is its power to anticipate results, or to falsify predictions for the conjectures that need proof. As such, any suggested modified gravity theory should be able to predict the evolution of time of the Universe ruled by it.

2.2 Criteria for a viable theory

In order to properly illustrate gravitational interaction through a proposed theory, the theory itself should be able to explain observational facts and have as outcome the predicted results within the suitable limits. The theory of gravity already imposes such limits, which are in terms of distance scales, cosmological perturbations and gravitational potentials [60]. In order to satisfy the distance scales, Newtonian dynamics are extremely important when the non-relativistic weak field limits is

being taken into account by the proposed theory. In other words, the theory should be able to replicate the results from tests on the solar system, which are initially well described by GR.

In addition, the gravitational potential which the theory predicts should match to some extent, the Newtonian potential. The latter already provides a good explanation with regards to radiation and baryonic matter that stars and galaxies hold, which implies that the new theory should be of an appropriate level to describe large scale structure formation using perturbation theory. The proposed theory should demonstrate cosmological perturbations which in turn need to be in tune with observational data that the CMB provides. This theory need to be able to describe and predict observations of the accelerated expansion of the Universe [60].

Not only should the proposed theory for modified gravity satisfy the above conditions, but it should also, without an explicit cosmological constant term, give an explanation for the late-time acceleration of the Universe, while challenging GR. The equivalence principle, the principles of relativity, general covariance and causality are assumed to be valid for the alternative theories of gravity in question. As such, several methods of modifying and generalizing GR have been put forward with great effort in GR to establish a semi-classical scheme in which we could replicate the same successes [10].

The ETGs are founded Einstein's theory with some additive corrections, and thus, became a paradigm in the study of gravitational interaction next to Einstein's theories. For instance, as summarised in [87], Lovelock's theorem implies that, in order to come up with metric gravity theories with field equations diverging from the standard GR ones, certain criteria apply. One should consider fields other than the metric tensor, accept derivatives of the curvature and related invariants to be of order higher than two for the metric, and add extra dimensions to the standard three space and one time, all while giving up locality. Some examples of such theories are Tensor-Vector-Scalar gravity (TeVes), Brane-World (BW) gravity and the well-known scalar-tensor gravity.

In this thesis, our focus is on higher-order theories of gravity (HOTG), in which corrections are made to generalise the EH action, as well as the power form $f(R) = R^{1+\epsilon}$. Two such examples are Teleparallel gravity, known as $f(\tau)$ theories, where τ is the usual torsion scalar, and $f(R)$ theories

of gravity. The difference between both theories is seen through the gravitational field equations: the ones for $f(\tau)$ theories are second order whereas those for $f(R)$ theories are of higher-order. Additional reading about Teleparallel gravities can be done in [63], from which an eye-catching observation of $f(\tau)$ theories is made: every solution of GR is also a solution for Teleparallel gravity although not every solution of $f(\tau)$ is a solution of GR. We will specifically deal with classes of $f(R)$ gravity theories.

This category of modified $f(R)$ theories involve invariants of order much higher than the scalar curvature. $f(R)$ theories, being just an extension from GR, were first studied by Weyl, followed by Eddington in 1923 [32] in trying to bring modifications to General Relativity by adding curvature invariants of higher-order in the EH action. Essentially, the standard procedure involves adding curvature invariants of the form, for instance, $R^{\mu\kappa}R_{\mu\kappa}, R^{\mu\kappa\delta\gamma}R_{\mu\kappa\delta\gamma}, R\Box R, R^2, R\Box^k R$ or non-minimally coupled scalar field into the dynamics emerging from an effective quantum gravity action [10].

The identities shown below [2] are valid for spacetime with maximally symmetric spatial parts. Therefore the Lagrangians involving the quadratic invariants $R^{\mu\kappa}R_{\mu\kappa}$ or $R^{\mu\kappa\delta\gamma}R_{\mu\kappa\delta\gamma}$ can be expressed in terms of R^2, on the assumption that the Lagrangian involves a linear combination of those quadratic invariants.

$$(\delta/\delta g_{\alpha\beta})\int \mathrm{d}^4x\sqrt{-g}(R^{\alpha\beta\delta\gamma}R_{\alpha\beta\delta\gamma} - 4R^{\alpha\beta}R_{\alpha\beta} + R^2) = 0 \tag{2.2.1}$$

$$(\delta/\delta g_{\alpha\beta})\int \mathrm{d}^4x\sqrt{-g}\epsilon^{\alpha\beta\delta\gamma}R_{\alpha\beta\delta\gamma}R^{\kappa\lambda}_{\delta\gamma} = 0 \tag{2.2.2}$$

$$(\delta/\delta g_{\alpha\beta})\int \mathrm{d}^4x\sqrt{-g}(3R^{\alpha\beta}R_{\alpha\beta} - R^2) = 0 \tag{2.2.3}$$

What this implies is that any Lagrangian which comprises a linear combination of such quadratic invariants of higher-order, is identical to a form of universal power law function involving R.

These alternative theories of gravitation, which arise by making a replacement in the Ricci Scalar, R, with some $f(R)$ function of the Ricci Scalar in the Einstein-Hilbert action, were first

studied by Buchdahl in 1970 in his paper on "Non-linear Lagrangians and cosmological theory" [96]. Moreover, conceptually, there would be no *a priori* reason to impose limitations on the the gravitational Lagrangian to be a linear function of the Ricci scalar R, minimally coupled with matter [60, 94, 95, 96]. As a matter of fact, if $f(R)$ is nonlinear, fourth order field equations are obtained when varying the action relative to the metric. These theories are known as fourth-order theories of gravity. In the quest of a suitable modification of Einstein's theory, $f(R)$ modifications of gravity seem to be a possible candidate to be able to explain Dark Matter [60].

$f(R)$ theories have been applied to several studies: for example, studies about black holes in $f(R)$ modified gravity [90], yielded solutions on constant curvature solutions for black holes, as well as the black hole thermodynamics and perturbative analysis. In [91], the cosmological dynamics of viable $f(R)$ theories of gravity were analysed and emphasis on and important fact was made; in order to maintain consistency with nucleosynthesis from the Big Bang, the expansion history in the early Universe should not deviate from GR. The authors also explained that, without inserting a cosmological constant, $f(R)$ theories would show a late-time accelaration that would avoid hindrance with what has already been detected.

Now that we have motivated the importance of modified gravity as a viable theory in dealing with gravitational interaction, more especially $f(R)$ theories, and briefed about some existing studies on this, we will now discuss $f(R)$ gravity theories in more depth. Additionally to the viability conditions mentioned above, we will see at the level of our equations, after the derivation of our field equations, what further constraints should be considered.

2.3 $f(R)$ gravity

In this subsection, we will address the question of why $f(R)$ functions are chosen as only the Ricci Scalar instead of other functions of other higher-order invariants such as $R_{\mu\kappa}R^{\mu\kappa}$, $R^{\mu\kappa\delta\gamma}R_{\mu\kappa\delta\gamma}$ or the Riemann tensor itself.

The very simple answer to this question is that $f(R)$ theories appear to be one of the higher-order theories of gravity which can prevent what is called the Ostrogradsky instability. Another

such type of theory is $f(Gauss-Bonnet)$. This instability, which emerges from Classical Mechanics, has implications that a non-degenerate Lagrangian relying on time derivatives of higher-order, conforms to a Hamiltonian which is linearly unstable. This is precisely what was first proved by Ostrogradsky, then by Woodard in [100], where he shows that this instability is avoided due to the uniqueness of $f(R)$ theories. In other words, the Ostrogradsky instability can be barred within the class of $f(R)$ theories because, according to the Ostrogradsky theorem, any modified Lagrangian that relies on the traces of $R_{\mu\kappa}$ or $R_{\mu\kappa\delta\gamma}$ should be precluded. Furthermore, in [92], Motohashi *et al.* explained that the instability is able to justify why differential equations of second and higher-orders do not describe certain physical phenomena. Additional details about the Ostrogradsky instability can be found in [93].

From a realistic point of view, $f(R)$ theories, being functions of the curvature scalar, R, are not only easy and straightforward to manipulate, but they are sufficiently universal to enclose certain essential properties of higher-order gravity, as explained by Sotiriou *et al.* in [60]. For instance, if $f(R)$ is expanded as a series, i.e. [60]

$$f(R) = ... + \frac{\alpha_2}{R^2} + \frac{\alpha_1}{R} - 2\Lambda + R + \frac{R^2}{\beta_2} + \frac{R^3}{\beta_3} + ... \tag{2.3.1}$$

where the coefficients α_i and β_i are given the suitable dimensions, it can be observed that the action includes quite some stimulating terms. This makes $f(R)$ theories of gravity one which helps us gain insight on the principles, dynamics and limitations of the intended modifications to gravity in an easier way.

$f(R)$ theories of gravity also give us an opportunity to comprehend and reflect on the validity in certain theories of gravity concerning some results which are accepted as being valid in GR, for example Birkhoff's theorem. This theorem states that all spherically symmetric solutions arising from Einstein equations in vacuum must be static and asymptotically flat in the absence of the cosmological constant [87]. As a matter of fact, Birkhoff's theorem and asymptotic flatness in the vacuum solutions of generalised fourth-order theories of gravity are not guaranteed, as is the case for GR [61]. In some later section, we will see that Birkhoff's theorem does not hold for general $f(R)$ gravity theories.

However, this issue arising from the shortcomings of Birkhoff's theorem can be remedied by adding an Einstein-Hilbert term proportional to the Ricci Scalar to the Lagrangian. In the low curvature limit, the field equations are dominated by this term and at asymptotically large distances from source, this guarantees that the usual behaviour of solutions get even closer to Minkowski space [62]. The method also enables perturbative expansions about a Minkowski background [86]. This certifies both the investigation of the weak-field limit of fourth-order gravity in an easy way, and its comparison to experiments.

2.3.1 Shortcomings with $f(R)$ gravity

As with other theories, $f(R)$ theories of gravity also come with disadvantages, one of them being that the consequent theories are quite complicated, and thus make it difficult to analyse and understand. Functions which produce late-time acceleration of the scale factor can be found, but their hurdles come with adhering to local gravity tests, cosmological observations and being sufficiently different to ΛCDM. In order to identify the most favorable set of data for $f(R)$ models, one should resort to comparison with experimental data. As a general observation, the weak field limits of modified gravity theories can be retrieved from chameleon mechanisms. Another instance of such limitation arises with testing $f(R)$ the same way that GR can be tested using the solar system. It is hard to satisfy the same tests along with achieving the accelerated expansion.

A low mass scalar field, appearing as a long range gravity force, is brought in by $f(R)$ theories of gravity. This eventually ensues spacetime to be curved and the local energy density of spacetime to be decoupled, implying that high density is now dissociated from high curvature [64, 65]. The metrics which were well characterised in GR in the solar system now diverge from what is observed.

2.3.2 Derivation of field equations for $f(R)$

Gravitational interaction that is represented by field equations can actually be extracted from what is called the variational principle. Three such methods are known. The two main principles can be applied to the EH action in order to derive the Einstein Field Equations in GR, namely the standard metric formalism (metric variation) and the Palatini formalism (Palatini variation). In the former,

assuming that the independent variable is the metric, the action is varied with respect to the metric alone, whereas for the Palatini variation, both connection and metric are taken as the independent variables, and therefore variation of the action occurs with respect to both. Interestingly, we make a critical observation in the latter, which is that the matter Lagrangian does not depend on the connection.

The third kind of variational principle is the metric-affine formalism. It is simply a generalization of both Metric formalism and Palatini formalism. Variation of the action in this case occurs to both the metric and the connection, which are assumed to be the independent variables, but the assumption that the matter Lagrangian depends solely on the connection is made. Additional reading and details about these variational methods can be found in [60].

All three variational techniques lead to Einstein field equations, on the condition that the EH action has a Lagrangian which is linear in R. This is because in GR, equations for the connection $\Gamma^{\lambda}_{\mu\kappa}$ end at the Levi-Civita connection of the metric, $g_{\mu\kappa}$ [60]. However, although the techniques bring us to the same field equations for an action which is linear in R, there is no guarantee that the same will apply for a more general action. For this reason, depending on the type of formalism used, the slightest corrections made in any $f(R)$ gravity Lagrangian may induce distinct theories.

Depending on the variational techniques used, the $f(R)$ theories of gravity are named accordingly. Those emerging from the metric formalism are known as *metric $f(R)$ theories of gravity*. Similarly, those arising from the metric-affine principle are called *metric-affine $f(R)$ theories of gravity* and likewise, those appearing from the Palatini technique are referred to as *Palatini $f(R)$ theories of gravity* [60]. We stick to the first approach in this thesis.

2.3.3 Metric $f(R)$ gravity field equations

In this subsection, we present the detailed derivation of the field equations for the general $f(R)$ function, assuming the general definitions of the Riemann and Ricci tensors.

Before we do so, we recall some of the main results from Chapter 1.3.2, where we explained how the Einstein-Hilbert action, in the presence of matter, could be varied using variational principles,

to yield the Einstein Field Equations described by Eqs.(1.3.8 -1.3.9).

As mentioned earlier, field equations for $f(R)$ theories are obtained by substituting, in the Einstein-Hilbert action, the Ricci Scalar R by a certain $f(R)$ function, composed of the Ricci Scalar. This can be done either by adding any $F(R)$ function to the known GR part (which is described by R alone, in the action) or by simply replacing R by $f(R)$. Thereafter, the same variational procedures, as known in GR, apply to the new action.

For example, we consider an action of the form

$$S = \frac{1}{2k}\int \mathrm{d}^4x\sqrt{-g}\big[R + F(R)\big], \tag{2.3.2}$$

As said before, $f(R)$ is a generalization of the Ricci Scalar, therefore, if we let $f(R) = R+F(R)$, where $F(R)$ contains corrective terms, then as $F(R) \to 0$, we retrieve GR.

For our case of $f(R)$ gravity, we will generalise the Einstein-Hilbert action as follows

$$S_{f(R)} = \frac{1}{2k}\int \mathrm{d}^4x\sqrt{-g}\big[f(R) + 2k\mathcal{L}_M\big] \tag{2.3.3}$$

whose variation is given as

$$\frac{\delta S_{f(R)}}{\delta g^{\mu\kappa}} = \frac{1}{2k}\int \mathrm{d}^4x\sqrt{-g}\left[\frac{\delta f(R)}{\delta g^{\mu\kappa}} + \frac{f(R)}{\sqrt{-g}}\frac{\delta\sqrt{-g}}{\delta g^{\mu\kappa}} + \frac{2k}{\sqrt{-g}}\frac{\delta(\sqrt{-g}\mathcal{L}_M)}{\delta g^{\mu\kappa}}\right] \tag{2.3.4}$$

From $\delta S_{f(R)} = 0$, we have the following implication

$$\frac{\delta f(R)}{\delta g^{\mu\kappa}} + \frac{f(R)}{\sqrt{-g}}\frac{\delta\sqrt{-g}}{\delta g^{\mu\kappa}} + \frac{2k}{\sqrt{-g}}\frac{\delta(\sqrt{-g}\mathcal{L}_M)}{\delta g^{\mu\kappa}} = 0 \tag{2.3.5}$$

Which (using Eq.1.3.9) implies

$$\frac{\delta f(R)}{\delta g^{\mu\kappa}} + \frac{f(R)}{\sqrt{-g}}\frac{\delta\sqrt{-g}}{\delta g^{\mu\kappa}} = kT_{\mu\kappa} \tag{2.3.6}$$

We then apply the following definitions to Eq.(2.3.6)

$$\delta(f(R)) = f_R \delta R \tag{2.3.7}$$

where, $f_R = \frac{\mathrm{d}f(R)}{\mathrm{d}R}$ We also note, from (2.3.7), that

$$\delta R = \delta(g^{\mu\kappa} R_{\mu\kappa}) = (\delta g^{\mu\kappa}) R_{\mu\kappa} + g^{\mu\kappa}(\delta R_{\mu\kappa}) \tag{2.3.8}$$

The variation of the metric determinant is determined from the Jacobi's formula, which sets the rule for differentiating a determinant [18]. Therefore, we have

$$\delta(\sqrt{-g}) = -\frac{1}{2}\sqrt{-g} g_{\mu\kappa} \delta g^{\mu\kappa} \tag{2.3.9}$$

such that

$$\frac{f(R)}{\sqrt{-g}} \delta\sqrt{-g} = -\frac{1}{2} f(R) g_{\mu\kappa} \delta g^{\mu\kappa} \tag{2.3.10}$$

In order to simplify Eq.(2.3.8), the following definitions and respective variations are required. For the Riemann curvature tensor generally defined as

$$R^{\sigma}_{\mu\nu\kappa} = \partial_\nu \Gamma^{\sigma}_{\mu\kappa} - \partial_\kappa \Gamma^{\sigma}_{\mu\nu} + \Gamma^{\sigma}_{\nu\lambda}\Gamma^{\lambda}_{\mu\kappa} - \Gamma^{\sigma}_{\kappa\lambda}\Gamma^{\lambda}_{\mu\nu} \tag{2.3.11}$$

The variation of the Riemann tensor is now

$$\delta R^{\sigma}_{\mu\nu\kappa} = \partial_\nu \delta\Gamma^{\sigma}_{\mu\kappa} - \partial_\kappa \delta\Gamma^{\sigma}_{\mu\nu} + \delta\Gamma^{\sigma}_{\nu\lambda}\Gamma^{\lambda}_{\mu\kappa} + \Gamma^{\sigma}_{\nu\lambda}\delta\Gamma^{\lambda}_{\mu\kappa} - \delta\Gamma^{\sigma}_{\kappa\lambda}\Gamma^{\lambda}_{\mu\nu} - \Gamma^{\sigma}_{\kappa\lambda}\delta\Gamma^{\lambda}_{\mu\nu} \tag{2.3.12}$$

The connection given by $\Gamma^{\sigma}_{\mu\kappa}$ is not a tensor, but since $\delta\Gamma^{\sigma}_{\mu\kappa}$ is a tensor, we obtain its covariant derivative as

$$\nabla_\nu(\delta\Gamma^{\sigma}_{\mu\kappa}) = \partial_\nu(\delta\Gamma^{\sigma}_{\mu\kappa}) + \Gamma^{\sigma}_{\nu\lambda}\delta\Gamma^{\lambda}_{\mu\kappa} - \Gamma^{\lambda}_{\nu\mu}\delta\Gamma^{\sigma}_{\lambda\kappa} - \Gamma^{\lambda}_{\nu\kappa}\delta\Gamma^{\sigma}_{\mu\lambda} \tag{2.3.13}$$

By inspection, we find that Eq.(2.3.12) is actually given by the difference of two terms such that,

$$\delta R^{\sigma}_{\mu\nu\kappa} = \nabla_\nu(\delta\Gamma^{\sigma}_{\mu\kappa}) - \nabla_\kappa(\delta\Gamma^{\sigma}_{\mu\nu}) \tag{2.3.14}$$

We now deal with the variation of the Ricci tensor. Similar to contracting on the third index for the general Ricci curvature tensor, the same contraction can be applied on the third index of the variation result at (2.3.14), and we obtain as follows, what is known as the Palatini identity:

$$\delta R_{\mu\kappa} = \delta R^{\sigma}_{\mu\sigma\kappa} = \nabla_\sigma(\delta\Gamma^\sigma_{\mu\kappa}) - \nabla_\kappa(\delta\Gamma^\sigma_{\mu\sigma}) \tag{2.3.15}$$

Substituting this identity into (2.3.8), we arrive at

$$\delta R = (\delta g^{\mu\kappa})R_{\mu\kappa} + g^{\mu\kappa}\big[\nabla_\sigma(\delta\Gamma^\sigma_{\mu\kappa}) - \nabla_\kappa(\delta\Gamma^\sigma_{\mu\sigma})\big] \tag{2.3.16}$$

The last remaining variation is for the the connection. For our Christoffel symbol described as

$$\Gamma^\lambda_{\mu\kappa} = \frac{1}{2}g^{\lambda\sigma}(\partial_\mu g_{\sigma\kappa} + \partial_\kappa g_{\sigma\mu} - \partial_\sigma g_{\mu\kappa}), \tag{2.3.17}$$

the respective variation is

$$\delta\Gamma^\lambda_{\mu\kappa} = \frac{1}{2}g^{\lambda\sigma}(\partial_\mu \delta g_{\sigma\kappa} + \partial_\kappa \delta g_{\sigma\mu} - \partial_\sigma \delta g_{\mu\kappa}) \tag{2.3.18}$$

Since $\delta\Gamma^\lambda_{\mu\kappa}$ is a tensor, and transforms as tensors do, we can write the partial derivatives as covariant derivatives. It can be shown to be [18],

$$\delta\Gamma^\lambda_{\mu\kappa} = \frac{1}{2}g^{\lambda\sigma}(\nabla_\mu \delta g_{\sigma\kappa} + \nabla_\kappa \delta g_{\sigma\mu} - \nabla_\sigma \delta g_{\mu\kappa}) \tag{2.3.19}$$

Therefore Eq.(2.3.16) can be written as

$$\delta R = (\delta g^{\mu\kappa})R_{\mu\kappa} + g_{\mu\kappa}\Box\delta g^{\mu\kappa} - \nabla_\mu\nabla_\kappa\delta g^{\mu\kappa} \tag{2.3.20}$$

where $\Box = g^{\mu\kappa}\nabla_\mu\nabla_\kappa$ is the D'Alembertian operator.

Rewriting Eq.(2.3.7), we have that

$$\delta f(R) = f_R\big[(\delta g^{\mu\kappa})R_{\mu\kappa} + g_{\mu\kappa}\Box\delta g^{\mu\kappa} - \nabla_\mu\nabla_\kappa\delta g^{\mu\kappa}\big] \tag{2.3.21}$$

Now that we have all the missing pieces, we can assemble Eq.(2.3.6) using (2.3.10) and (2.3.21). We have the field equations for any $f(R)$ model given as

$$R_{\mu\kappa}f_R - \frac{1}{2}g_{\mu\kappa}f(R) + (g_{\mu\kappa}\Box - \nabla_\mu\nabla_\kappa)f_R = kT_{\mu\kappa} \tag{2.3.22}$$

In order to make the above correspond to Einstein Equations, in terms of the Einstein Tensor $G_{\mu\kappa}$, we rewrite it by adding and subtracting $\frac{1}{2}g_{\mu\kappa}Rf_R$ to the left hand side of Eq.(2.3.22). So, we obtain

$$R_{\mu\kappa}f_R - \frac{1}{2}g_{\mu\kappa}Rf_R + \frac{1}{2}g_{\mu\kappa}Rf_R - \frac{1}{2}g_{\mu\kappa}f(R) + (g_{\mu\kappa}\Box - \nabla_\mu\nabla_\kappa)f_R = kT_{\mu\kappa} \tag{2.3.23}$$

$$f_R(R_{\mu\kappa} - \frac{1}{2}g_{\mu\kappa}R) + \frac{1}{2}g_{\mu\kappa}(Rf_R - f(R)) + (g_{\mu\kappa}\Box - \nabla_\mu\nabla_\kappa)f_R = kT_{\mu\kappa} \tag{2.3.24}$$

It is now easy to see that

$$G_{\mu\kappa} = R_{\mu\kappa} - \frac{1}{2}g_{\mu\kappa}R = \frac{1}{f_R}\Big[kT_{\mu\kappa} + (\nabla_\mu\nabla_\kappa - g_{\mu\kappa}\Box)f_R + \frac{1}{2}g_{\mu\kappa}(f(R) - Rf_R)\Big] \tag{2.3.25}$$

The trace of equation (2.3.22) is given by

$$Rf_R + 3\Box f_R - 2f(R) = kT \tag{2.3.26}$$

where $T = g^{\mu\kappa}T_{\mu\kappa}$. With the presence of $\Box$, this relation is no longer algebraic, but dynamical.

Our interest lies in homogeneous and isotropic spacetimes, that is, spacetimes which conform with spatial sections which are maximally symmetric. We therefore consider the solutions of the $f(R)$ gravity field equations which are maximally symmetric, that is, considering solutions arising from surfaces with constant curvature (R = constant and $T_{\mu\kappa} = 0$). Therefore from equation (2.3.26) we have

$$Rf_R - 2f(R) = 0 \tag{2.3.27}$$

If $R = 0$ is a root of the above, what the field equations (2.3.22) imply is that $R_{\mu\kappa} = 0$ and this describes a flat and maximally symmetric Minkowski spacetime. On the other hand, if $R = C$, where C is a constant, we then have $R_{\mu\kappa} = g_{\mu\kappa}C/4$, which, depending on the sign of C, is known

to describe a de Sitter/anti de Sitter space time, which is comparable with a cosmological constant in GR, responsible for late-time speed ups [97, 10].

On an end note to this section, we write about the theoretical viability conditions and constraints on the choice of $f(R)$ functions. As it turns out, severe constraints are in place so as to provide a consistency in these theories of gravity, for instance, constraints have to be imposed on the form of $f(R)$ so that the model is linearly stable and passes local tests of gravity [99]. Following [98] we look at both gravitational and cosmological conditions therein. The four conditions for the $f(R)$ theory to be viable are summarised as:

For high curvatures, $f_{2R} \geq 0$

This requirement is essential for classically stable high-curvature and existence of a cosmological phase dominated by matter during the cosmological evolution. On the contrary, if this condition is not followed, what we come across is the "Dolgov Kawasaki" or "matter" or "Ricci scalar" instability. The Dolgov-Kawasaki instability happens whenever, in a very short time interval, higher-order derivative theories are brought down to a strong curvature regime. Thus the need to impose this constraint in on the form $f(R)$. As a matter of fact, if $f_{2R} < 0$, then the extra degree of freedom of the $f(R)$ theory behaves as a ghost.

For all curvature scalar values, $1 + f_R > 0$

This is a necessary condition for ensuring a positive value of the Newton's constant and graviton energy, at all times. It is an important condition, also because, it is required to recover standard thermodynamics of Schwarzschild anti de Sitter black holes in $f(R)$ theories [90].

For General Relativity behaviour, $f_R < 0$

This condition allows us to recover the basic General Relativity behaviour at early times. Alongside $f_{2R} > 0$, the implication of this is that f_R has to be negative, as well as a monotonically growing function of R in the range $-1 < f_R < 0$.

At recent epochs, $|f_R| \ll 1$

Local gravity tests impose this condition. Resulting implications are that the cosmological evo-

lution as predicted by $f(R)$ viable models, needs to be similar to that of ΛCDM at late-times. However, if there is no interest in constructing models with regards to cosmic acceleration, this constraint can be disregarded. As a matter of fact, this condition is simply sufficient, but not necessary since it does not take into account the chameleon mechanism.

As for the choices of the $f(R)$ function, we have to ensure that cosmological requirements are met. These conditions should impose on the function a behaviour similar to that of ΛCDM at high redshift regimes, where it is well-tested by the CMB. Furthermore, it should, without adding on an ad-hoc cosmological constant term, accelerate the cosmological expansion at low redshift [65]. Lastly, as an obvious requirement, the $f(R)$ function needs to have standard GR solutions in the low curvature limit. So if for example, our $f(R)$ function is chosen to be the usual Lagrangian linear in R plus a corrective term, which is also a function of R, as in the case of Eq.(2.3.2), where $f(R) = R + F(R)$, what this condition implies, is that the two limits below have to be true [65]

$$\begin{aligned} \lim_{R\to\infty} F(R) &= \text{constant} \\ \lim_{R\to 0} F(R) &= 0 \end{aligned} \tag{2.3.28}$$

Now that we have seen the nature of $f(R)$ theories, the kind of functions they encompass, their shortcomings and field equations derivations, and conditions for viable functions, we take a step into the next section, where we look at some known examples of $f(R)$ theories of gravity.

2.4 Some $f(R)$ models

Birkhoff's theorem is a statement that any spherically symmetric solution of the field equations in vacuum, must not only be asymptotically flat, but should also be static. This theorem and asymptotic flatness might be successful conditions fulfilled for the solutions in GR in vacuum, but the same cannot be said in principle for the generalised fourth-order theories of gravity [61]. By considering theories, in which the Lagrangian contains an EH term that, in the limit for low-curvature, has an upper hand on the field equations, is the standard approach in overcoming the problem related with this theorem. In this manner, from asymptotically large distances, it is possible to achieve before Minkowski, Schwarzschild spacetime, such that one can then perform perturbative analysis and expansions about a Minkowski background [86].

2.4.1 $f(R) \propto R^2$ Model

Over the past few years, the growing interest in higher-order theories of gravity (HOTG) came from the fact that these theories contained information that could impersonate cosmological evolution, associated with Dark Matter or Dark Energy. This is because such theories contain extra terms related to curvature in their equations of motions. An instance of this was the plausible explanation for a inflation, known as the R^2-inflation [48].

Studies on modifed $f(R)$ gravity were done by Buchdahl back in the 1970s [96]. This led to an active field of research arising from Starobinsky's explanation on cosmic inflation. His claim was that quantum corrections to the previously founded General Relativity would have important explanations for the early Universe, thus the reason for adopting a change to the Einstein-Hilbert action by adding curvature-squared corrections. From a Lagrangian of the form $\mathcal{L} = R + F(R)$, the quadratic $F(R)$ term he added was $R^2/6M^2$, where M has dimensions of mass [48].

The fact that the quadratic function, $f(R) \propto R^2$, when used with Einstein Field Equations, resulted in an effective cosmological constant when high curvatures are involved, such that the early Universe underwent an inflationary de Sitter epoch. This explanation solved some cosmological problems and allowed for some important predictive corrections to be made in the CMB. Thereon, several other modifications of this function were attempted, from which different results were obtained. The Starobinsky model, just as certain other $f(R)$ models, introduces no new type of matter.

One interesting aspect of this modified gravity model, in contrast to models involving the Ricci or Riemann tensor in the action, is that the Ostrogradski ghost is avoided, even though the equations of motion derived from the quadratic Lagrangian are of fourth order. Additionally, the $f(R) = R + \alpha R^2$ Starobinsky model, being the first internally consistent inflationary model, explains an accelerated epoch in the early Universe through the R^2 term [49]. Proofs are from results received from Planck data [20] , which astonishingly match with the Starobinsky model. The full exact solution for neutron stars, using this model, and with the spacetime of the star's exterior matched to Schwarzschild, can be found in [49], while numerical solutions, using the same model can be found in [85]. We will also investigate this model in the next chapter.

2.4.2 $f(R) = R + eR^q$ Models

$f(R)$ gravity theory functions can be of several types of forms, the majority of them being of the kind $R + eR^q$. Alternatives to sources of Dark Energy have been proposed throught theories with $q = -1$, which aided in explaning the cosmic acceleration observed [66, 67, 68, 69]. However, for any corrections higher than R^2, the theories are constrained by solar system experiments. [70, 71]. While in quadratic gravity theories, a new length scale is added to the characteristic length scale of GR by the constant e, there exists other forms of $f(R)$ which bring no such changes.

2.4.3 $f(R) = R^n$ Models

These forms are the functions described by $f(R) = R^n$, in which, in the limit

$$\lim_{n \to 1} = 1, \tag{2.4.1}$$

we recover GR. Such gravity theories have several attractive features, such as exact solutions which are simple to compare with observations [89]. Other approaches, such as solving with dynamical systems, were used in[88] in order to find out to which extent exact solutions could be considered as attractors of spatially flat Universes at late-times [66].

In [68], it is shown that, due to very small corrections in the R^n form of gravitational action from GR, there can be cosmic acceleration when $n < 0$. Although this case excludes the requirement of Dark Energy, it does not explain the situation with the cosmological constant. However, for $n > 0$, bringing a modification to the Einstein-Hilbert action with the same power series function can address inflation in the early times. The proposal from [68] gives a unified and purely gravitational origin and explanation of the acceleration in the early and late-times in our expanding Universe.

Additionally, the Minkowski background is very simple and useful in investigations of the weak-field, but it is unclear if a theory ought to be overlooked or not, by the mere fact that this limit does not exist. Several gravitational theories which do not take up the Minkowski space as solution exist. Some of these theories have been derived from Lagrangians of the form $R^{1+\epsilon}$ where $\epsilon \neq 0$ (as will be seen in the next chapter) [72, 73, 74, 75, 88], as well as others of the form $R + \alpha/R^n$, where $n > 0$ [44].

2.4.4 The Hu-Sawicki Model

As highlighted from the previous section, a few important constraints need to be applied to the choice of $f(R)$ function we make. While we need to ensure that these constraints are algebraically followed, we also need to make sure that these chosen models are also feasible cosmological models satisfying the aforementioned conditions. One such model, within the limits described at (2.3.28) is the Hu-Sawicki model, in which without the need for a cosmological constant, a class of metric-variation $f(R)$ models causing the accelerated expansion, and satisfying both solar-system and cosmological tests, is analysed. It is described by the following function [65]

$$f(R) = R - m^2 \frac{c_1 (R/m^2)^n}{c_2 (R/m^2)^n + 1} \tag{2.4.2}$$

with $n > 0$ and mass scale

$$m^2 \equiv \frac{\kappa^2 \bar{\rho}_0}{3} = (8315\mathrm{Mpc})^{-2} \Big(\frac{\Omega_\mathrm{m} \mathrm{h}^2}{0.13} \Big),$$

where c_1 and c_2 are dimensionless parameters, $\Omega_m h^2$ is the physical matter density inferred from the CMB and $\bar{\rho}_0 = \bar{\rho}(\ln a = 0)$ is the mean density of the present time.

Identifying Eq.(2.4.2) with the general form $f(R) = R + F(R)$ that we described previously, we can identify

$$F(R) = -m^2 \frac{c_1 (R/m^2)^n}{c_2 (R/m^2)^n + 1}, \tag{2.4.3}$$

the sign of which is chosen in a way so that the following condition is satisfied for $R \gg m^2$

$$f_{2R} \equiv \frac{\mathrm{d}^2 F(R)}{\mathrm{d}R^2} > 0 \tag{2.4.4}$$

This condition is also an implication that at high redshifts, cosmological tests are similar to those in GR.

The Hu-Sawicki model is one of the models which successfully implements the desired conditions and limits for a viable $f(R)$ theory, most interestingly with the fact that a true cosmological constant is not included (in this instance, the limiting case of $c_1/c_2^2 \to 0$ at a fixed ratio c_1/c_2 is a

cosmological constant in both local and cosmological test of gravity [65]). However, not all $f(R)$ functions successfully fulfill these conditions. For instance, in [44], the function advanced forward by Caroll *et al.*, described by $f(R) = R - \mu^{2(n+1)}/R^n$ does not fulfill these constraints, but eventually, models following these conditions were found [45].

2.5 Conclusion

In this chapter, we motivated the implementation of modified $f(R)$ gravity theories due to the limitations arising from the popular ΛCDM model. However, like many other gravitational theories available in literature, $f(R)$ theories cannot be randomly used; they need to be plausible. We described the criteria and constraints which need to be followed.

We have also seen the drawbacks arising from these theories and went into detail into deriving the field equations for the general $f(R)$ model, using the metric formalism approach, while giving a very brief description of other possible methods of deriving different field equations.

Last in this chapter, we looked at some of the most used $f(R)$ models that already exist, among which the famous Starobinsky model which was successful in explaining cosmic inflation in the early Universe. Other successful models include the Hu-Sawicki model, which without a cosmological constant, successfully satisfied all the conditions and constraints for a viable $f(R)$ model and provides late-time acceleration naturally. We also introduced $f(R) = R^n$ models, the analysis of which we do in the next chapter, along with the quadratic, $f(R) \propto R^2$ model.

Part II

Static and Spherically Symmetric Geometry

Chapter 3

3 Static and Spherically Symmetric solutions in $f(R)$ Models

3.1 On Neutron Stars First

The direct detection of gravitational-wave signals has been a phenomenal discovery, first by LIGO, followed by Virgo collaborations, in this 21st century. It was in 2015, in the case of a black hole merger, that these collaborating observatories opened a new window on the search and detection of gravitational waves (GW) in the Universe [76]. Later on, in 2017, with the discovery of GWs from a new kind of astrophysical object, the resulting signal (GW170817) was in fact emitted by a low-mass coalescing compact binary of neutron stars (NSs) [77, 78]. The nature of the kind of stars in question, was confirmed from the fact that their masses and other various electromagnetic observations, were consistent with stars.

Neutron stars (NSs) are known to be the kind of smallest and densest kind of stars. They are born from the collapsing of the cores of giant stars. NSs are characterised by radii of order of 10 km and masses lower than 2.16 $M_\odot$ (solar masses) [79], while the Chandrasekhar limit is about 1.4 $M_\odot$, which is the maximum mass of a stable white dwarf star. Once these stars are formed, there is no more heat generation and undergo cooling with time. Notwithstanding, they can still evolve by colliding and accretion. For this reason, neutron stars are great candidates for the studies of the behaviour of high-density cold nuclear matter [78].

Stars are "protected" against collapse by certain processes and principles such as "electron degeneracy pressure" and "neutron degeneracy pressure". While in the case of white dwarfs, the stars are saved from futher collapse by the "electron degeneracy pressure", in the case of neutron stars, "neutron degeneracy pressure" is what saves the stars from collapsing more. However, this mechanism cannot sufficiently support the star beyond 0.7 $M_\odot$ [80], and thus, more massive neutron stars are supported by nuclear forces of repulsive nature [81].

In the event that a remnant star is heavier than the limit imposed by the Tolman-Oppenheimer-Volkoff (TOV), the star collapses, which results in black hole formation. The TOV limit is an upper bound value for the mass of cold and static neutron stars. Recent studies on the observations of GW170817 and radius of the neutron star have imposed on this limit to be no more than 2.17 $M_\odot$ [82]. However, the idea of a neutron star being the source has been a debate, as that particular binary was thought to have collapsed into a black hole [83].

Several authors have addressed the topic of neutron star existence in the field of modified $f(R)$ gravity [51, 52, 53], although some do not stick to the constraints that need to be imposed onto these theories, one of them being that the interior must be carefully matched to the exterior spacetime of the star with utmost care. Conditions about the continuity of the curvature scalar and its first derivative need to be followed, as have been done in [49, 90]. Conclusions are that the neutron plasma equations of state being used in calculations play a huge part in determining the existence or non-existence of these stellar objects. We address this in the next section, as well as in the results from our analysis.

3.2 Neutron Plasma Equations of State

Equations for neutron stars, or for any stellar objects, are very important as they describe the relation of their radii to their respective masses, usually through a pressure-density related equation. However, for a neutron star, its EoS is still unknown. Several accurate values for neutron star masses have been obtained by observing radio pulsars in binary systems, but it could only be concluded that the radii of neutron stars should be of order 10 km [84]. However, current researches are being done in order to constrain the gravitational theories that can make predictions about neutron star matter, as in the research work performed in [103], from which we model our $f(R)$ functions. Methods and procedures for obtaining EoS as accurate as possible are discussed therein, as well as in [85].

As mentioned earlier, several works have been done with regards to neutron stars in $f(R)$ modified gravity, from which were concluded that results for the existence or non-existence of neutron stars, depended on the type of EoS used, as well as on the specific form of the $f(R)$ model and parameters. For instance, in the quadratic $f(R) = R + \alpha R^2$ model from [49], with careful matching

of the continuity conditions about the Ricci scalar and its prime derivative, allowing for the interior to be consistently matched to the Schwarzschild exterior solution, only a specific class of EoS is consistent with the quadratic model used therein. When a constant density and polytropic EoS is used along with high values of the coupling constant α, it was found that the exterior could not be matched to Schwarzschild, but as smaller values of this constant parameter were used, the system deviated more from Schwarzschild.

In [51] for example, the FPS, SLy, other EoS as well as one piecewise form were used for stars with quark cores. The different $f(R)$ models used evidently produced different results, of which stable stars were observed from the SLy EoS, with minimal radius ~ 9 km and mass ~ 1.9 $M_\odot$. In the same analysis, a similar case was also reported from the use of AP4 and BSK20 EoS, and it was concluded that more massive stars were formed, than in GR. If these phenomena are observed, this would be a groundbreaking feature for theories of modified gravity at astrophysical level. It was thus concluded that if upper bound of the mass of neutron star increased, the EoS used could describe realistic star configurations [51].

For the case of this thesis, we use the data from [103] to construct EoS, which also appear in [85, 102]. These are labelled as "soft" (or "min"), "intermediate" (or "mid") and "stiff" (or "max"). The "Max" EoS is defined for a pressure range of 0 to 4×10^{-4} km^{-2} and density range of 0 to 8×10^{-4} km^{-2}. The "Mid" EoS is defined for a pressure range of 0 to 8×10^{-4} km^{-2} and density range of 0 to 1.5×10^{-3} km^{-2}. The "Min" EoS is defined for a pressure range of 0 to 8.8×10^{-4} km^{-2} and density range of 0 to 1.8×10^{-3} km^{-3}. However, due to time restrictions, we perform our analysis with only the last two. Below we include a profile with all three EoS as also shown in [85], relating pressure p, to density ρ, both in units of km^{-2}

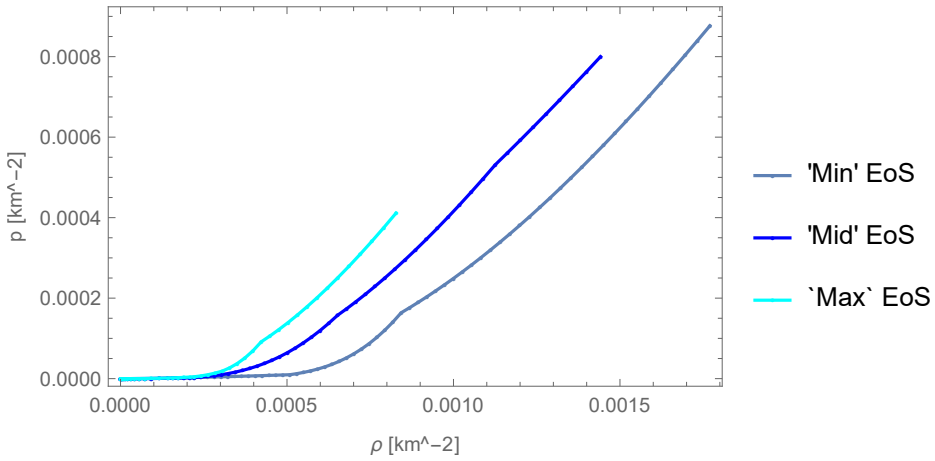

Figure 4: Pressure-density profiles

Having gone through all the technicalities regarding the derivation of our $f(R)$ field equations, as well as the different models in this kind of modified gravity theory and the equations of state for which we seek neutron star solutions, we are now ready to present our analysis and results in the next section.

3.3 Static Spherically symmetric solutions

For field equations defined as [101]

$$R_{\mu\kappa} - \frac{1}{2}Rg_{\mu\kappa} = \frac{1}{f_R}\Big[- kT_{\mu\kappa} - (\nabla_\mu\nabla_\kappa - g_{\mu\kappa}\Box)f_R + \frac{1}{2}g_{\mu\kappa}(f(R) - Rf_R)\Big] \tag{3.3.1}$$

with the energy-momentum tensor

$$T_{\mu\kappa} = \frac{2}{\sqrt{-g}}\frac{\delta(\mathcal{L}_M\sqrt{-g})}{\delta g^{\mu\kappa}} \tag{3.3.2}$$

and trace

$$R = \frac{-kT + 3\nabla^\alpha\nabla_\alpha f_R + 2f(R)}{f_R} \tag{3.3.3}$$

we are ready to solve our system of equations, bearing in mind that, our definition for the Riemann tensor as from this part of the thesis, is

$$R^\sigma_{\mu\nu\kappa} = \partial_\kappa\Gamma^\sigma_{\mu\nu} - \partial_\nu\Gamma^\sigma_{\mu\kappa} + \Gamma^\sigma_{\kappa\lambda}\Gamma^\lambda_{\mu\nu} - \Gamma^\sigma_{\nu\lambda}\Gamma^\lambda_{\mu\kappa} \tag{3.3.4}$$

For neutron stars, we assume the most general form of a static and spherically symmetric four dimensional metric tensor, described as

$$\mathrm{d}s^2 = B(r)\mathrm{d}t^2 - A(r)\mathrm{d}r^2 - r^2(\mathrm{d}\theta^2 + \sin^2\theta\mathrm{d}\phi^2) \tag{3.3.5}$$

The conservation of the energy-momentum $\nabla_\mu T^{\mu\kappa} = 0$ and substitution of Eq.(3.3.5) and (1.3.10) in the field equation (3.3.1) gives the set of independent equations below, the derivations of which, as well as their respective components can be found in Appendix B.2

$$A' = \frac{2rA}{3f_R}\left[kA(\rho+3p) + Af(R) - f_R\left(\frac{A}{2}R + \frac{3B'}{2rB}\right) - \left(\frac{3}{r} + \frac{3B'}{2B}\right)f_{2R}R'\right] \tag{3.3.6}$$

$$B'' = \frac{B'}{2}\left(\frac{A'}{A} + \frac{B'}{B}\right) + \frac{2A'B}{rA} + \frac{2B}{f_R}\left[-kAp + \left(\frac{B'}{2B} + \frac{2}{r}\right)f_{2R}R' - \frac{A}{2}f(R)\right] \tag{3.3.7}$$

$$R'' = R'\left(\frac{A'}{2A} - \frac{B'}{2B} - \frac{2}{r}\right) - \frac{A}{3f_{2R}}\left[k(\rho-3p) + f_R R - 2f(R)\right] - \frac{f_{3R}}{f_{2R}}R'^2 \tag{3.3.8}$$

$$p' = -\frac{\rho+p}{2}\frac{B'}{B} \tag{3.3.9}$$

where prime represents the derivative with respect to the radial coordinate r and, as before, $f_R \equiv \mathrm{d}f(R)/\mathrm{d}R$, $f_{2R} \equiv \mathrm{d}f_R/\mathrm{d}R$ and $f'_R = f_{2R}R'$ etc.

3.3.1 Numerical Procedure

For our numerical procedure, we make use of the *Mathematica* software, from which we have tested and concluded that the best method for solving our system of equations is the built-in "PDEDiscretization" solver. Using this method, we have adjusted our accuracy and precision for which the best results were obtained, in a fair amount of computation time.

Solving the above set of equations comes in two stages - one, where we solve for the interior solution, and second, where we solve for the exterior part. The solutions that we seek are for the unknown functions $R(r), A(r), B(r), \rho(r)$ and $p(r)$, where, as mentioned before, the pressure, $p(r)$ and density, $\rho(r)$, vanish on the outside space of our static neutron star.

To close the system, a fluid EoS which relates pressure and density is required, for example, $\rho = \rho(p)$ or alternatively, $p = p(\rho)$. To begin integrating outwards numerically from the star's centre, six initial conditions need to be provided for R, R', A, B, B' and p, all evaluated at $r = 0$. For the existence of the static star, the pressure which is a physical quantity, has to be finitely defined everywhere.

Therefore, as derived in [85], we have the initial conditions for our system of equation to be $A(0) = 1$, $B'(0) = 0$, $p(0) = p_0$ (central pressure) and $R'(0) = 0$. $B(0)$ and $R(0)$ (B_0 and R_0 respectively) remain two free initial conditions, which are usually determined by the shooting method, in order to fulfill the boundary condition requirements as $r \to \infty$. This step is necessary so that the exterior solution of the star can be matched to the one for Schwarzschild at infinity. Motivations for this condition can be found in [49], which are elaborated in later sections.

Once we obtain the interior solutions, with careful matching of the boundary conditions, we can solve for the exterior part. As we have imposed that the pressure and density have to be zero at the radius of the star, what this implies, is that in vacuum, we have one less equation for solving our system of equations. We reduce the number of differential equations, since the EoS at Eq.(3.3.9) is no longer needed.

However, before we attempt solving, we introduce another step which helps simplify our system of equations (3.3.6 - 3.3.9) as well as the initial conditions which are required. We introduce the function $\psi(r)$ such that

$$\psi(r) = \frac{B'(r)}{B(r)} \tag{3.3.10}$$

and,

$$\psi'(r) = \frac{B''(r)}{B(r)} - \frac{B'(r)}{B(r)^2} \tag{3.3.11}$$

From Eq.3.3.10, we can then recover $B(r)$ as

$$B(r) = D \exp^{\int \psi(r) \mathrm{d}r} \tag{3.3.12}$$

where D is the constant of integration, the value of which will depend on the conditions that we want to impose, and whether we are seeking the interior or exterior solution. This constant is important as it enables us to match the interior to the exterior solution, as well as the other way around. We will see this in the next sections.

From the introduction of this new function, we now have the following set of equations to solve, as have been found in [101] :

$$A' = \frac{2rA}{3f_R}\left[kA(\rho + 3p) + Af(R) - f_R\left(\frac{A}{2}R + \frac{3\psi}{2r}\right) - \left(\frac{3}{r} + \frac{3\psi}{2}\right)f_{2R}R'\right] \tag{3.3.13}$$

$$\psi' = \frac{\psi}{2}\left(\frac{A'}{A} - \psi\right) + \frac{2A'}{rA} + \frac{2}{f_R}\left[- kAp + \left(\frac{\psi}{2} + \frac{2}{r}\right)f_{2R}R' - \frac{A}{2}f(R)\right] \tag{3.3.14}$$

$$R'' = R'\left(\frac{A'}{2A} - \frac{\psi}{2} - \frac{2}{r}\right) - \frac{A}{3f_{2R}}\left[k(\rho - 3p) + f_R R - 2f(R)\right] - \frac{f_{3R}}{f_{2R}}R'^2 \tag{3.3.15}$$

$$p' = -\frac{\rho + p}{2}\psi \tag{3.3.16}$$

where as before, prime is the derivative with respect to the radial coordinate r and $f_R \equiv \mathrm{d}f(R)/\mathrm{d}R$, $f_{2R} \equiv \mathrm{d}f_R/\mathrm{d}R$ and $f'_R = f_{2R}R'$ etc.

The introduction of this function also relieves us from the shooting method which is required to

find the previous initial condition for B_0. Now, we simply have that $\psi(0) = 0$

In the next part, we will see how with particular choices of $f(R)$ functions, we can retrieve the Schwarzschild solution for GR (using the proper limits etc.). As a test, we will use results we know from GR already, to test whether or not, our code in *Mathematica* is giving us the results we want. As we should expect, both numerical and analytical well-known solutions should match for the interior part, while behaving as purely Schwarzschild-like on the exterior.

3.4 Test case: General Relativity

We have derived the field equations in Appendix A.1 and the interior solutions for GR in Appendix A.2 (for the non-realistic case of a constant density star), and as explained there, after careful matching with the definition of our metric in this thesis, we have [17]

$$A(r) = \left(1 - \frac{2GMr^2}{r_*^3}\right)^{-1} \tag{3.4.1}$$

$$B(r) = \frac{1}{4}\left[3\sqrt{\left(1 - \frac{2GM}{r_*}\right)} - \sqrt{\left(1 - \frac{2GMr^2}{r_*^3}\right)}\right]^2 \tag{3.4.2}$$

where M is the total mass energy of the system, and r_* is the radius of the star.

The above solutions were obtained after solving the famous Tolman-Oppenheimer-Volkoff (TOV) equations, for the case of a constant density star, and the latter definitions are what can be used as a check, versus the numerical solutions that we obtain, provided that in our case, we also set the density to a constant value. Alternatively, we can obtain solutions by solving the TOV Eq.(A.1.22), alongside Eq.(A.1.17), to obtain $A(r)$ and $B(r)$, and after careful matching with the definition of our metric, we can compare both solutions. This exercise is only to check the validity of our code.

3.4.1 Interior Solutions

The solutions displayed below, as highlighted before, are merely a check of the validity of our code. Instead of using a realistic EoS, we have simply used a constant value of $\rho = 7 \times 10^{-4}$ km^{-2}, and respective central pressure value of $p_0 = 1.9 \times 10^{-4}$ km^{-2} from the "Mid" EoS, from which the radius of the star was computed as $r_* = 9.28$ km. We have the following agreement between both analytical solutions from Eqs. (3.4.1-3.4.2) and numerical ones obtained after solving Eqs.(3.3.6-3.3.8). This can be shown by the fact that the two curves, both in analytical and numerical cases, lie exact on top of each other, with "pgr(r)", "Agr(r)" and "Bgr(r)" denoting the analytical solutions, and "pfinal(r)", ''Afinal(r)" and "Bfinal(r)" denoting the numerical solutions from our system of equations. We have performed checks on the relative differences of both solutions in each case, and conclude that both numerical and analytical cases perfectly agree with each other.

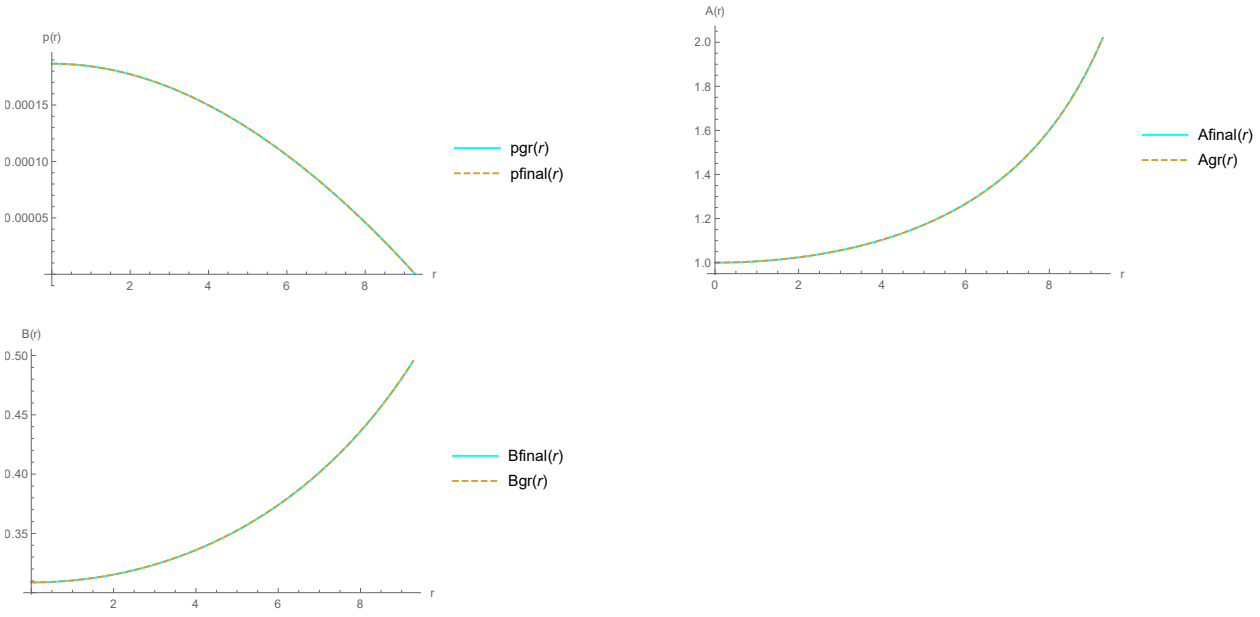

Figure 5: Checking GR with a constant density case ($f(R) = R$)

3.5 Test case: $f(R) = R + \alpha R^2$

In recent years, in the context of astrophysical applications, a lot of attention was drawn to this quadratic model in $f(R)$, with one of the leading researches in this area done by Strarobinsky with his model, as mentioned in the last section of the previous chapter. This model has been widely used in an attempt to geometrically describe Dark Matter abundances [85]. One will naively

assume that the nonlinearity arising from this kind of model will make it difficult to approximate solutions to those of GR, but if small enough deviations are considered, this can be made possible too.

In this part, we address a function of the Ricci scalar of the form $f(R) = R + \alpha R^2$, remembering that in the event that the quadratic term goes to zero, we retrieve GR solutions. A more intensive analysis is done in [85], which we follow very closely.

The important part of this function is the following definitions of the derivatives, which are then substituted in Eqs.(3.3.13 - 3.3.16). We recall that

$$\begin{aligned} f_R &= \frac{\mathrm{d}f(R)}{\mathrm{d}R} = 1 + 2\alpha R \\ f_{2R} &= 2\alpha \\ f_{3R} &= 0 \end{aligned} \tag{3.5.1}$$

where α is just a parameter fixed at a value $\alpha = -0.05$ km^2. The choice of the value of the parameter, is because we want to have only a slight deviation from GR, but the choice of the sign of it depends on the perturbative analysis, as performed in [85], in the curvature scalar around R_o (the GR solution) by R_p, such that $R = R_o + R_p$ with

$$R_p \ll R_o = kT \tag{3.5.2}$$

In order to ensure that the solution is stable, the perturbation must imperatively be bounded and rapid growth should be prevented. This perturbation is substituted in Eq.(3.3.15), where only first order terms in R_p are considered. On the right-hand side of Eq.(3.5.2), R_o is known, and we have the following dynamical equation for R_p as outcome

$$\begin{aligned} R_p'' = &- R_o'' + R_o'\left(\frac{A'}{2A} - \frac{\psi}{2} - \frac{2}{r}\right) - \frac{f_{3R}(R_o)}{f_{2R}(R_o)} {R_o'}^2 \\ &- \frac{A}{3f_{2R}(R_o)}(R_o f_R(R_o) - 2f(R_o)) + \gamma R_p' + \xi R_p \end{aligned} \tag{3.5.3}$$

where the coefficients γ and ξ adopt the following definitions [85]

$$\gamma = \frac{A'}{2A} - \frac{\psi}{2} - \frac{2}{r} - \frac{2R_o f_{3R}(R_o)}{f_{2R}(R_o)} \tag{3.5.4}$$

and

$$\begin{aligned}\xi =& \frac{A}{3f_{2R}(R_o)}\left[R_o f_{2R}(R_o) + f_R(R_o) - \frac{f_{3R}(R_o)}{f_{2R}(R_o)}(2f(R_o) + R_o f_R(R_o))\right] \\ &+ \frac{{R_o'}^2}{f_{2R}(R_o)}\left(f_{4R}(R_o) - \frac{f_{3R}^2(R_o)}{f_{2R}(R_o)}\right)\end{aligned} \tag{3.5.5}$$

Shifting our focus to the exterior solution, that is, when $R_o = R_o' = 0$, we have

$$\xi = \frac{A}{3f_{2R}(0)}\left(f_R(0) - \frac{2f_{3R}(0)f(0)}{f_{2R}(0)}\right) \tag{3.5.6}$$

As said earlier, it is imperative to prevent the exponential growth of the perturbation. Therefore, the condition $\xi < 0$ has to be fulfilled so that the tension term which is proportional to R_p in Eq.(3.5.3) makes the perturbation in R_p an oscillatory function of r [85].

The explanation for this restriction is because if we consider the homogeneous part of Eq.(3.5.3), $R_p'' = \xi R_p + ...$, then we would have a general solution comprising of both one exponentially increasing and one exponentially decreasing solution, the former imposing on R to be further away from 0 at the star's exterior. This disobeys any agreement with what is known from GR, and therefore we have to dismiss the case when $\xi > 0$.

Another interesting fact to notice is that, in the exterior of the star, γ is negative. Looking at Eq.(3.5.4), since in GR the exterior solution is Schwarzschild, the perturbation that arises is close to the famous solution [90]

$$B(r) = \frac{1}{A(r)} = 1 - \frac{2M}{r}$$

. As a consequence, all of A, B and B' are positive, while A' is negative and R_o no longer exists. Using all of these facts in Eq.(3.5.4), we have that $\gamma < 0$.

It can then be concluded that the term we previously identified as the tension term from Eq.(3.5.3) is as a matter of fact, a term which causes damping. Therefore, for $\xi < 0$, damped oscillations are born from a small perturbation of the Schwarzschild solution, and since $\xi < 0$, a direct implication of this is that, $\alpha < 0$ too.

From [90], since it was studied that $f(R)$ models with $f(0) \neq 0$ did not exhibit exterior solutions that could be matched to a Schwarzschild spacetime at very large distances [85], it is necessary to concentrate on cases where $f(0) = 0$. Consequently we arrive at the conclusion that Eq.(3.5.7) below becomes a crucial hypothetical stability condition

$$\xi = \frac{A}{3f_{2R}(0)}(f_R(0)) < 0 \tag{3.5.7}$$

In GR, the Jebsen-Birkhoff theorem is a statement that the unique spherically symmetric solution of the vacuum Einstein field equations is given by the Schwarzschild solution. Therefore, for a spherical star, the gravitational field around it in vacuum must be static, which can be described by the Schwarzschild metric (for $r > 2M$)

$$\mathrm{d}s^2 = -\Big(1 - \frac{2M}{r}\Big)\mathrm{d}t^2 + \Big(1 - \frac{2M}{r}\Big)^{-1}\mathrm{d}r^2 + r^2\mathrm{d}\Omega^2 \tag{3.5.8}$$

This metric, to a very good approximation, represents the spacetime of the Solar Sytem, and all other spherically symmetric stellar systems [49]. As mentioned before, for theories of gravity of higher-order, Birkhoff's theorem is violated. However, since our interest lies in generating models of realistic and compact astrophysical objects, it is imperative that the exterior spacetime of these static objects be at least asymptotically flat and approximately Schwarzschild, just as has been decreed by solar system tests.[49].

Interestingly, an extension to the exterior solution of a compact static star can be made to black holes, from the fact that these spatial phenomena are born from the gravitational collapse of these stars. Assuming the Schwarzschild spacetime implies two very important conditions which need to be satisfied: both the curvature scalar and its first derivative from the edge of the star should be

zero, that is, $R = 0$ and $R' = 0$. Once these conditions are satisfied, one can find suitable exterior solutions for the stars in two ways. The interior can be matched with an exact asymptotically flat static solution or the interior can be matched to an intermediate static vacuum solution that can be matched to Schwarzschild at larger distances. Futher details about these methods are found in [49].

Having explained the choice of our exterior spacetime, we now consider the physical boundary conditions (BCs). As mentioned before, the solution occurs in two stages. The matching of the interior to the exterior solution is done at the radius of the star, r_* which is found by solving the pressure equation, Eq.(3.3.9) as $p(r_*) = 0$. Thereafter, for the exterior solution, which exist as from the radius of the star until infinity, we integrate in vacuum, that is, $\rho = p = 0$. Minkowski spacetime is the asymptotic requirement, just like is the case for standard GR. We will therefore have [85]

$$\begin{aligned} \lim_{r\to\infty} B &= \lim_{r\to\infty} A = 1 \\ \lim_{r\to\infty} R &= \lim_{r\to\infty} R' = 0 \end{aligned} \tag{3.5.9}$$

Results from the perturbative analysis indicate that damped oscillations as from the star's exterior are expected from the scalar curvature R. On the condition that $\xi < 0$, very far away, both R and R' will approach zero. Thus,

$$\lim_{r\to\infty} B = \lim_{r\to\infty} A = 1$$

are the two BCs which remain to be satisfied, alongside two free ICs, B_0 and R_0 at the centre of the star (see Appendix B.2). We can say that the system of Eqs.(3.3.6-3.3.9) is a well-posed initial value problem, for all the times that the solutions for $A(r)$ and $B(r)$ asymptotically reach fixed values for large radii values.

3.5.1 Interior and Exterior solutions

We solve the system of equations described by Eqs.(3.3.13 - 3.3.16), for this case, with the ICs $A(0) = 1$, $\psi(0) = 0$, $p(0) = p_0 = 2.40 \times 10^{-4}$ km^{-2} (this is just one random value in the range

satisfied by our EoS), $R(0) = kT(0)$ and $R'(0) = 0$. For R_0, the density at the centre of the star, ρ_0, therein assumes a value of 7.80×10^{-4} km^{-2} (correct to two significant figures). We make use of the "intermediate" EoS from [103], which is also one of the EoS used in [85].

As said above, the algorithm is such that we solve for the interior part as described by Eqs. (3.3.13 - 3.3.16) with the aforementioned ICs and solve for r_*, which is the radius of the star, by letting $p(r_*) = 0$. Then at r_* we make the link to the exterior solution. If for instance, our interior solutions are denoted by $A_{\rm in}(r)$, $\psi_{\rm in}(r)$,$R_{\rm in}(r)$ and $\rho_{\rm in}(r)$, then the ICs for now solving the exterior part (described by the set of equations below) are given by $A_{\rm in}(r_*)$, $\psi_{\rm in}(r_*)$, $R_{\rm in}(r_*)$ and $R'_{\rm in}(r_*)$, bearing in mind that we no longer have any EoS nor pressure equation to solve in vacuum.

$$A' = \frac{2rA}{3f_R}\left[Af(R) - f_R\left(\frac{A}{2}R + \frac{3\psi}{2r}\right) - \left(\frac{3}{r} + \frac{3\psi}{2}\right)f_{2R}R'\right] \tag{3.5.10}$$

$$\psi' = \frac{\psi}{2}\left(\frac{A'}{A} - \psi\right) + \frac{2A'}{rA} + \frac{2}{f_R}\left[\left(\frac{\psi}{2} + \frac{2}{r}\right)f_{2R}R' - \frac{A}{2}f(R)\right] \tag{3.5.11}$$

$$R'' = R'\left(\frac{A'}{2A} - \frac{\psi}{2} - \frac{2}{r}\right) - \frac{A}{3f_{2R}}\left[f_R R - 2f(R)\right] - \frac{f_{3R}}{f_{2R}}R'^2 \tag{3.5.12}$$

Results from the "Intermediate" EoS:

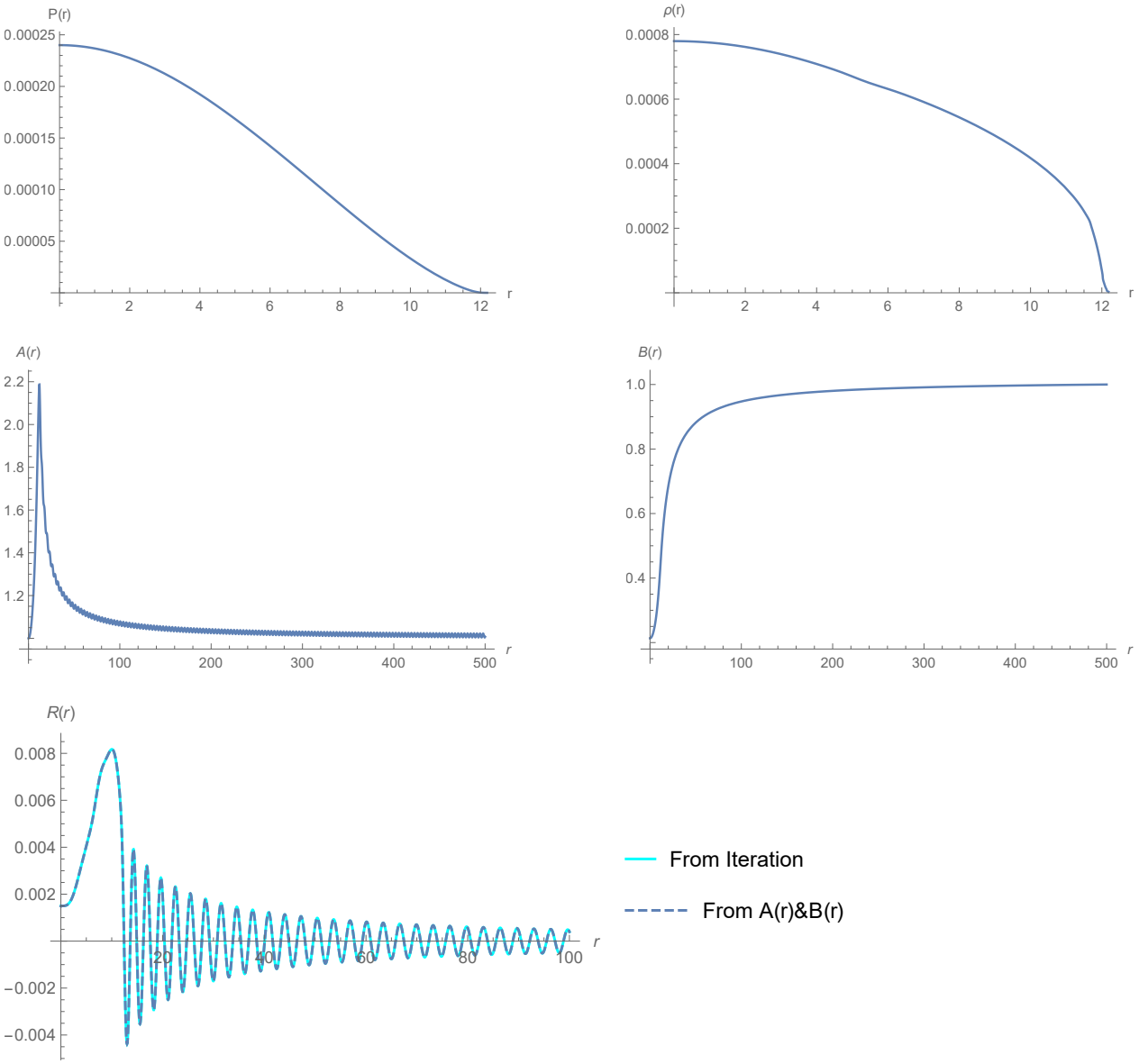

Figure 6: Solutions to $f(R) = R + \alpha R^2$, with $\alpha = -0.05$, $p_0 = 2.4 \times 10^{-4}$ km^{-2}, $r_* = 12.19$ km from "Mid" EoS

The solutions to the field equations above are obtained using the "Intermediate" or "Middle" EoS, after using the "Spline fit" in order to obtain our EoS from the sets of data. From top left, we show the graphs for $p(r)$, $\rho(r)$, $A(r)$, $B(r)$ and $R(r)$. The curvature scalar, $R(r)$ displays oscillations which are damped. The same can be seen in $A(r)$. The oscillations occurring in $B(r)$ are much smaller, thus negligibly seen in the diagrams above. The direct computation of the Ricci scalar

(from $A(r)$ and $B(r)$ as described by Eq.(B.1.12)), as well as the iterated one agree very well within our numerical precision. We can see outside the $f(R)$ star, the standing wave of the curvature scalar.

We can also see that the pressure and density profiles agreeing to the initial conditions. This is only for the interior, and thus, our integration for these two quantities stops at $r_* = 12.19$ km (correct to two decimal places), which is exactly what we want. We can check with Fig. 5 from [85], that we have the same solutions describing our quantities. For the case of the integration constant at Eq.(3.3.12), we choose it to be one, so it matches with Schwarzschild at infinity.

We have also checked the accuracy of our code by running the simulations in the forward direction, that is, from the centre of the star till the radius, then from the radius of the star until infinity, and also in the backward direction, that is, from infinity till the radius of the star (which we know from the forward integration), then from the radius till the centre of the star. We present the solutions in Appendix C, where we conclude that the integration techniques we use, agree very well within numerical precision in the code.

This check is important, as its accuracy constitutes a crucial part of the analysis that we perform in later sections of this thesis, where we will be integrating the exterior solutions that the author presents in [86], to check whether these solutions are solutions for stars, and whether they are realistic or not.

The plots presented below now show the exterior solutions from both forward and backward integration. We also plot the Schwarzschild solutions, as a reference, to show that our solutions behave Schwarzschild-like at infinity. Curve labeled "asolexf(r)" is the exterior solution of $A(r)$ from the forward integration, and "asolexoutf(r)" from the backward integration. "SchAsolex(r)" is the Schwarzschild solution that we plot as reference. The same reasoning applies for $B(r)$. The results from the forward and backward integration perfectly agree with each other, which is why the respective coloured curves lie on top of each other in both $A(r)$ and $B(r)$ in each case.

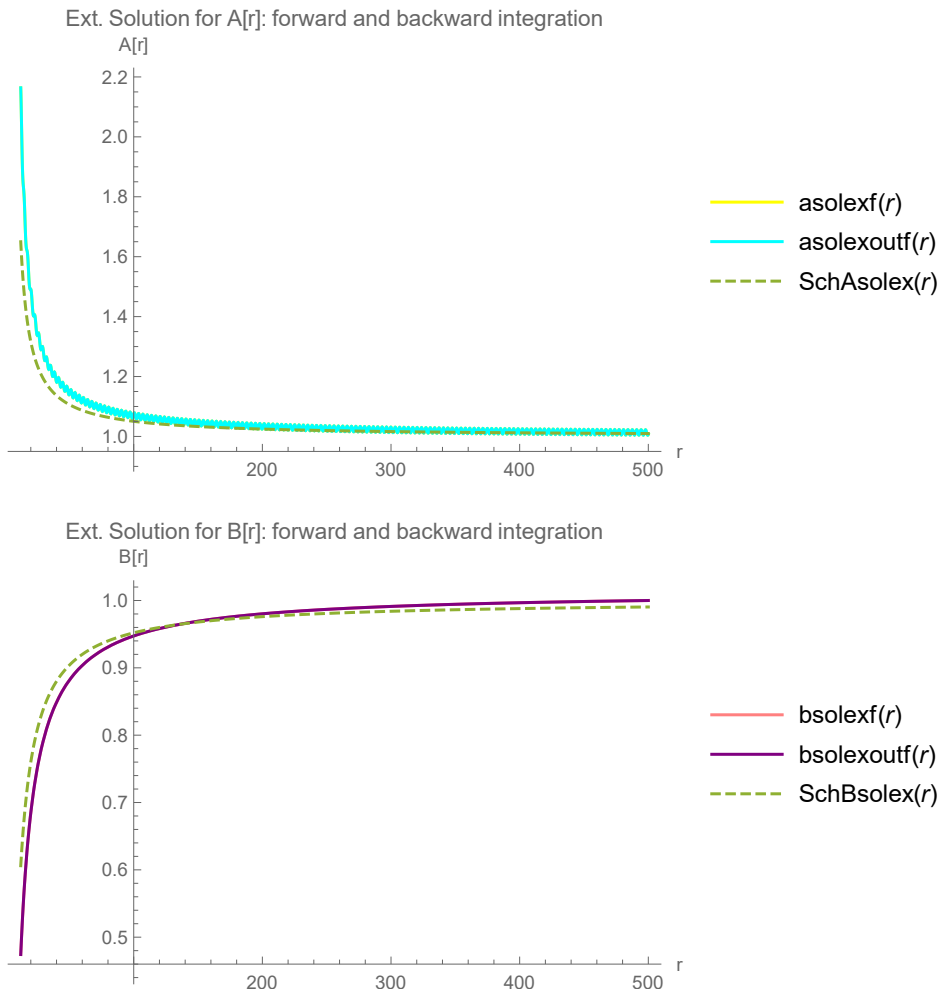

Figure 7: Comparison of exterior solution for $A(r)$ and $B(r)$ for both integration methods for $f(R) = R + \alpha R^2$, with $\alpha = -0.05$ from "Mid" EoS

From the upper panel of Figure 7 above, the yellow curve, representing the exterior solution for $A(r)$ from the forward integration technique, cannot be distinguished from the blue curve also in the upper panel, which is in turn the same exterior solution for $A(r)$, but obtained from the backward integration technique (refer to Section 3.3.1 for the description of our numerical procedure). The same reasoning applies for the lower panel of Figure 7, which displays the exterior solution of $B(r)$, where the pink curve representing solution from the forward integration technique, cannot be distinguished from the purple curve, which is the same exterior solution, but from the backward integration technique.

As can be seen from Figure 7 above, our solutions for $A(r)$ and $B(r)$ are asymptotically flat but do not coincide exactly with Schwarzschild solution. This is because our choice of coefficients and idea of "infinity" have a role to play in the results obtained, thus, we can conclude that our solutions for $A(r)$ and $B(r)$ tend to one at infinity but not at the same speed, which explains the "discrepancy" from the Schwarzschild solution.

Results from the "Stiff" EoS:

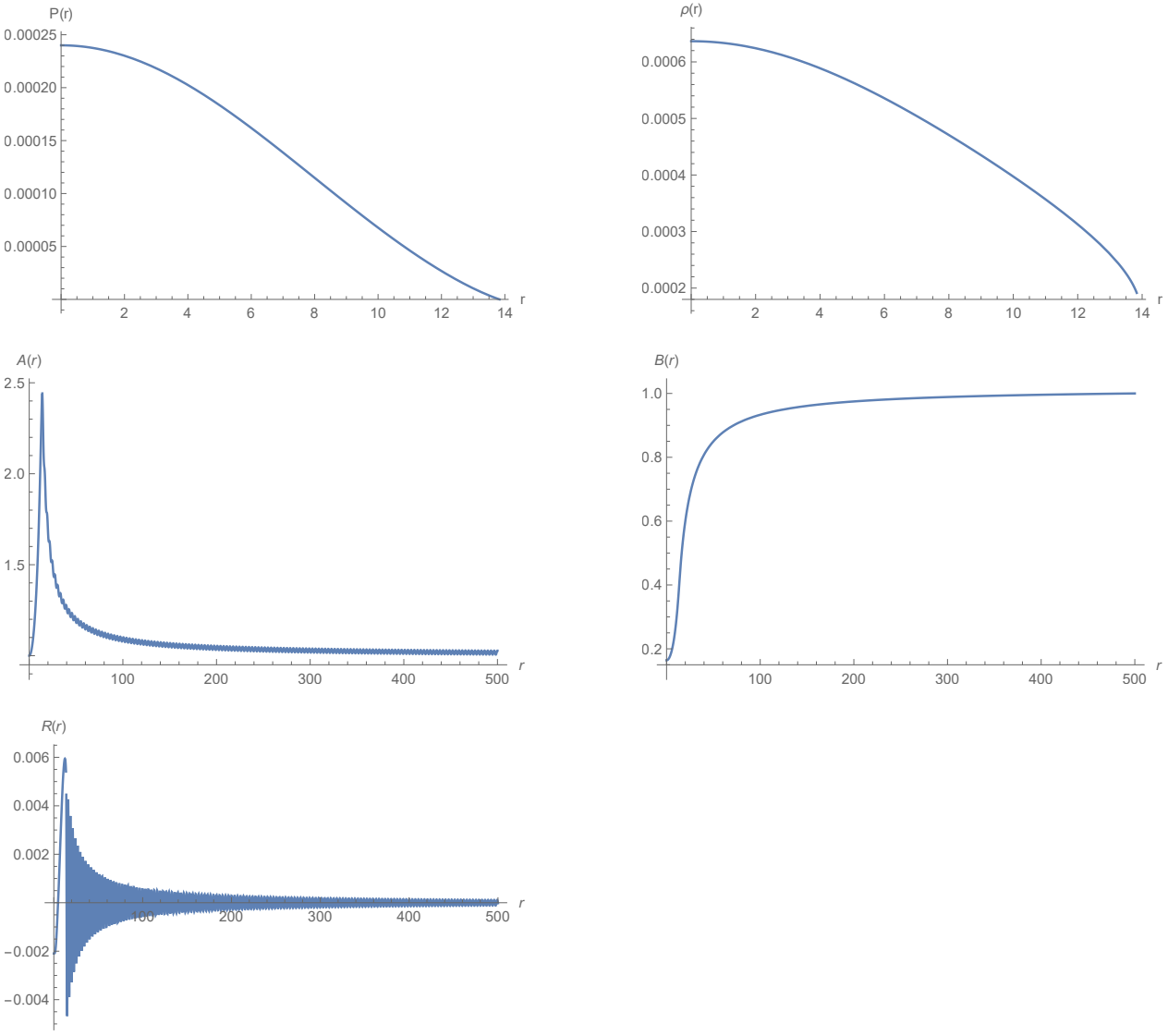

Figure 8: Solutions to $f(R) = R + \alpha R^2$, with $\alpha = -0.05$, $p_0 = 2.4 \times 10^{-4}$ km^{-2}, $r_* = 13.83$ km from "Max" EoS

The solutions to the field equations above are obtained using the "Stiff" or "Max" EoS, after using a polynomial fit in order to obtain our EoS from the sets of data. Once again, from top left, we show the graphs for $p(r)$, $\rho(r)$, $A(r)$, $B(r)$ and $R(r)$. The curvature scalar, $R(r)$ displays oscillations which are damped once again. A similar situation is seen in $A(r)$. The oscillations occurring in $B(r)$ are much smaller, thus negligibly seen in the diagrams above. Outside the $f(R)$ star, for this different EoS, we can see the standing wave of the curvature scalar.

3.5.2 Mass-Radius Diagrams

The mass definitions in $f(R)$ gravity adopts quite a different path as compared to what we know in GR. In GR, one can assume the mass to be defined as the volume integral of energy density of the body. As can be seen from Eq.(A.1.19) in Appendix A.1, the mass is what is contained within the radius of the star, In fact, the integral

$$M = m(r_*) = 4\pi \int_0^{r_*} \rho(r) r^2 \mathrm{d}r \tag{3.5.13}$$

acts as just a parameter which characterises a family of solutions in GR [85]. In the plots below, we show the results for the mass-radius diagrams, that we generated from our codes, for the neutron star, as defined by the volume integral, for the respective EoS, where "Mass($M_\odot$)" is defined by Eq.(3.5.13) and "Radius" is the radius of the star

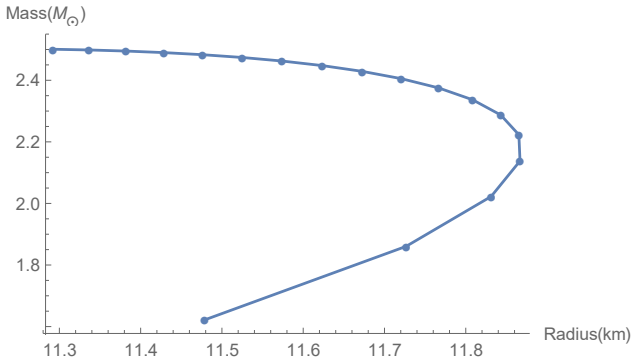

Figure 9: Mass-Radius Diagram for $f(R) = R + \alpha R^2$, with $\alpha = -0.05$ from "Mid" EoS

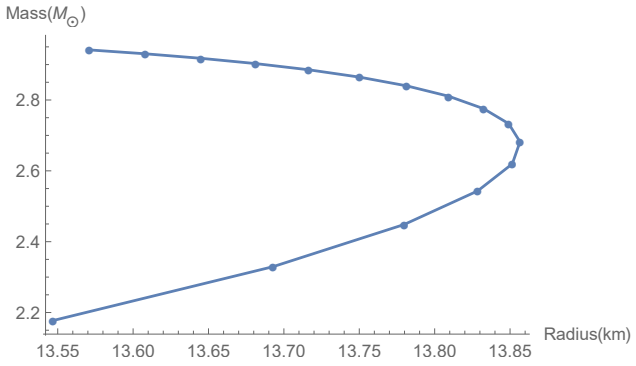

Figure 10: Mass-Radius Diagram for $f(R) = R + \alpha R^2$, with $\alpha = -0.05$ from "Max" EoS

In the case of $f(R)$ gravity, we parameterise the coefficients from our metric defined by Eq.(3.3.5) such that

$$\begin{aligned} B(r) &= A^{-1}(r) = 1 - \frac{2\tilde{M}(r)}{r} \\ A(r) &= \frac{1+\tilde{U}(r)}{B(r)} \end{aligned} \tag{3.5.14}$$

From the definitions above, we can rewrite, the same way as in [101]

$$\tilde{M}(r) = \frac{r}{2}\Big(1 - A^{-1}(r)\Big) \tag{3.5.15}$$

and

$$\tilde{U}(r) = A(r)B(r) - 1 \tag{3.5.16}$$

which allow us to define the gravitational mass function (or so-called $f(R)$ mass) as [85]

$$M_{f(R)}(r) = \frac{\tilde{M}(r)}{1+\tilde{U}(r)} \tag{3.5.17}$$

where, much further away from the star, the gravitational mass is given by

$$M^{\infty}_{f(R)} = \lim_{r\to\infty} M_{f(R)}(r) \tag{3.5.18}$$

In the scatter plots below, we show the results for the mass-radius diagrams, for the neutron star, as defined by gravitational mass, denoted as "f(R) Mass($M_\odot$)" defined at Eq.(3.5.17), for the respective EoS, for a value of r very close to the value of "infinity" that we use in the code. Thus we have here

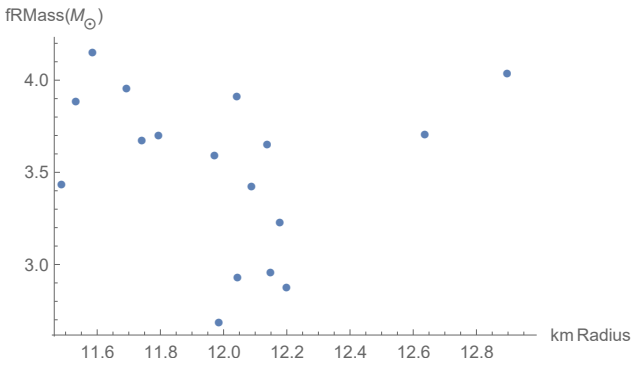

Figure 11: f(R) Mass-Radius Diagram for $f(R) = R + \alpha R^2$, with $\alpha = -0.05$ from "Mid" EoS

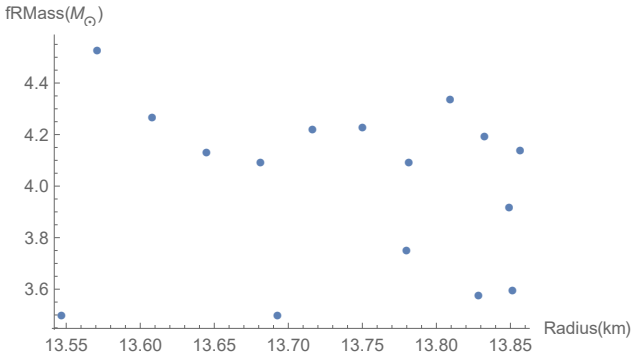

Figure 12: f(R) Mass-Radius Diagram for $f(R) = R + \alpha R^2$, with $\alpha = -0.05$ from "Max" EoS

Mass extraction for this $f(R)$ model is very tricky if enough attention is not given to the kind of matching approach being used. As the results show, these solutions, as have been concluded in several other researches, are quite sensitive to the kind of EoS that is being investigated. Further reading about retrieving the gravitational mass can be found in [49, 90, 101].

3.6 Test case: $f(R) = R^{1+\epsilon}$

In this type of $f(R)$ model, as mentioned from the previous chapter, there is one advantage over quadratic functions, and this is because these power series functions do not bring additive changes to the characteristic length scale of GR. Exact solutions from these theories are very simpler to compare with observations. We define the following trivial derivatives, keeping the value of ϵ constant to

± 0.05

$$\begin{aligned} f_R(R) &= (1+\epsilon)R^{\epsilon} \\ f_{2R}(R) &= \epsilon(1+\epsilon)R^{\epsilon-1} \\ f_{2R}(R) &= \epsilon(\epsilon-1)(1+\epsilon)R^{\epsilon-2} \end{aligned} \tag{3.6.1}$$

Motivation for the range of values for ϵ is given through the same perturbative analyses performed in Chapter 3.5. We recall the following results therein

$$\gamma = \frac{A'}{2A} - \frac{\psi}{2} - \frac{2}{r} - \frac{2R_o f_{3R}(R_o)}{f_{2R}(R_o)} \tag{3.6.2}$$

and

$$\begin{aligned} \xi =& \frac{A}{3f_{2R}(R_o)}\left[R_o f_{2R}(R_o) + f_R(R_o) - \frac{f_{3R}(R_o)}{f_{2R}(R_o)}(2f(R_o) + R_o f_R(R_o))\right] \\ &+ \frac{{R_o'}^2}{f_{2R}(R_o)}\left(f_{4R}(R_o) - \frac{f_{3R}^2(R_o)}{f_{2R}(R_o)}\right), \end{aligned} \tag{3.6.3}$$

from which we had the stability condition

$$\xi = \frac{A}{3f_{2R}(0)}\left(f_R(0) - \frac{2f_{3R}(0)f(0)}{f_{2R}(0)}\right) \tag{3.6.4}$$

Using the derivatives defined by Eqs.(3.6.1), we subsitute them into Eq.(3.6.4), (but not evaluating at $R = 0$ yet, we recall that our interest is in the exterior, where this condition applies) . After simplifying, we arrive at

$$\xi = \frac{AR}{3\epsilon} - \frac{2A(\epsilon-1)}{3\epsilon(1+\epsilon)}\left(R - R^{1-\epsilon}\right) \tag{3.6.5}$$

Since we are only considering solutions for which $f(0) = 0$, for the same reason that $f(0) \neq 0$ hosted no exterior solutions [85], we find that $f(0) = 0 \iff 1 + \epsilon \geq 0$, that is, $\epsilon \geq -1$. Similarly from Eq.(3.6.5), we see that, for the equation to be properly defined in the second denominator, $\epsilon \neq -1$ and in $(R - R^{1-\epsilon})$, we need to have that $1 - \epsilon \geq 0$ to prevent any "blow-ups" of the stability

condition. Putting all the pieces together, we have that ϵ needs to be in the range

$$-1 < \epsilon \leq 1$$

.

In the next part, we present the interior-exterior solutions that we have for the differet EoS that we use.

3.6.1 Interior and Exterior solutions

One interesting thing to observe in our analysis with this power series function, is that, for a positive ϵ value, we are faced with cosmological horizons at different radii for the different values of central pressure (p_0), chosen, which prevents us from reaching the limit $r \to \infty$. This can be seen with our solutions "blowing-up to infinity" at a certain point. The same phenomenon were found for the Hu-Sawicki model, in [85], with a value of $d = 10^{-3}$ km^{-2} and $b = 2.5$, when Eq.(2.4.2) was expanded from a reparameterised form, such that [85]

$$f(R) \sim -d + \frac{d^2}{bR} \tag{3.6.6}$$

where b is an adimensional parameter and d and R have dimensions $[L^{-2}]$. In the case $|R| > |d|$, the cosmological horizon was produced in a Schwarzschild-de Sitter spacetime, at $\mathcal{O}\,(10\,\mathrm{r}_\odot)$. From the fact that the cosmological constant does not agree with observations, the solutions in this spacetime cannot be considered for stellar applications is the field of Cosmology and Astrophysics, and thus, we ignore such values of these parameters.

In the Tables below, we summarise our findings, for the different EoS and central pressure values. Analysis were only performed for $\epsilon \pm 0.05$. In Tables 2 - 5, we show the results from both "Mid" and "Max" EoS, with one respective set of plots of the solutions, right below the table. We start with computing for $\epsilon = 0.05$ in Tables 2 and 3 below.

p_0 [km^{-2}]	Star Existence	Radius, r_* [km]	Horizon at [km]	Asymptotic Behaviour
1.10×10^{-9}	Yes	2.816	142.920	Non-Schwarzschild
2.02×10^{-9}	Yes	5.886	127.042	Non-Schwarzschild
4.59×10^{-7}	Yes	10.080	24.628	Non-Schwarzschild
4.94×10^{-7}	Yes	9.965	24.233	Non-Schwarzschild
5.87×10^{-6}	Yes	7.158	17.700	Non-Schwarzschild
1.29×10^{-5}	Yes	9.265	17.887	Non-Schwarzschild
7.85×10^{-5}	Yes	10.220	22.752	Non-Schwarzschild
1.00×10^{-4}	Yes	10.602	25.363	Non-Schwarzschild
1.50×10^{-4}	Yes	10.708	35.825	Non-Schwarzschild
2.00×10^{-4}	Yes	10.653	54.947	Non-Schwarzschild
2.27×10^{-4}	Yes	10.505	78.360	Non-Schwarzschild
2.40×10^{-4}	Yes	10.467	99.172	Non-Schwarzschild
2.76×10^{-4}	Yes	9.458	1040.687	Non-Schwarzschild
2.77×10^{-4}	No	-	-	-
5.72×10^{-4}	No	-	-	-

Table 2: Analysis of $f(R) = R^{1+\epsilon}$ for $\epsilon = 0.05$ from "Mid" EoS

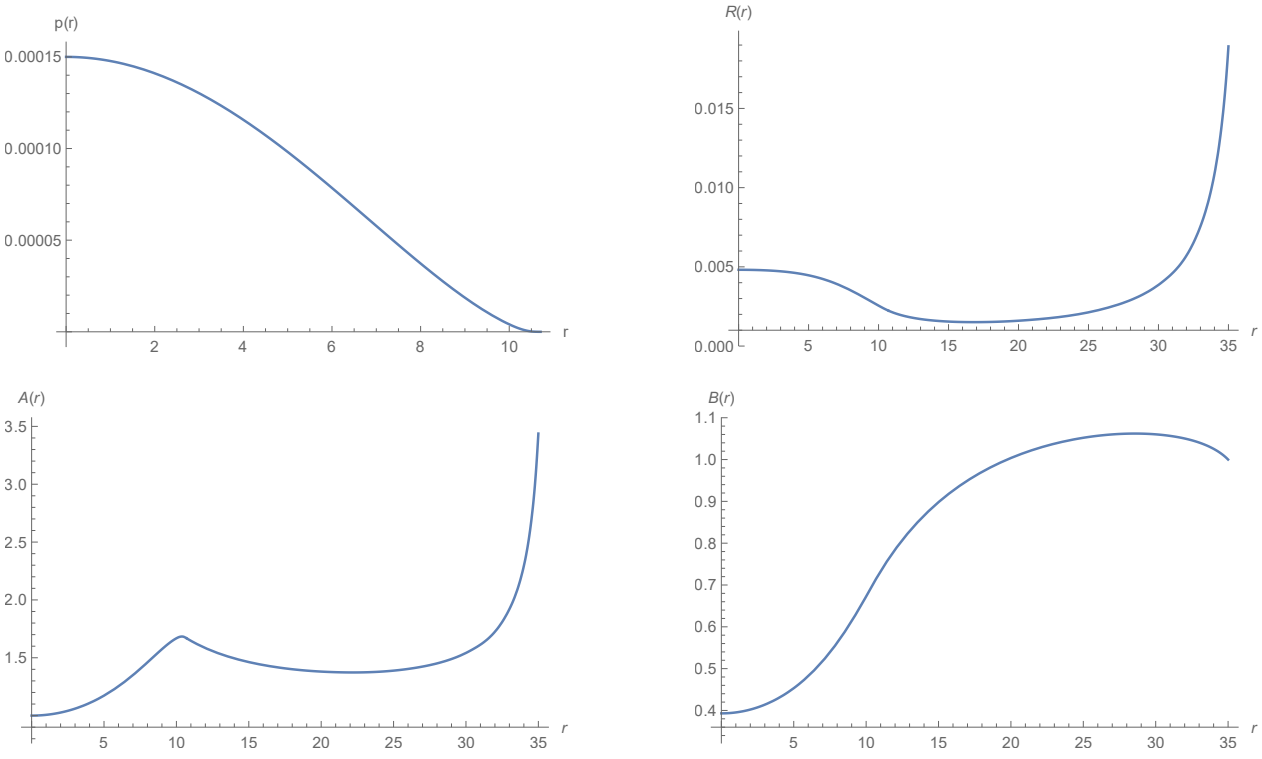

Figure 13: Solutions to $f(R) = R^{1+\epsilon}$, with $p_0 = 1.50 \times 10^{-4}$ km^{-2}, $\epsilon = 0.05$ from "Mid" EoS.

As can be seen from Table 2 and the respective graphical results with Figure 13, in the case of "Mid" EoS and for a central pressure value of $p_0 = 1.50 \times 10^{-4}$ km^{-2}, we have, from solving the

interior solution, a value of $r_* = 10.708$ km as the radius. Further to solving on the exterior part, we can only solve until $r = 35.825$ km, thereafter our solutions start to shoot up to infinity.

In Table 3 below, we perform the same kind of analysis and numerical procedure and we can see a similar situation that arises with the "Max" EoS. For the same value of central pressure that we use, that is $p_0 = 1.50 \times 10^{-4}$ km^{-2}, we have the radius of the star occurring at $r_* = 11.394$ km, which is further away than the radius found from the "Mid" EoS, and the cosmological horizon occurring at $r = 79.599$ km, which is over two times more than the value of the cosmological horizon for the "Mid" EoS.

p_0 [km^{-2}]	Star Existence	Radius, r_* [km]	Horizon at [km]	Asymptotic Behaviour
6.27×10^{-10}	Yes	0.079	16.479	Non-Schwarzschild
1.10×10^{-9}	Yes	0.105	16.479	Non-Schwarzschild
2.02×10^{-9}	Yes	0.142	16.480	Non-Schwarzschild
4.59×10^{-7}	Yes	2.090	16.841	Non-Schwarzschild
4.94×10^{-7}	Yes	2.164	16.864	Non-Schwarzschild
5.87×10^{-6}	Yes	6.327	18.913	Non-Schwarzschild
1.29×10^{-5}	Yes	8.214	20.470	Non-Schwarzschild
7.85×10^{-5}	Yes	12.761	36.588	Non-Schwarzschild
9.00×10^{-5}	Yes	12.912	41.462	Non-Schwarzschild
1.00×10^{-4}	Yes	11.868	39.280	Non-Schwarzschild
1.50×10^{-4}	Yes	11.394	79.599	Non-Schwarzschild
1.89×10^{-4}	Yes	11.145	506.767	Non-Schwarzschild
1.91×10^{-4}	Yes	10.712	1172.904	Non-Schwarzschild
1.92×10^{-4}	No	-	-	-
2.00×10^{-4}	No	-	-	-

Table 3: Analysis of $f(R) = R^{1+\epsilon}$ for $\epsilon = 0.05$ from "Max" EoS

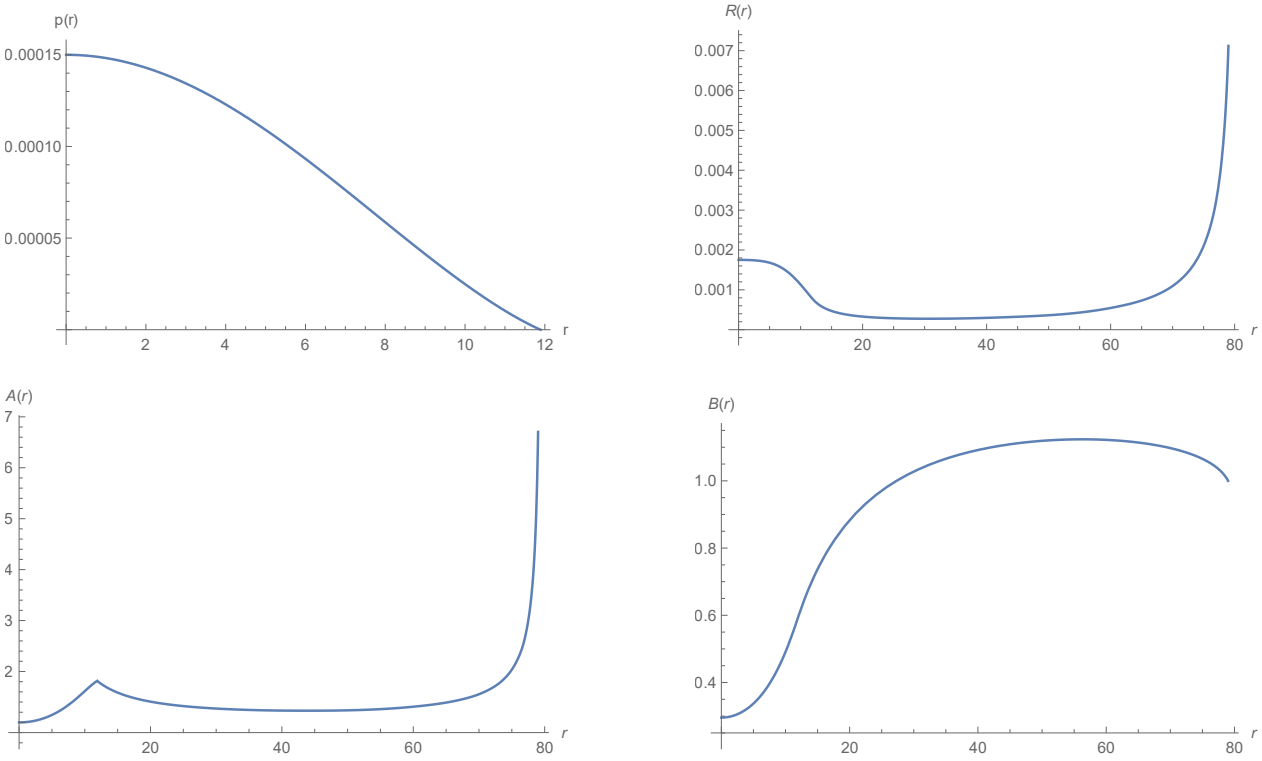

Figure 14: Solutions to $f(R) = R^{1+\epsilon}$, with $p_0 = 1.50 \times 10^{-4}\text{km}^{-2}$, $\epsilon = 0.05$ from "Max" EoS.

As we can see from Tables 2 and 3 and plots displayed in Figures 13 and 14 , for $\epsilon > 0$, we have the presence of cosmological horizons, due to which the limit $r \to \infty$ cannot be taken. For the different values of central pressure, we have a respective value for the occurrence of the horizon.

Below in Tables 4 and 5, we present the results for a case where $\epsilon < 0$. As can be concluded, there are no horizons and we can safely take the limit $r \to \infty$. However, although our solutions display an asymptotically flat behaviour, they cannot be matched to the Schwarzschild spacetime. Due to this, we cannot compute any value for the apparent (gravitational) mass (see section 3.5.2), and therefore we present our results for the convergence of the mass-to-radius ratio as

$$\lim_{r\to\infty} \frac{\tilde{M}(r)}{r}, \tag{3.6.7}$$

where $\tilde{M}$ assumes the same definition as at Eq.(3.5.15).

In Table 4 below, we display the results from our analysis, where, as before, p_0 is the central pressure value and in the second column, we conclude the existence or non-existence of stars.

p_0 [km^{-2}]	Star	Radius r_* [km]	Horizon	Convergence of $\frac{1}{A(r)}$ and $B(r)$ as $r \to \infty$	$\frac{\tilde{M}(r)}{r}$ limit	Asymptotic Behaviour
4.94×10^{-7}	Yes	32.195	None	0.909388660368, 0.909479599234	0.0452942348311	Flat, not Schwarzschild
5.87×10^{-6}	Yes	13.576	None	0.90707344716, 0.907164154512	0.04646327641611	Flat, not Schwarzschild
1.29×10^{-5}	Yes	11.672	None	0.907073465672, 0.907164173019	0.0464632671637	Flat, not Schwarzschild
7.85×10^{-5}	Yes	13.075	None	0.907078513825, 0.907169221677	0.04646074308717	Flat, not Schwarzschild
1.00×10^{-4}	Yes	13.240	None	0.907077286210, 0.907167993939	0.04646135689479	Flat, not Schwarzschild
1.50×10^{-4}	Yes	13.484	None	0.907079196618, 0.907169904537	0.04646040169099	Flat, not Schwarzschild
2.00×10^{-4}	Yes	13.650	None	0.907074173525, 0.907164880943	0.04646291323713	Flat, not Schwarzschild
2.27×10^{-4}	Yes	13.775	None	0.90707349717, 0.907164204525	0.046463251412309	Flat, not Schwarzschild
2.40×10^{-4}	Yes	13.839	None	0.907079648842, 0.907170356807	0.04646017557874	Flat, not Schwarzschild
2.60×10^{-4}	Yes	14.082	None	0.907051621834, 0.90714232699	0.04647418908258	Flat, not Schwarzschild
2.75×10^{-4}	Yes	14.862	None	0.907043111928, 0.907133816244	0.0464784440355514	Flat, not Schwarzschild
2.76×10^{-4}	Yes	15.389	None	0.9070273731, 0.9071180758	0.04648631343762	Flat, not Schwarzschild
2.77×10^{-4}	No	-	-	-	-	-
3.09×10^{-4}	No	-	-	-	-	-
5.72×10^{-4}	No	-	-	-	-	-

Table 4: Analysis of $f(R) = R^{1+\epsilon}$ for $\epsilon = -0.05$ from "Mid" EoS

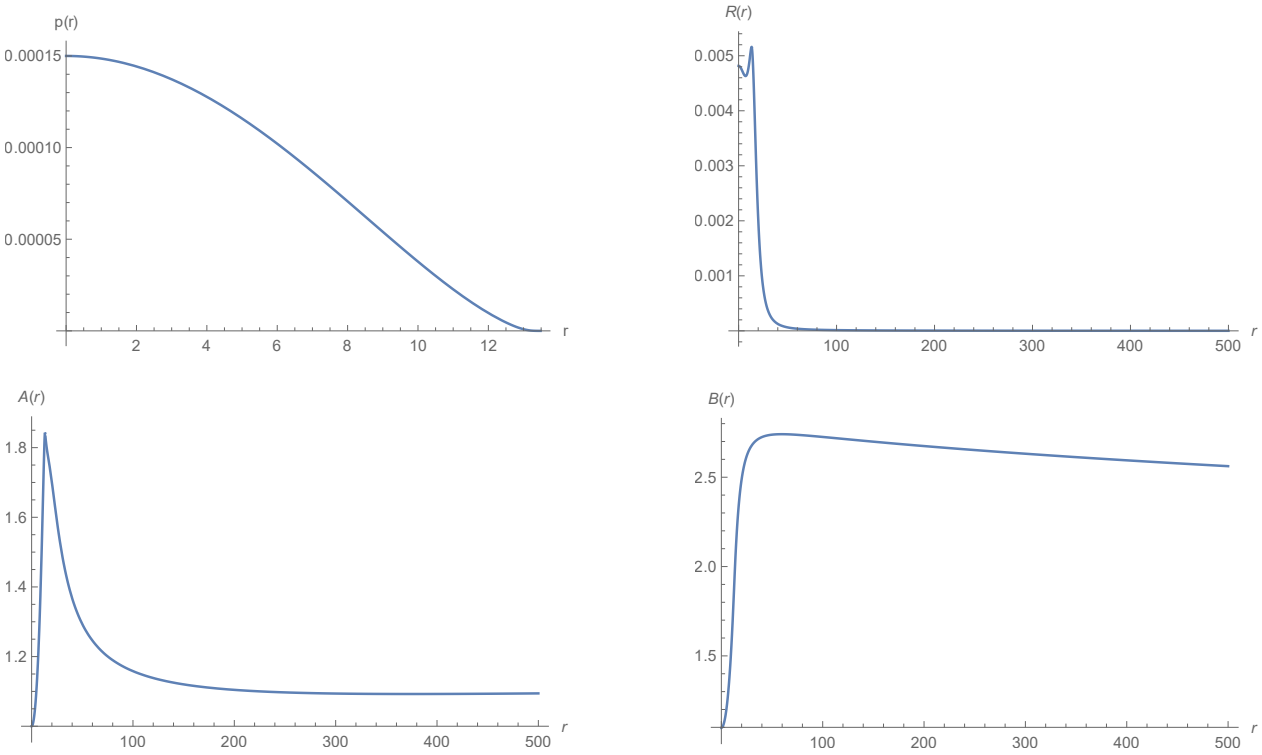

Figure 15: Solutions to $f(R) = R^{1+\epsilon}$, with $p_0 = 1.50 \times 10^{-4}\text{km}^{-2}$, $\epsilon = -0.05$ from "Mid" EoS.

As can be seen from Table 4 and the respective graphical results with Figure 15, in the case of "Mid" EoS, $\epsilon = -0.05$ and for a central pressure value of $p_0 = 1.50 \times 10^{-4}$ km^{-2}, we have, from solving the interior solution, a value of $r_* = 13.484$ km as the radius. Further to solving on the exterior part, we can very safely reach $r \to \infty$.

A similar observation is made in Table 5: as we take $r \to \infty$, we can conclude that with the relation $M(r) \propto r$, there exists no realistic stars. As can be seen, we do not recover the Schwarzschild spacetime and therefore, we cannot compute the $f(R)$ gravitational mass as described at Eq.(3.5.17).

p_0 [km^{-2}]	Star	Radius r_* [km]	Horizon	Convergence of $\frac{1}{A(r)}$ and $B(r)$ as $r \to \infty$	$\frac{\tilde{M}(r)}{r}$ limit	Asymptotic Behaviour
6.27×10^{-10}	Yes	0.104	None	0.9070654394941, 0.907156146038	0.04646728025291	Flat, not Schwarzschild
1.10×10^{-9}	Yes	0.137	None	0.907068105861, 0.9071588126723	0.04646594706910	Flat, not Schwarzschild
2.02×10^{-9}	Yes	0.186	None	0.9070667365996, 0.9071574432732	0.046466631700186	Flat, not Schwarzschild
4.59×10^{-7}	Yes	2.738	None	0.9070652908305, 0.9071559973596	0.046467354584728	Flat, not Schwarzschild
4.94×10^{-7}	Yes	2.835	None	0.9070680887988, 0.907158795607	0.046465955600593	Flat, not Schwarzschild
5.87×10^{-6}	Yes	8.156	None	0.9070718383614, 0.9071625455452	0.046464080819296	Flat, not Schwarzschild
1.29×10^{-5}	Yes	10.484	None	0.9070734405240, 0.907164147868	0.04646327973795	Flat, not Schwarzschild
7.85×10^{-5}	Yes	14.783	None	0.9070749376207, 0.9070749376207	0.04646253118961	Flat, not Schwarzschild
9.00×10^{-5}	Yes	14.978	None	0.9070743225717, 0.907165030003	0.046462838714138	Flat, not Schwarzschild
1.00×10^{-4}	Yes	15.117	None	0.9070756753979, 0.9071663829654	0.04646216230103	Flat, not Schwarzschild
1.50×10^{-4}	Yes	15.633	None	0.907070456399, 0.9071611634450	0.04646477180030	Flat, not Schwarzschild
1.89×10^{-4}	Yes	16.755	None	0.9070433528897, 0.9071340572250	0.046478323555110	Flat, not Schwarzschild
1.91×10^{-4}	Yes	17.425	None	0.9070480595662, 0.9071387643722	0.04647597021685	Flat, not Schwarzschild
1.92×10^{-4}	No	-	-	-	-	-
2.00×10^{-4}	No	-	-	-	-	-

Table 5: Analysis of $f(R) = R^{1+\epsilon}$ for $\epsilon = -0.05$ from "Max" EoS

The graphical results below in Figure 16 are computed for a same central pressure value, in a way as to compare both solutions, using the same central pressure value but different EoS. We find that for $p_0 = 1.50 \times 10^{-4}$ km^{-2}, we have the radius of the star at $r_* = 15.633$ km, which, as expected from previous observations, is further away than the one calculated with the "Mid" EoS.

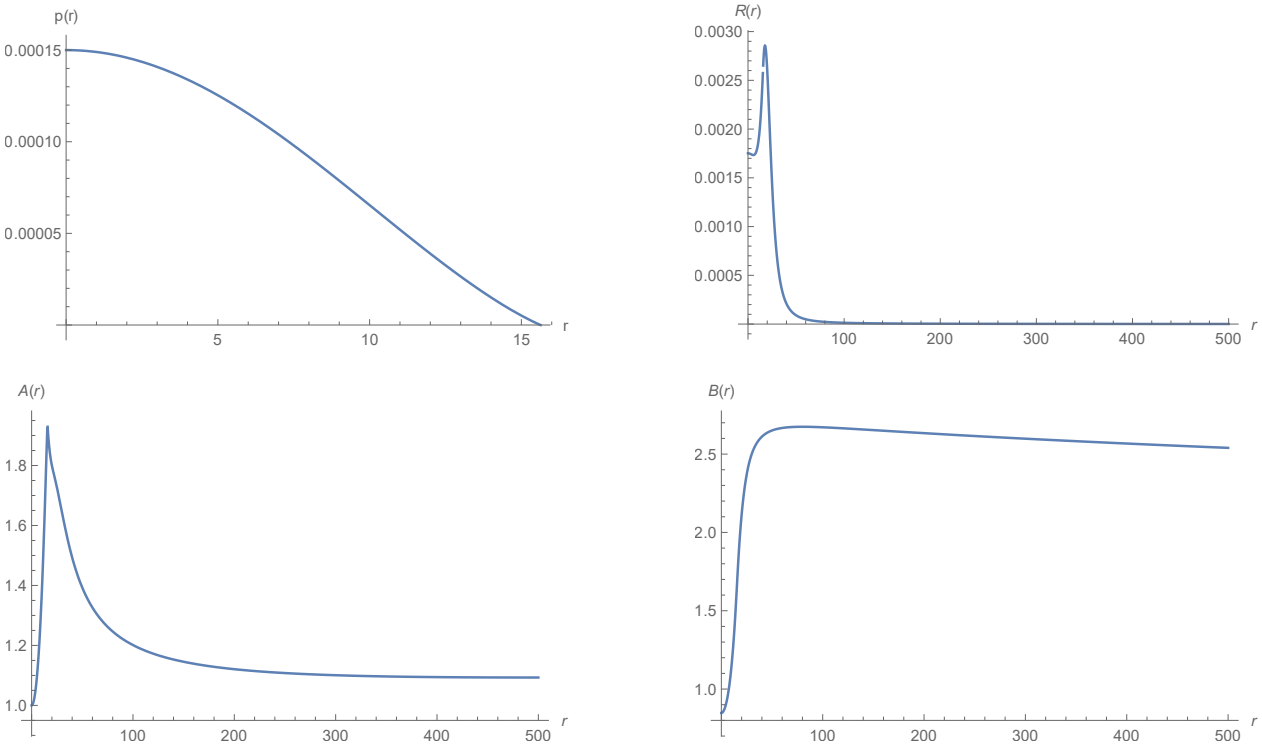

Figure 16: Solutions to $f(R) = R^{1+\epsilon}$, with $p_0 = 1.50 \times 10^{-4}$ km^{-2}, $\epsilon = -0.05$ from "Max" EoS.

3.7 Exact Spherically Symmetric Vacuum Solutions

In this section, we analyse the exact solutions provided by Clifton in [86] for $f(R) = R^{1+\epsilon}$ models. The exact spherical and symmetric solutions in vacuum for the line element

$$\mathrm{d}s^2 = -\tilde{A}(r)\mathrm{d}t^2 + \frac{1}{\tilde{B}(r)}\mathrm{d}r^2 + r^2\mathrm{d}\Omega^2 \,. \tag{3.7.1}$$

are given by [86]

$$\begin{aligned} \tilde{A}(r) &= r^{2\epsilon\frac{(1+2\epsilon)}{(1-\epsilon)}} + \frac{C_1}{r^{\frac{(1-4\epsilon)}{(1-\epsilon)}}} \\ \tilde{B}(r) &= \frac{(1-\epsilon)^2}{(1-2\epsilon+4\epsilon^2)(1-2\epsilon(1+\epsilon))}\left(1 + \frac{C_1}{r^{\frac{(1-2\epsilon+4\epsilon^2)}{(1-\epsilon)}}}\right) \end{aligned} \tag{3.7.2}$$

where C_1 is an arbitrary constant.

In order for these solutions to match with ours (obtained using the line element defined at

Eq.(3.3.5)), we have to adhere to the following mapping

$$A \to \frac{1}{\tilde{B}} \quad \text{and} \quad B \to \tilde{A}\,. \tag{3.7.3}$$

Full derivations of these results and mapping conditions can be found in Appendix D. Once we have made the appropriate mapping, we can now compare the numerical and the analytical exterior solutions for $f(R) = R^{1+\epsilon}$, which we present in the next section.

3.8 Comparison of results

In this part of the thesis, we compare the exterior solutions for a value of the central pressure value from the numerical code we have implemented, against the analytical solution proposed in [86], and we show both results in the following plots, in Figures 17 and 18, where "asolexf(r)", "bsolexf(r)" and "Rsolexf(r)" are the numerical exterior solutions and "Aex(r)", "Bex(r)" and "Rex(r)" are the analytical solutions obtained from Eqs.(3.7.2). For this comparison, we safely choose $\epsilon < 0$, as we had seen from our analysis in section 3.6.1 that for $\epsilon > 0$, the presence of horizons did not allow us to take the limit $r \to \infty$.

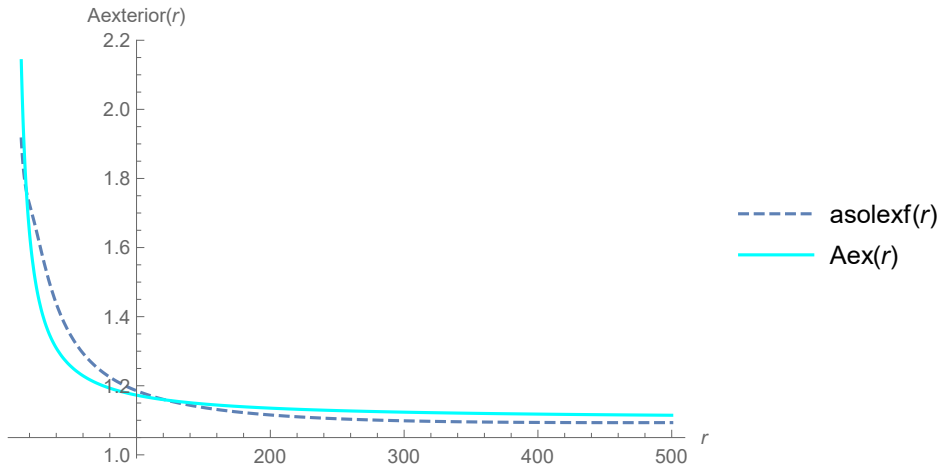

Figure 17: Numerical vs. Analytical Exterior Solutions for $A(r)$, with $p_0 = 2.4 \times 10^{-4}$ km$^{-2}, \epsilon = -0.05$ from "Mid" EoS.

It can be seen from Figures 17 and 18, that the numerical and analytical exterior results display a similar behaviour. The reason for which the numerical and analytical results are not precisely the same, is because of the choices of certain coefficients, for example, the integration constant in

Eq. (3.3.12) as well as the one in Eq.(3.7.2). This implies that with some fine tuning, it is possible to bring both numerical and analytical solutions as close as possible since we have also rigorously checked that the analytical solutions indeed satisfy our system of equations (3.5.10 - 3.5.12).

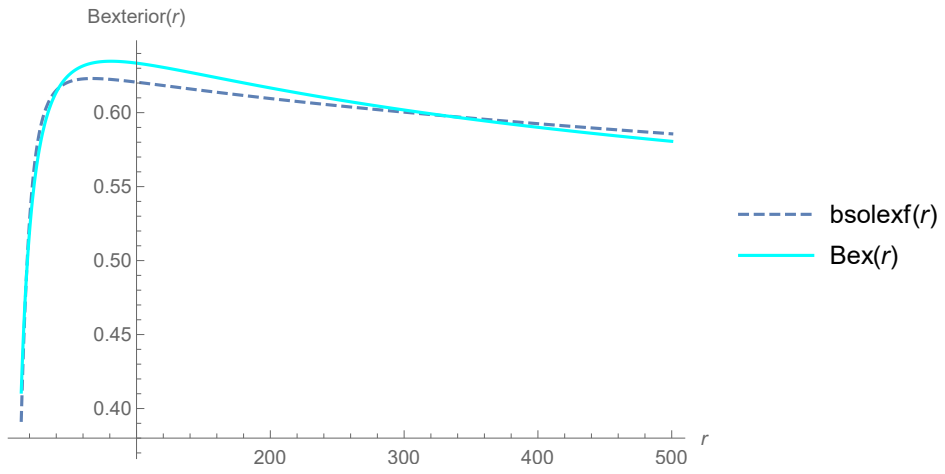

Figure 18: Numerical vs. Analytical Exterior Solutions for $B(r)$, with $p_0 = 2.4 \times 10^{-4}$ km$^{-2}, \epsilon = -0.05$ from "Mid" EoS.

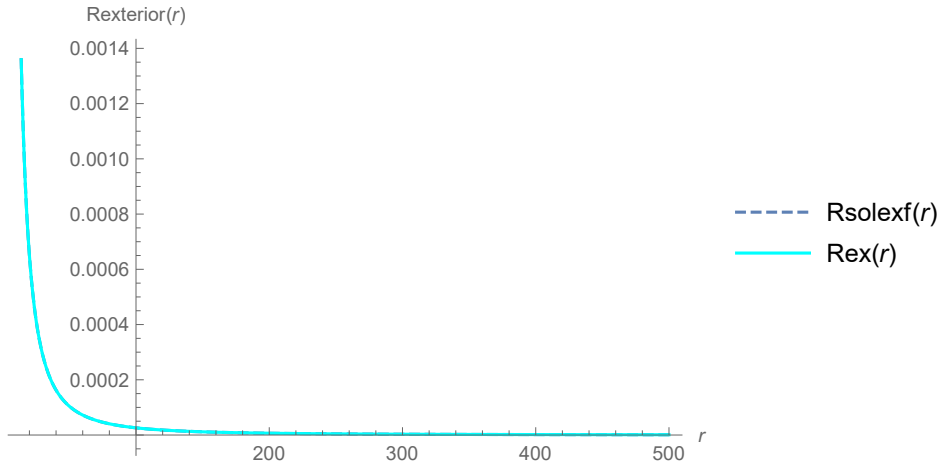

Figure 19: Numerical vs. Analytical Exterior Solutions for $R(r)$, with $p_0 = 2.4 \times 10^{-4}$ km$^{-2}, \epsilon = -0.05$ from "Mid" EoS.

In what follows, we want to prove whether or not, from the exact spherically symmetric vacuum solutions given by Eqs.(3.7.2), we can obtain realistic star solutions in the case of NSs. We therefore perform a thorough analysis from the "backward integration" method that we have developed, since Eqs.(3.7.2) are defined in vacuum, which trivially implies that we have to start integrating from

"infinity".

The numerical procedure, as outlined in section 3.6.1, is such that we solve the system of equations (3.5.10-3.5.12), while imposing ICs at infinity using the known solutions at Eqs.(3.7.2) (with the careful matching from 3.7.3) . Once our equations are set up and that we have all the ICs ready, we solve the system by imposing a random range of radii values (which we denote in our tables of analysis by "Trial r_*"), at which we think the star is formed. Now, this is where our EoS plays an important role.

The condition for accepting that a solution exists, is that, once we solve our equations and can get a decent density and pressure profile through this backward integration technique, we check for the value of the central pressure obtained. We should be cautious, as for example, the "Mid" EoS only takes up maximum pressure values to the order of 10^{-4}, and of order 10^{-3} for the respective maximum density. Therefore, for any values bigger than these thresholds, might be a solution, but not a realistic one.

The results tabulated below in Table 6 were shown to be dependent on the value of the constant C_1 in Eqs.(3.7.2). From the fact that we have $\tilde{B} \to \left(1 + \frac{C_1}{r}\right)$ in the limit that $\epsilon \to 0$, as a start, we assign $C_1 = -2M$ in comparison to the Schwarzschild coefficient. Therefore, we look for solutions for different values of M, and as soon as we see potential solutions (from a central pressure of the upto order 10^{-4} and respective density value), we dive deeper into the random range of radii values that we first suggested, in an attempt to locate a more accurate value and solution.

One very important thing to note hereon is that M is just a parameter assigned in our analysis, in units of kilometers, assuming geometrised units $c = G = 1$, but is not a physical mass.

The tables below display the analysis that we did with the "Mid" EoS, where trial r_* is the approximate value we claim to be the radius of the star, $p(r_*)$ is the pressure of the star at the radius of the star, p_0 is the initial pressure defined at the centre of the star, $\rho(r_*)$ is the density at the edge of the star and at last, ρ_0 is the density at the centre of the star. For all the analysis we made, we started with a range of radii values from 6 km (since we know approximately from the

"forward integration technique, which values we could use as starting values) to 20 km. Thereon, we narrowed down our range, until the best results could be obtained.

Trial r_* [km]	$p(r_*)$ [km^{-2}]	p_0 [km^{-2}]	$\rho(r_*)$ [km^{-2}]	ρ_0 [km^{-2}]	Star Solution
12.7	$2.587667918790 \times 10^{-9}$	2.37002×10^{11}	$3.5143980306843 \times 10^{-6}$	68.02901069372018	No
12.8	$2.587667918790 \times 10^{-9}$	1.04212×10^{11}	$3.5143980306843 \times 10^{-6}$	51.73115589850199	No
12.9	$2.587667918790 \times 10^{-9}$	6.14222×10^{10}	$3.5143980306843 \times 10^{-6}$	43.37338928934668	No
13.0	$2.587667918790 \times 10^{-9}$	4.71882×10^{10}	$3.5143980306843 \times 10^{-6}$	39.72469616570360	No
13.1	$2.587667918790 \times 10^{-9}$	4.67299×10^{10}	$3.5143980306843 \times 10^{-6}$	39.59567414342206	No
13.2	$2.587667918790 \times 10^{-9}$	5.86273×10^{10}	$3.5143980306843 \times 10^{-6}$	42.70529946276240	No
13.3	$2.587667918790 \times 10^{-9}$	9.19726×10^{10}	$3.5143980306843 \times 10^{-6}$	49.62105702129883	No
13.4	$2.587667918790 \times 10^{-9}$	1.7618×10^{11}	$3.5143980306843 \times 10^{-6}$	61.62593478629539	No
13.5	$2.587667918790 \times 10^{-9}$	3.81193×10^{11}	$3.5143980306843 \times 10^{-6}$	79.70591871373031	No
13.6	$2.587667918790 \times 10^{-9}$	1.09372×10^{12}	$3.5143980306843 \times 10^{-6}$	113.2595214438863	No

Table 6: Analysis of existence of stars for $f(R) = R^{1+\epsilon}$ for $\epsilon = -0.05$, $M = 1.3$ km from "Mid" EoS

What we can conclude from Table 6 is that, due to the extremely high values of the central pressure, there are no star solutions. Therefore, we reject these values for M.

Trial r_* [km]	$p(r_*)$ [km^{-2}]	p_0 [km^{-2}]	$\rho(r_*)$ [km^{-2}]	ρ_0 [km^{-2}]	Star Solution
13.780	$2.587667918790 \times 10^{-9}$	7.68239	$3.5143980306843 \times 10^{-6}$	0.022995897328001745	No
13.782	$2.587667918790 \times 10^{-9}$	7.66843	$3.5143980306843 \times 10^{-6}$	0.022982738130324425	No
13.788	$2.587667918790 \times 10^{-9}$	7.63012	$3.5143980306843 \times 10^{-6}$	0.022946546355760083	No
13.794	$2.587667918790 \times 10^{-9}$	7.59712	$3.5143980306843 \times 10^{-6}$	0.022915269158132487	No
13.800	$2.587667918790 \times 10^{-9}$	7.56935	$3.5143980306843 \times 10^{-6}$	0.022888890556176027	No
13.806	$2.587667918790 \times 10^{-9}$	7.54678	$3.5143980306843 \times 10^{-6}$	0.022867397048517486	No
13.812	$2.587667918790 \times 10^{-9}$	7.52936	$3.5143980306843 \times 10^{-6}$	0.022850777821858786	No
13.816	$2.587667918790 \times 10^{-9}$	7.52059	$3.5143980306843 \times 10^{-6}$	0.022842402426181931	No
13.820	$2.587667918790 \times 10^{-9}$	7.51409	$3.5143980306843 \times 10^{-6}$	0.022836188715998644	No
13.860	$2.587667918790 \times 10^{-9}$	7.57371	$3.5143980306843 \times 10^{-6}$	0.022893038383131580 3	No

Table 7: Analysis of existence of stars for $f(R) = R^{1+\epsilon}$ for $\epsilon = -0.05$, $M = 1.98$ km from "Mid" EoS

In the case of Table 7 above, where we randomly assigned M to be 1.98 km, once again, we find that the values of both central pressure and central density are way too high to be accepted as solutions, and thus, we conclude that there exists no stars, for which no graphical results could even be shown.

One interesting case is what we observe with the table below. Here, we have increase M from 1.98 km to 2.4 km Interestingly, although the central pressure and density values are higher than those described from the "Mid" EoS, we can still retrieve proper pressure and density profiles with

these solutions. However, once again, due to the fact that these values are still high, we conclude that these results are solutions, but not solutions of realistic stars. This remains to be investigated further, in order to figure out what stellar objects do these results model.

Trial r_* [km]	$p(r_*)$ [km^{-2}]	p_0 [km^{-2}]	$\rho(r_*)$ [km^{-2}]	ρ_0 [km^{-2}]	Star Solution	Realistic
14.2000	$2.587667918790 \times 10^{-9}$	0.114224	$3.5143980306843 \times 10^{-6}$	0.006574448655811823	Yes	No
14.2500	$2.587667918790 \times 10^{-9}$	0.107402	$3.5143980306843 \times 10^{-6}$	0.006464104669029631	Yes	No
14.3000	$2.587667918790 \times 10^{-9}$	0.105161	$3.5143980306843 \times 10^{-6}$	0.006426821559719190	Yes	No
14.3025	$2.587667918790 \times 10^{-9}$	0.105154	$3.5143980306843 \times 10^{-6}$	0.006426707689949802	Yes	No
14.3050	$2.587667918790 \times 10^{-9}$	0.105157	$3.5143980306843 \times 10^{-6}$	0.006426763583619416	Yes	No
14.3075	$2.587667918790 \times 10^{-9}$	0.105171	$3.5143980306843 \times 10^{-6}$	0.006426989722041595	Yes	No
14.3100	$2.587667918790 \times 10^{-9}$	0.105194	$3.5143980306843 \times 10^{-6}$	0.006427386595038115	Yes	No
14.3125	$2.587667918790 \times 10^{-9}$	0.105228	$3.5143980306843 \times 10^{-6}$	0.006427954636639545	Yes	No
14.3400	$2.587667918790 \times 10^{-9}$	0.106287	$3.5143980306843 \times 10^{-6}$	0.006445621159883353	Yes	No
14.3500	$2.587667918790 \times 10^{-9}$	0.106991	$3.5143980306843 \times 10^{-6}$	0.006457305223327092	Yes	No

Table 8: Analysis of existence of stars for $f(R) = R^{1+\epsilon}$ for $\epsilon = -0.05$, $M = 2.4$ km from "Mid" EoS

As can be seen in Table 9 below, we changed the value of M from 2.4 km to 3.9 km and we can see that solutions are obtained, in the sense that, the values of p_0 and ρ_0 are well within the range of the EoS being used. We can see at for example, $r_* = 14.7$ km, the central pressure is of order 10^{-3} and although the value of central density is of an order acceptable in our EoS, we reject this value on the basis that the central pressure range is not adhered to. However, since for trial radii values from $r = 14.706$ km to even 14.900 km, we have potential solutions. Both central pressure values and central density values are of the correct range as modelled by the "Mid" EoS. Therefore, we conclude that these values, are indeed realistic neutron star solutions.

Trial r_* [km]	$p(r_*)$ [km^{-2}]	p_0 [km^{-2}]	$\rho(r_*)$ [km^{-2}]	ρ_0 [km^{-2}]	Star Solution	Realistic
14.700	$2.587667918790 \times 10^{-9}$	0.00104293	$3.5143980306843 \times 10^{-6}$	0.0016828431003600609	Yes	No
14.706	$2.587667918790 \times 10^{-9}$	0.00098124	$3.5143980306843 \times 10^{-6}$	0.0016275792775041523	Yes	Yes
14.718	$2.587667918790 \times 10^{-9}$	0.000866872	$3.5143980306843 \times 10^{-6}$	0.0015141224688543264	Yes	Yes
14.730	$2.587667918790 \times 10^{-9}$	0.000763938	$3.5143980306843 \times 10^{-6}$	0.0014010878075463935	Yes	Yes
14.742	$2.587667918790 \times 10^{-9}$	0.000671533	$3.5143980306843 \times 10^{-6}$	0.0012946115414965002	Yes	Yes
14.766	$2.587667918790 \times 10^{-9}$	0.000514342	$3.5143980306843 \times 10^{-6}$	0.0011071896323374268	Yes	Yes
14.778	$2.587667918790 \times 10^{-9}$	0.000447368	$3.5143980306843 \times 10^{-6}$	0.0010355353130287008	Yes	Yes
14.802	$2.587667918790 \times 10^{-9}$	0.000332449	$3.5143980306843 \times 10^{-6}$	0.0009016313692627330	Yes	Yes
14.826	$2.587667918790 \times 10^{-9}$	0.00023950	$3.5143980306843 \times 10^{-6}$	0.0007789780891544669	Yes	Yes
14.850	$2.587667918790 \times 10^{-9}$	0.000165096	$3.5143980306843 \times 10^{-6}$	0.0006641690481557799	Yes	Yes
14.862	$2.587667918790 \times 10^{-9}$	0.000133823	$3.5143980306843 \times 10^{-6}$	0.0006202384640167196	Yes	Yes
14.874	$2.587667918790 \times 10^{-9}$	0.000105731	$3.5143980306843 \times 10^{-6}$	0.0005577873906953477 4	Yes	Yes
14.886	$2.587667918790 \times 10^{-9}$	0.0000806758	$3.5143980306843 \times 10^{-6}$	0.0005340366539775809	Yes	Yes
14.900	$2.587667918790 \times 10^{-9}$	0.0000551374	$3.5143980306843 \times 10^{-6}$	0.0004795691762855270	Yes	Yes
15.000	$2.587667918790 \times 10^{-9}$	-1.75195×10^{130}	$3.5143980306843 \times 10^{-6}$	-4.0×10^{40}	No	No

Table 9: Analysis of existence of stars for $f(R) = R^{1+\epsilon}$ for $\epsilon = -0.05$, $M = 3.9$ km from "Mid" EoS

Given the fact that we obtain solutions through this "backward integration" technique, we present below, in Figure 20, the results obtained from the numerical integration. We consider

the case where $r_* = 14.850$ km, with respective central pressure value $p_0 = 1.651 \times 10^{-4}$ km^{-2} and respective central density $\rho_0 = 6.642 \times 10^{-4}$ km^{-2}, and show the graphical results from our integration.

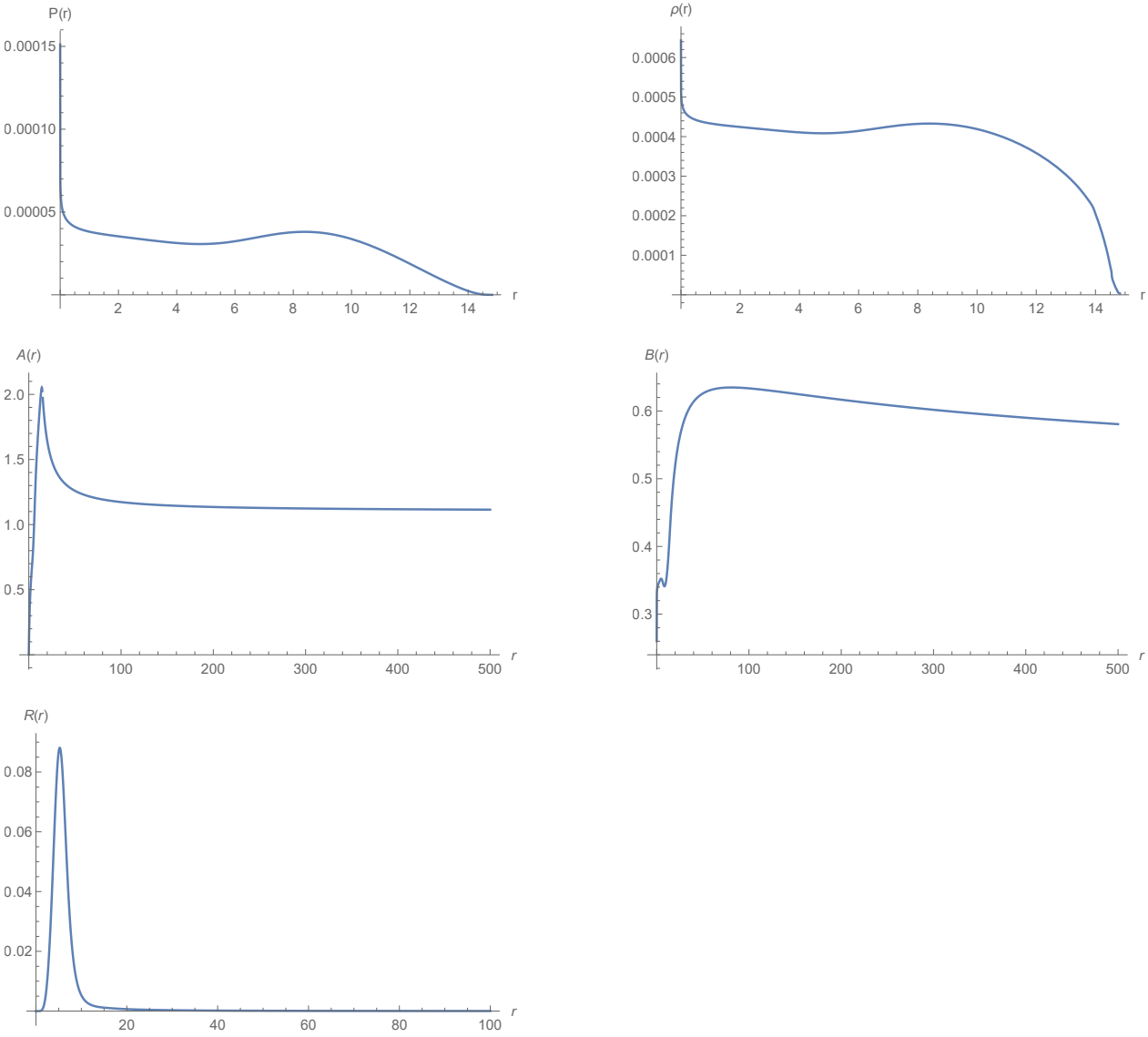

Figure 20: (Backward Integration) Solutions to $f(R) = R^{1+\epsilon}$, with $r_* = 14.850$ km, $\epsilon = -0.05$ from "Mid" EoS.

From these results, we can safely confirm that as we increased the value for M, we were able to retrieve neutron star solutions. However, due to time constraints, we were unable to check up until which values of M do these solutions exist, nor the several other initial and boundary conditions

which we could have imposed, and this goes as a scope for future projects.

3.9 Conclusion

In this chapter, before presenting the results from our analysis of the modified $f(R)$ models, we introduced neutrons stars and the reason why their studies are of prime interest at the moment. Since $f(R)$ quadratic models were shown to exhibit neutron star solutions [85], we translated the field equations of the general $f(R)$ model into our case, with respect to our definition of the metric and Riemann tensor.

Once the equations were derived, we dived into the numerical analysis part, all while considering the perturbative analysis and the conditions of a viable model. We tested our code for GR, and presented the interior and exterior solutions for $f(R) = R + \alpha R^2$, with careful matching occuring at the edge of our star, and explanation regarding the choice of our constant α. We then presented the mass-radius relations for this model, both in the case of the spherical mass and $f(R)$ gravitational mass. All results were presented using two different equations of state, namely "Mid" and "Max".

Additionally, we provided the analysis for the $f(R) = R^{1+\epsilon}$ model. Once again, we provided plots of the solutions with two EoS, from which we concluded that for $\epsilon > 0$, horizons are obtained and the limit $r \to \infty$ could not be reached, while for $\epsilon < 0$, we had asymptotically flat solutions, but which were not Schwarzschild.

As a final part of this chapter, we analysed the exact exterior solutions provided by Clifton in [86]. The aim of this part of the study was to check whether or not, these proposed solutions were indeed solutions of realistic stellar objects. From our research on this, we found out that for certain values of the arbitrary constant therein, which we matched analogously to the Schwarzschild coefficient of $(2M)/r$, stars existed, while for some other values, although admissible pressure and density profiles were retrieved, we concluded that those were solutions of certain bodies, but not of realistic stars, due to their mismatch in ranage of the EoS used.

Part III

Conclusion and Future Projects

4 Conclusion

In this final part of the thesis, we present main conclusions of the chapters, as well as the results obtained from this piece of research. We also provide suggestions for future work.

4.1 Summary

Chapter 1 was an introductory chapter in which we talked about the foundations of cosmology. We gave an overview of the fundamental ideas in this field, in view as how the Big Bang theory is the accepted theory about the formation of the Universe, and how its shortcomings in the flatness, horizon and monopole situations were resolved with inflation. This chapter reports on the standard cosmological model of the Universe, and how the Friedmann-Robertson-Walker metric is best at describing a flat universe following the Cosmological Principle. We then ended the discussions with the ΛCold Dark Matter model, which through its limitations does not help in the detection of Dark Matter particles and Dark Energy, given the fact that Dark Energy is responsible for the accelerated expansion phase of the Universe. As an attempt to explain these, theories of modified gravity were brought forward.

In Chapter 2, we precisely address the part where modified gravity theories are considered. This type of modifications aims at generalizing field equations from General Relativity in an attempt to explain late-time acceleration. We specifically considered $f(R)$ modified gravity theories, whose field equations were derived from the metric formalism. We also looked at conditions for which these types of theories are considered as acceptable, as well as some models which had successful explanations about the problems we face in Cosmology, such as Starobinsky and Hu-Sawicki.

In Chapter 3 lies the most part of the research done in this thesis. We presented details about the Equations of State that we used in this thesis. After deriving our field equations, using the Riemann tensor expressed in a different way, we explain our numerical procedure for solving our system of equations. Thereafter, we analysed some test cases of the functions of $f(R)$ that were considered. General Relativity remains a threshold for the test of any modified $f(R)$ function, in the sense that, for the case of $f(R) = R + \alpha R^2$, we retrieve General Relativity in the limit that

$\alpha \to 0$. Similarly for the case of $f(R) = R^{1+\epsilon}$ when $\epsilon \to 0$, we have General Relativity again.

4.2 Results

One of the purpose of this piece of research was to devise a method in which the spherically symmetric and analytical solutions in vacuum proposed by [86], were indeed solutions that could represent stellar objects like neutron stars.

With the perturbative analysis performed in section 3.5, we ensure that our parameters are of the correct magnitude. Using $\epsilon = \pm 0.05$, we analyse the kind of solutions we obtain in what we called the "forward integration", starting our integration from the centre of our star, until infinity. It was found, in this method, that for $\epsilon > 0$, the presence of cosmological horizons. These singularities prevented us from considering the limit $r \to \infty$ for any further investigation. This phenomena was observed in with both "Mid" and "Max" equations of state.

On the contrary, for the case of $\epsilon < 0$, we noticed that we could go until "infinity" in our analysis, with both equations of state. We thus concluded that, for this particular case, we had asymptotic solutions with a flat behaviour, but which could not be matched to a Schwarzschild spacetime.

The interesting part of this thesis, is the analysis performed in section 3.8. Starting from "infinity", we suggested radii values at which we claim the potential existence of a star. From thereon, we manipulate the values in such a way until we refined the range of such values we had randomly estimated. Tables 6, 7, 8 and 9 in section 3.8, for the analysis from the "Mid" equation of state, clearly conclude the presence or absence of stars, as well as whether these solutions are realistic or not, for the $f(R)$ model with function $f(R) = R^{1+\epsilon}$ with $\epsilon = -0.05$.

It turns out that, this presence/absence situation is dependent on the constant C_1 in the solutions at (3.7.2). We naively matched this constant to the Schwarzschild coefficient, given the fact that $\tilde{B} \to \left(1 + \frac{C_1}{r}\right)$ in the limit that $\epsilon \to 0$. To conclude this part, we notice that for values of M, in [km], as small as 1.3 and 1.98, there were no possibility of stars, but as we increased the value of this parameter, we had some positive results. Out of all the values used in the analysis, $M = 3.9$ km

gave the best results in terms of agreement with the equation of state that we were using, for which we even presented the graphical results.

5 Future Projects

5.1 Analysis involving other equations of state

For the most part of this thesis, we have been using only the "Mid" and "Max"equations of state. A large part of the work that we performed, could also be analysed using different equations of state. Unfortunately, due to time constraints, we were not able to model the backward integration technique for the "Max" EoS in section 3.5, nor for the existence of neutron stars in section 3.8, and thus these remain a future work that can be investigated.

Moreover, we found the existence of neutron stars from our analysis in section 3.8, but we were unfortunately able to check for a few values of M only. We concluded that as M increased, there were greater chances of finding solutions, however, we could not investigate up until which maximum value of M that we could obtain solutions.

Additionally, it would be very interesting to consider the EoS used in [77] in order to inspect the behaviour of these modified $f(R)$ functions and to test with these, whether or not, for our $f(R) = R^{1+\epsilon}$ model, we do find the existence of neutron stars.

5.2 Analysis of non-static objects

We have considered in this thesis, only static and spherically symmetric solutions, and the analysis therein were also constrained to the static case. It would be interesting to extend this work to the cases of rotating/expanding neutron stars which would be a description for the case of bouncing scenarios, with respect to the time-dependent metric. Thereafter, the same numerical analysis could be performed for the analysis of the second kind of exact solutions proposed in [86].

At last, for all of the above suggestions, it would be a good task to perform the analysis for the different values of ϵ, as well as using different initial and boundary conditions where suitable.

Part IV

Appendix

A General Relativity - Interior Solution

A.1 Derivation of the field equations and the TOV equations

These derivations are taken from a previous project[104].

We know that the metric of a non-rotating and fixed object in a symmetric spacetime can be represented by

$$\mathrm{d}s^2 = -A(r)\mathrm{d}t^2 + B(r)\mathrm{d}r^2 + r^2\mathrm{d}\Omega^2 \tag{A.1.1}$$

or as well as

$$\mathrm{d}s^2 = -e^{2\Phi(r)}\mathrm{d}t^2 + e^{2\Lambda(r)}\mathrm{d}r^2 + r^2\mathrm{d}\Omega^2 \tag{A.1.2}$$

where the introduction $\Phi(r)$ and $\Lambda(r)$ are made through exponential functions instead of the two unknowns $g_{tt}(r)$ and $g_{rr}(r)$, on the condition that both $g_{rr} > 0$ and $g_{tt} < 0$ wherever they are defined. And $\mathrm{d}\Omega^2 = \mathrm{d}\theta^2 + \sin^2\theta\mathrm{d}\phi^2$

Our interest is in the non-vacuum case, therefore we solve the full Einstein equations

$$G_{\mu\kappa} = R_{\mu\kappa} - \frac{1}{2}Rg_{\mu\kappa} = kT_{\mu\kappa} \tag{A.1.3}$$

where $k = 8\pi G/c^4$. Once again, one should not confuse k with the index κ.

On the assumption that the interior of our star takes as model a perfect fluid with energy-momentum tensor, we have the following relation

$$T_{\mu\kappa} = (\rho + p)U_\mu U_\kappa + pg_{\mu\kappa} \tag{A.1.4}$$

where, pressure p and energy density ρ are both functions of radial distance r only.

For full static and timelike solutions $(U^t, \mathbf{0})$ we impose the normalization condition $g_{\mu\kappa}U^\mu U^\kappa = -1$. We then obtain $U^t = e^{-\Phi(r)}$, and $g_{tt}U^t = U_t = -e^{\Phi(r)}$. The interior energy-momentum tensor has

the following non-zero components

$$T_{tt} = \rho(r)e^{2\Phi(r)} \tag{A.1.5}$$

$$T_{rr} = p(r)e^{2\Lambda(r)} \tag{A.1.6}$$

$$T_{\theta\theta} = r^2 p(r) \tag{A.1.7}$$

$$T_{\phi\phi} = \sin^2\theta T_{\theta\theta} \tag{A.1.8}$$

For the conservation of energy and momentum, we compute the covariant derivative (∇_κ) of the energy-momentum tensor, i.e. $\nabla_\kappa T^{\mu\kappa} = 0$. We obtain

$$\dot{U}^\mu = U^\mu_{;\kappa} U^\kappa \tag{A.1.9}$$

and

$$\dot{U}^\mu \big[\rho(r) + p(r)\big] = -h^\mu_\kappa p(r)^{;\kappa} \tag{A.1.10}$$

We substitute equation (A.1.9) into (A.1.10) and taking into account the radial component only, we arrive at the following relation

$$\big[\rho(r) + p(r)\big]\frac{\mathrm{d}\Phi(r)}{\mathrm{d}r} = -\frac{\mathrm{d}p(r)}{\mathrm{d}r} \tag{A.1.11}$$

The non-zero components of the Einstein Tensor are given as

$$G_{tt} = \frac{1}{r^2}e^{2\Phi(r)}\frac{\mathrm{d}}{\mathrm{d}r}\Big[r(1 - e^{-2\Lambda(r)})\Big] \tag{A.1.12}$$

$$G_{rr} = -\frac{1}{r^2}e^{2\Lambda(r)}(1 - e^{-2\Lambda(r)}) + \frac{2}{r}\frac{\mathrm{d}\Phi(r)}{\mathrm{d}r} \tag{A.1.13}$$

$$G_{\theta\theta} = r^2 e^{-2\Lambda(r)}\left[\frac{\mathrm{d}^2\Phi(r)}{\mathrm{d}r^2} + \left(\frac{\mathrm{d}\Phi(r)}{\mathrm{d}r}\right)^2 + \frac{1}{r}\frac{\mathrm{d}\Phi(r)}{\mathrm{d}r} - \frac{\mathrm{d}\Phi(r)}{\mathrm{d}r}\frac{\mathrm{d}\Lambda(r)}{\mathrm{d}r} - \frac{1}{r}\frac{\mathrm{d}\Lambda(r)}{\mathrm{d}r}\right] \tag{A.1.14}$$

$$G_{\phi\phi} = \sin^2\theta G_{\theta\theta} \tag{A.1.15}$$

Having calculated all the components, we are now able to find solutions to our Einstein equations.

From the Einstein tensor $G_{\mu\kappa} = kT_{\mu\kappa}$, the tt-component is therefore,

$$\frac{1}{r^2}e^{2\Phi(r)}\frac{\mathrm{d}}{\mathrm{d}r}\left[r(1-e^{-2\Lambda(r)})\right] = k\rho(r)e^{2\Phi(r)} \tag{A.1.16}$$

If we introduce a mass function $m(r) = \frac{1}{2}r(1-e^{-2\Lambda(r)})$, we arrive at the following first order differential equation in mass relative to radial component r,

$$\frac{\mathrm{d}m(r)}{\mathrm{d}r} = 4\pi r^2\rho(r) \tag{A.1.17}$$

The associated boundary condition is $m(0) = 0$ so as to make sure that $e^{2\Lambda(r)} = 1\Big/\left[1-\frac{2Gm(r)}{r}\right]$ is finitely defined.

We note that the $e^{2\Lambda(r)}$ term is simply an analogy to the Schwarzschild coefficient with $M \sim m(r)$. From equation (A.1.17) we can write [17]

$$m(r) = 4\pi\int_0^r \rho(\tilde{r})\tilde{r}^2\mathrm{d}\tilde{r} \tag{A.1.18}$$

On the assumption that r_* is the radius of our neutron star in vacuum, it implies that the M is computed by the integral of the energy density contained within the star

$$M = m(r_*) = 4\pi\int_0^{r_*} \rho(r)r^2\mathrm{d}r \tag{A.1.19}$$

The value of M is in fact the total mass contained within the radius of the star.

Taking into account the rr-component, we have

$$-\frac{1}{r^2}e^{2\Lambda(r)}(1-e^{-2\Lambda(r)}) + \frac{2}{r}\frac{\mathrm{d}\Phi(r)}{\mathrm{d}r} = kpe^{2\Lambda(r)} \tag{A.1.20}$$

We can rewrite Eq.(A.1.20) in terms of the mass function $m(r)$, and get the relation

$$\frac{\mathrm{d}\Phi(r)}{\mathrm{d}r} = \frac{m(r)+4\pi r^3p(r)}{r[r-2m(r)]} \tag{A.1.21}$$

When we substitute equation (A.1.11) into (A.1.21), we obtain the well-known Tolman-Oppenheimer-

Volkoff (TOV) equation:

$$\frac{\mathrm{d}p(r)}{\mathrm{d}r} = -\frac{\big[\rho(r) + p(r)\big]m(r) + 4\pi r^3 p(r)}{r[r - 2m(r)]} \tag{A.1.22}$$

A.2 Case of constant density neutron star

For simplicity, we look at the case of a neutron star of constant density. It is then described by the following relations, in addition to the ones already derived above

$$\rho(r) = \begin{cases} \rho\ , & \mathrm{r} \leq r_* \\ 0, & r > r_* \end{cases} \tag{A.2.1}$$

with mass function [17]

$$m(r) = \begin{cases} \frac{4}{3}\pi\rho r^3\ , & \text{for r} \leq r_* \\ \frac{4}{3}\pi\rho r_*^3 = M, & \text{for } r > r_* \end{cases} \tag{A.2.2}$$

now, for r_* as the radius of the star of constant density. Using the central pressure condition defined at the centre of the star, $p_c = p(0) = p_0$ to solve equation (A.1.22) , we can show that the expressions for central pressure, pressure and radius r_* respectively [17]

$$p_c = \rho\frac{1 - \sqrt{(1 - \frac{2GM}{r_*})}}{3\sqrt{(1 - \frac{2GM}{r_*})} - 1} \tag{A.2.3}$$

$$p(r) = \rho\frac{\sqrt{(1 - \frac{2GMr^2}{r_*^3})} - \sqrt{(1 - \frac{2GM}{r_*})}}{3\sqrt{(1 - \frac{2GM}{r_*})} - \sqrt{(1 - \frac{2GMr^2}{r_*^3})}} \tag{A.2.4}$$

$$r_*^2 = \frac{3}{8\pi G\rho}\left[1 - \left(\frac{\rho + p_c}{\rho + 3p_c}\right)^2\right] \tag{A.2.5}$$

The above equation, combined with equation (A.2.2), makes it easy to compute the central pressure,

at any radius, along with the pressure, in terms of the total mass M and radius r_* of the star.

The radius r_* is calculated from the condition $p(r_*) = 0$, a condition which is imposed as well as the following ICs and BCs. For the mass, the IC we assume is $m(0) = 0$, while that for the pressure has already been given as $p_c = p(0)$. Our forward integration is such that we start at the centre of the star, that is, at $r = 0$, until we reach $r = r_*$, that is, until we reach the edge (radius) of the star, at which the pressure vanishes.

Since $\mathrm{d}p(r)/\mathrm{d}r < 0$ [17], it can be seen that the pressure will decline as we move outwards from the origin towards the star's edge. Therefore, a chosen EoS should satisfy this criteria, that is, it should be such that, at a finite radius, it decreases to a null pressure value.

From equation (A.2.3), one can note that the expression diverges for $\frac{2GM}{r_*} \to \frac{8}{9}$. Consequently, for the solution to exist, we have to be in accordance with the limit $\frac{2GM}{r_*} < \frac{8}{9}$. Padmanabhan in [17] outlines that the same condition also holds for non-constant density.

After integrating within the proper limits and substituting, we obtain the following expressions as our constant density neutron star solutions

$$A(r) = e^{2\Phi(r)} = \frac{1}{4}\left[3\sqrt{\left(1 - \frac{2GM}{r_*}\right)} - \sqrt{\left(1 - \frac{2GMr^2}{r_*^3}\right)}\right]^2 \tag{A.2.6}$$

$$B(r) = e^{2\Lambda(r)} = \left(1 - \frac{2GMr^2}{r_*^3}\right)^{-1} \tag{A.2.7}$$

These solutions above will help in setting up our boundary conditions for the numerical part of this thesis. Given the fact that the case of constant density is a simple one, these explicit solutions were easy to derive. However, for the non-constant density case, a set of first order differential equations need to be solved, with careful attention paid to the initial and boundary conditions, and from which only numerical solutions are possible. For this instance, an EoS relating pressure and density needs to be provided.

B $f(R)$ theories - Interior Solution

B.1 Derivation of the Ricci scalar

The line element which describes a non-rotating and non-expanding neutron star can be represented by

$$\mathrm{d}s^2 = B(r)\mathrm{d}t^2 - A(r)\mathrm{d}r^2 - r^2(\mathrm{d}\theta^2 + \sin^2\theta\mathrm{d}\phi^2) \tag{B.1.1}$$

The matrix below represents the non-zero components along the main diagonal

$$g_{\mu\kappa} = \begin{pmatrix} B(r) & 0 & 0 & 0 \\ 0 & -A(r) & 0 & 0 \\ 0 & 0 & -r^2 & 0 \\ 0 & 0 & 0 & -r^2\sin^2\theta \end{pmatrix} \tag{B.1.2}$$

with matrix inverse

$$g^{\mu\kappa} = \begin{pmatrix} \frac{1}{B(r)} & 0 & 0 & 0 \\ 0 & -\frac{1}{A(r)} & 0 & 0 \\ 0 & 0 & -\frac{1}{r^2} & 0 \\ 0 & 0 & 0 & -\frac{1}{r^2\sin^2\theta} \end{pmatrix} \tag{B.1.3}$$

Here, we also assume that, for our neutron star, its matter content can be modeled by a perfect fluid that, in the comoving frame, can be modelled by the energy-momentum tensor as

$$T_{\mu\kappa} = \big[\rho(r) + p(r)\big]u_\mu u_\kappa - p g_{\mu\kappa} \tag{B.1.4}$$

.

A completely time-like four-velocity, U_μ is assumed for the case of non-rotating (static) solutions, which abides by the normalisation condition $g_{\mu\kappa}U^\mu U^\kappa = +1$. From this, we find that $U_t = \sqrt{B(r)}$. We compute the non-zero components of the energy-moment tensor as

$$T_{tt} = \rho(r)B(r) \tag{B.1.5}$$

$$T_{rr} = p(r)A(r) \tag{B.1.6}$$

$$T_{\theta\theta} = p(r)r^2 \tag{B.1.7}$$

$$T_{\phi\phi} = T_{\theta\theta}\sin^2\theta \tag{B.1.8}$$

From Eq.(B.1.1), we compute the following non-zero curvature tensors

$$R_{tt} = -\frac{B''}{2A} - \frac{B'}{rA} + \frac{B'}{4A}\left(\frac{A'}{A} + \frac{B'}{B}\right) \tag{B.1.9}$$

$$R_{rr} = \frac{B''}{2B} - \frac{A'}{rA} - \frac{B'}{4B}\left(\frac{B'}{B} + \frac{A'}{A}\right) \tag{B.1.10}$$

$$R_{\theta\theta} = \frac{r}{2A}\left(\frac{B'}{B} - \frac{A'}{A}\right) + \frac{1}{A} - 1 \tag{B.1.11}$$

The curvature scalar, R, calculated from $R = g^{\mu\kappa}R_{\mu\kappa}$ is found as the sum of the tt, rr, $\theta\theta$ and $\phi\phi$ components, given by the equation below:

$$R = \frac{B'}{2AB}\left(\frac{A'}{A} + \frac{B'}{B}\right) - \frac{B''}{AB} - \frac{2B'}{rAB} + \frac{2A'}{rA^2} - \frac{2}{Ar^2} + \frac{2}{r^2} \tag{B.1.12}$$

B.2 Derivation of the field equations in $f(R)$

We have for the respective $tt, rr, \theta\theta$ components, the following equations substituted into Eq.(3.3.1),

$$\begin{aligned} -\frac{B''}{2A} - \frac{B'}{rA} + \frac{B'}{4A}\left(\frac{A'}{A} + \frac{B'}{B}\right) = \frac{1}{f_R}\Bigg(&- k\rho B \\ &+ B\left(\frac{A'}{2A^2} - \frac{2}{rA}\right)f'_R - \frac{B}{A}f''_R + \frac{B}{2}f(R)\Bigg) \end{aligned} \tag{B.2.1}$$

$$\begin{aligned} \frac{B''}{2B} - \frac{A'}{rA} - \frac{B'}{4B}\left(\frac{B'}{B} + \frac{A'}{A}\right) = \frac{1}{f_R}\Bigg(&- kpA + \\ &\left(\frac{B'}{2B} + \frac{2}{r}\right)f'_R - \frac{A}{2}f(R)\Bigg) \end{aligned} \tag{B.2.2}$$

$$\frac{r}{2A}\left(\frac{B'}{B}-\frac{A'}{A}\right)+\frac{1}{A}-1=\frac{1}{f_R}\Bigg(-kpr^2+\frac{r^2}{A}f''_R \\ +\left(\frac{B'r^2}{2AB}-\frac{A'r^2}{2A^2}+\frac{r}{A}\right)f'_R-\frac{r^2}{2}f(R)\Bigg) \tag{B.2.3}$$

Equations of similar forms were derived by M. A. Resco *et al.* in [85], where a Lagrangian of the form $\mathcal{L}_M = R + f(R)$ was used, and where, in the limit that $f(R) \to 0$, GR solutions are retrieved for this case. Again, in our case, where we have $\mathcal{L}_M = f(R)$, setting $f(R) = R$ gives us GR solutions.

The components for G_{tt} and G_{rr} can be found by equations (B.2.1) and (B.2.2) respectively. The component for $G_{\phi\phi}$ is excluded as it holds the same information as equation (B.2.3), which leads to the $G_{\theta\theta}$ component.

One distinction to make is that the $'$ (prime) denotes the derivative with respect to the radial coordinate r, while $_R$ (subscript R), represents the derivative with respect to the curvature scalar R.

Combining equations $\frac{B.2.1}{2B}+\frac{B.2.2}{2A}+\frac{B.2.3}{r^2}$ yields

$$\frac{1}{Ar^2}-\frac{A'}{rA^2}-\frac{1}{r^2}=\frac{1}{f_R}\Bigg[-\frac{k}{2}(\rho+3p)+\frac{1}{2A}f''_R \\ +\left(\frac{3B'}{4AB}-\frac{A'}{4A^2}+\frac{1}{rA}\right)f'_R-\frac{1}{2}f(R)\Bigg] \tag{B.2.4}$$

In order to have an expression for $A'(r)$, we express f''_R in terms of derivatives of smaller order. Therefore, combining the equations in a new way and using Eq.(B.1.12), we obtain the following relation

$$f''_R=f_R\Big(\frac{AR}{2}-\frac{A'}{2rA}-\frac{2A}{r^2}+\frac{2}{r^2}+\frac{3B'}{2rB}\Big)+f'_R\Big(\frac{A'}{2A}+\frac{1}{r}\Big) \tag{B.2.5}$$

Using the above definition for f''_R into Eq.(B.2.4) and rearranging the result, we have an expression for A'. We define $f'_R=\frac{\mathrm{d}f_R}{\mathrm{d}r}=\frac{\mathrm{d}f_R}{\mathrm{d}R}\frac{\mathrm{d}R}{\mathrm{d}r}=f_{2R}R'$ and using all our findings, we arrive at Eq.(3.3.6), which is the first equation of our system of equations. One can manipulate Eqs.(B.2.1-B.2.3) and use the trace equation (3.3.3) as well as the fact that $f''_R=f_{3R}R'^2+f_{2R}R''$, to obtain Eq.(3.3.8) [85].

Additionally, Eqs.(3.3.9) and (B.2.2) can be used to extract the last two highest derivatives which are required to conclude the system of equations, and Eqs.(3.3.7) and (3.3.9) are then ob-

tained. Once we have all our equations, as presented in Chaper 3.3, we use iterative numerical methods with appropriate initial and boundary conditions to solve the system.

If we introduce smaller derivatives, for example, $Rr = R'$ such that trivially $Rr' = R''$, and $\psi(r) = \frac{B'(r)}{B(r)}$, then the system of equations described at (3.3.6-3.3.9) form a system of six differential equations of first-order, [85], for which six initial conditions are required: for R, R', A, B, B' and p, all evaluated at the centre of the star, that is, at $r = 0$.

Being a physical quantity, the pressure has to be finitely defined everywhere in order for the stagnant star to be existent, particularly at $r = 0$. We provide this initial condition as p_0, the value of which is provided from the data for which our EoS holds. Considering Eq.(B.2.3) where we take the limit $r \to 0$, we have one initial condition which is $A(0) = 1$ and by reviewing Eqs.(B.2.1) and (B.2.2) within the same limit, we find, from Eq.(3.3.9), in order to make sure we have a smooth pressure profile at the origin, that [85]

$$B'(0) = -A'(0)B(0) = \frac{2f_{2R}R'(0)}{f_R}B(0) \tag{B.2.6}$$

Since $p(0)$ (or p_0) is a free parameter characterizing the star (which in turn provides points for the Mass-Radius diagrams), we can obtain a series of stars depending on this IC that we provide. As such, we can say that only four important initial conditions are needed, and these are that $A_0 = 1, B_0' = 0, p(0) = p_0$ and $R_0' = 0$. B_0 and R_0 are the two remaining ICs which are free, and which are determined by a shooting method in order to satisfy the right BCs when $r \to \infty$.

The shooting method ensures that the proper matching is done at the star's exterior, to the one defined by the Schwarzschild metric also at infinity. However, as introduced $\psi = \frac{B'}{B}$, we have one less IC to worry about, we simply have that $\psi(0) = 0$. As for the other free initial condition for R, with some freedom, we can use $R(0) = kT(0)$ as an IC for R_0, which is the well-known GR value.

A careful comparison of the metrics described for GR in equation (A.1.1) and that for f(R) described by equation (B.1.1) show that the following mapping applies in respect of the metric coefficients described for both metrics. In other words, we can use the analytical solutions provided

in Appendix A to be those of the metric described at (B.1.1).

$$A(r) = \left(1 - \frac{2GMr^2}{r_*^3}\right)^{-1} \tag{B.2.7}$$

$$B(r) = \frac{1}{4}\left[3\sqrt{\left(1 - \frac{2GM}{r_*}\right)} - \sqrt{\left(1 - \frac{2GMr^2}{r_*^3}\right)}\right]^2 \tag{B.2.8}$$

Using the above expressions, one can write the initial and boundary conditions that are necessary in solving the system of equations described by (3.3.6 - 3.3.9) for the case of constant density neutron star. The conditions that are needed are

$$A(0) = 1 \tag{B.2.9}$$

$$B(0) = B_0 \tag{B.2.10}$$

where B_0 can be calculated from Eq.(B.2.8). The pressure part, for the same constant density star, modeled by equation (3.3.9), is now as follows

$$p(r) = \frac{\sqrt{B_0}}{\sqrt{B(r)}}(\rho_0 + p_0) - \rho \tag{B.2.11}$$

where ρ_0 is a value for the density at the centre of the star and p_0 is the central pressure.

C Exterior-Interior Solutions for $f(R) = R + \alpha R^2$

In this Appendix, we present the exterior-interior solutions, from the backward integration mentioned. As can be seen, the solutions match very accurately to the ones obtained from the forward integration. Here also, we make use of the "Intermediate" EoS, as well as impose for the solution for $B(r)$ to be Schwarzschild at infinity.

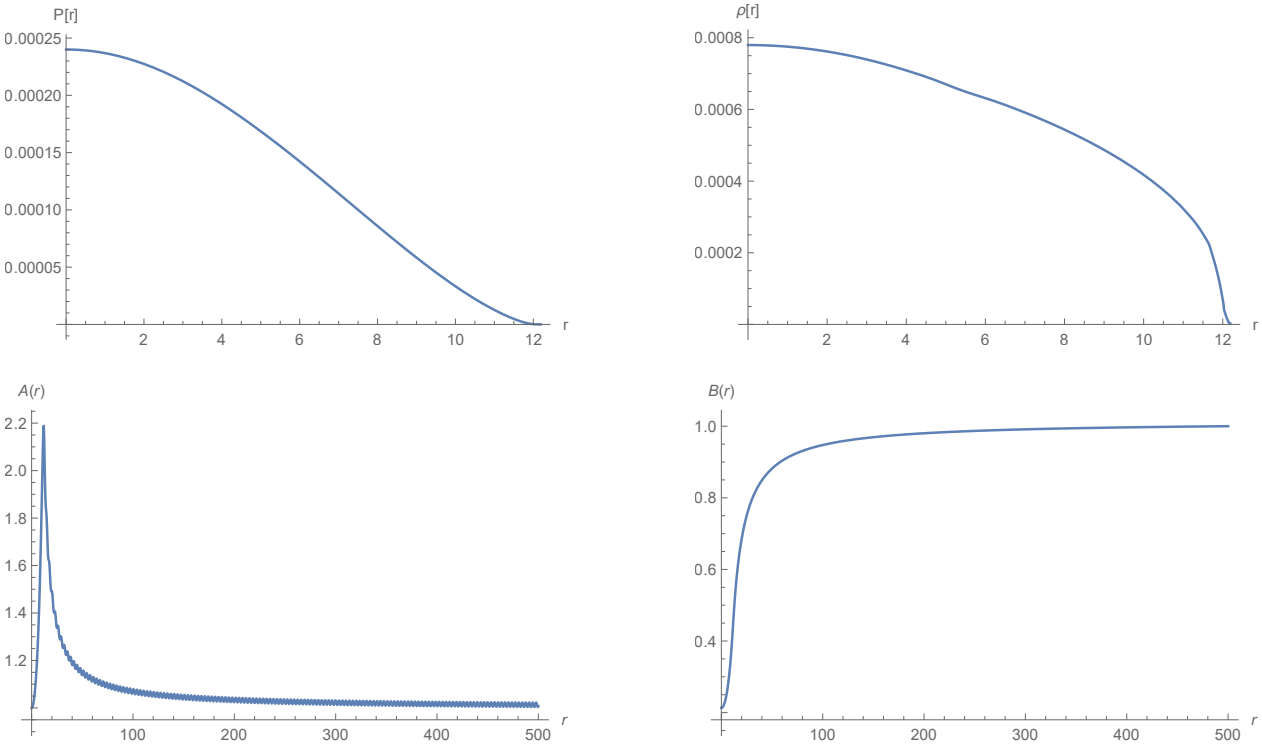

Figure 21: (Backward Integration) Solutions to $f(R) = R + \alpha R^2$, with $\alpha = -0.05$ from "Mid" EoS

Solutions to the field equations using the "Intermediate" EoS, with $r_* = 12.19$ km. From top left, $p(r)$, $\rho(r)$, $A(r)$, and $B(r)$. We retrieve the same in $A(r)$. The oscillations occurring in $B(r)$ are much smaller, thus negligibly seen in the diagrams above.

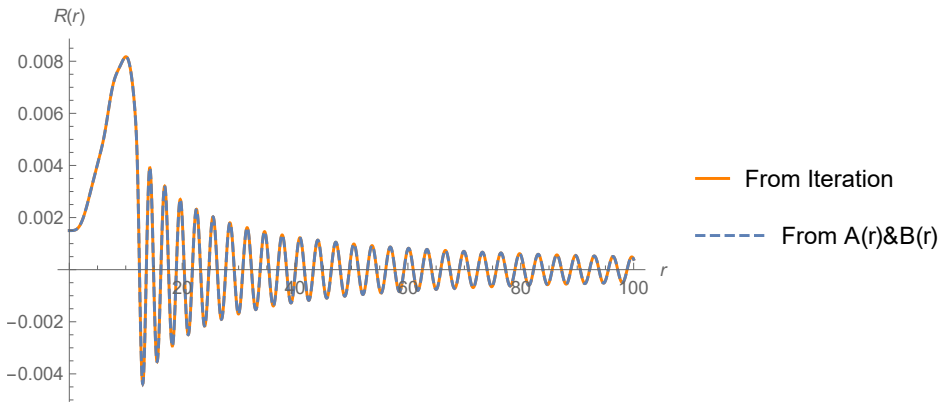

Figure 22: (Backward Integration) Solutions to $f(R) = R + \alpha R^2$, with $\alpha = -0.05$ from "Mid" EoS

Once again, the Ricci scalar, $R(r)$ displays damped oscillations. The direct computation of the Ricci scalar (from $B(r)$ and $A(r)$) as described by Eq.(B.1.12)), as well as the iterated one, once again, agree perfectly within numerical precision that we use.

The reason for plotting the curvature scalar, $R(r)$ only until $r = 80$ km, instead of a larger value, is only to properly show the oscillations which occur. We can see from the Ricci scalar, the standing wave which is outside the $f(R)$ star, even in this backward integration method.

D Mapping Conditions for Numerical and Analytical Static and Spherically Symmetric Solutions in Vacuum

In this Appendix, we analyse the exact solutions provided by Clifton in [86] for $f(R) = R^{1+\epsilon}$. The exact spherical and symmetric solutions in vacuum for the line element

$$\mathrm{d}s^2 = -\tilde{A}(r)\mathrm{d}t^2 + \frac{1}{\tilde{B}(r)}\mathrm{d}r^2 + r^2\mathrm{d}\Omega^2 \,. \tag{D.0.1}$$

are given by [86]

$$\begin{aligned} \tilde{A}(r) &= r^{2\epsilon\frac{(1+2\epsilon)}{(1-\epsilon)}} + \frac{C_1}{r^{\frac{(1-4\epsilon)}{(1-\epsilon)}}} \\ \tilde{B}(r) &= \frac{(1-\epsilon)^2}{(1-2\epsilon+4\epsilon^2)(1-2\epsilon(1+\epsilon))}\left(1 + \frac{C_1}{r^{\frac{(1-2\epsilon+4\epsilon^2)}{(1-\epsilon)}}}\right) \end{aligned} \tag{D.0.2}$$

where C_1 is an arbitrary constant.

Since these solutions are derived from a metric and Riemann tensor definition which are different from the ones that we have used in this thesis, we have to implement a careful matching in order to be able to compare the exterior solutions from our system of equations, to the analytical solutions proposed.

Starting with a Lagrangian of the form $\mathcal{L} = f(R)$, where $f(R)$ is a power-series function of the curvature scalar, which can be expanded, we consider the function,

$$f(R) = R^{1+\epsilon} \tag{D.0.3}$$

which, as we have seen before, reduces to GR when $\epsilon = 0$.

After substituting Eqs.(3.6.1) in our field equations, we now obtain for the general form

$$\begin{aligned} kT_{\mu\kappa} = {} & \epsilon(1+\epsilon)R^{\epsilon-2}\nabla_\mu R\nabla_\kappa R - \epsilon(1+\epsilon)R^{\epsilon-1}\nabla_\mu\nabla_\kappa R + (1+\epsilon)R^\epsilon R_{\mu\kappa} \\ & - \frac{1}{2}g_{\mu\kappa}R^{\epsilon+1} - g_{\mu\kappa}\epsilon(1-\epsilon^2)\nabla_c R\nabla^c R + \epsilon(1+\epsilon)g_{\mu\kappa}R^{\epsilon-1}\Box R \end{aligned} \tag{D.0.4}$$

With some manipulation, we can find the tt-component of (D.0.4) to be,

$$\begin{aligned}(1+\epsilon)R^{\epsilon}R_{tt} = kT_{tt} + \epsilon(1+\epsilon)R^{\epsilon-1}\nabla_t(\nabla_t R) + \frac{1}{2}g_{tt}R^{\epsilon+1} \\ + g_{tt}\epsilon(1-\epsilon^2)R^{\epsilon-1}\nabla_c R\nabla^c R - \epsilon(1+\epsilon)g_{tt}R^{\epsilon-1}\Box R\,.\end{aligned} \tag{D.0.5}$$

For the static and spherically symmetric Universe, we have the description of the line element as in Eq.(D.0.1) and the Christoffel symbols needed to simplify the covariant derivatives in (D.0.5) are as follows,

$$\Gamma^r_{tt} = \frac{1}{2}\tilde{A}'\tilde{B}\,, \quad \Gamma^r_{rr} = -\frac{\tilde{B}'}{2\tilde{B}}\,, \quad \Gamma^r_{\theta\theta} = -\tilde{B}r \quad \text{and} \quad \Gamma^r_{\phi\phi} = -\tilde{B}r\sin\theta\,, \tag{D.0.6}$$

where $'$ denotes the derivative with respect to r.

After simplifying the covariant derivative from Eq.(D.0.5) and using Eq.(D.0.6), we show that the tt-component now becomes

$$R_{tt} = \frac{\kappa\rho\tilde{A}}{(1+\epsilon)R^{\epsilon}} + \frac{\epsilon R'}{R}\left(\frac{\tilde{A}\tilde{B}'}{2} + \frac{2\tilde{A}\tilde{B}}{r} - \frac{(1-\epsilon)\tilde{A}\tilde{B}R'}{R}\right) + \frac{\epsilon R''}{R}\tilde{A}\tilde{B} - \frac{\tilde{A}R}{2(1+\epsilon)}\,. \tag{D.0.7}$$

For this thesis, the definition of the line element used is

$$\mathrm{d}s^2 = B(r)\mathrm{d}t^2 - A(r)\mathrm{d}r^2 - r^2\mathrm{d}\Omega^2\,, \tag{D.0.8}$$

and the Christoffel symbols needed to simplify the covariant terms are,

$$\Gamma^r_{tt} = -\frac{B'}{2A}\,, \quad \Gamma^r_{rr} = \frac{A'}{2A}\,, \quad \Gamma^r_{\theta\theta} = -\frac{r}{A} \quad \text{and} \quad \Gamma^r_{\phi\phi} = -\frac{r}{A}\sin\theta\,. \tag{D.0.9}$$

Therefore, R_{tt} component for this case is

$$R_{tt} = \frac{-k\rho B}{(1+\epsilon)R^{\epsilon}} + \frac{\epsilon R'}{R}\left(\frac{A'B}{2A^2} - \frac{2B}{rA} + \frac{(1-\epsilon)BR'}{AR}\right) - \frac{\epsilon R''}{R}\frac{B}{A} + \frac{BR}{2(1+\epsilon)}\,, \tag{D.0.10}$$

When comparing Eq.(D.0.7) with Eq.(D.0.10) we find that the only possible mapping for which both R_{tt} components agree, relative to all the respective sign conventions, is through the following

$$A \to \frac{1}{\tilde{B}} \quad \text{and} \quad B \to \tilde{A}\,. \tag{D.0.11}$$

References

[1] Caroll, B. W. and Ostlie, D. A., *An introduction to Modern AstroPhysics*, 2^{nd}*Ed.* Pearson Education (2006).

[2] Kandhai, S., *Exploring the cosmological dynamics of a viable theory for* $f(R)$*-gravity* (University of Cape Town, 2013).

[3] Kofman, L., *The Origin of Matter in the Universe: Reheating after Inflation* arXiv: 9605155 [astro-ph] (1996).

[4] Dodelson, S., *Modern Cosmology*, Academic Press (2003).

[5] Yoshida, N., *Structure Formation in the Early Universe*, arXiv: 0906.4372[astro-ph.CO] (2009).

[6] Miralda-Escude, J., *The Dark Age of the Universe*, arXiv: astro-ph/0307396 (2003).

[7] National Aeronautics and Space Administration, *Other WMAP Site Images*, URL: `https://map.gsfc.nasa.gov/resources/otherimages.html`.

[8] Planck Collaboration (Ade, P.A.R. *et al)*, *Planck 2013 results. XVI. Cosmological parameters* arXiv: 1303.5076 [astro-ph.CO] (2013).

[9] Planck Collaboration (Ade, P.A.R. *et al.*, *Planck 2013 results. XV. CMB power spectra and likelihood* arXiv: 1303.5075 [astro-ph.CO](2013).

[10] Sotiriou, T. P., and Faraoni, V., *f(R) theories of gravity* (2010) arXiv: 0805.1726 [gr-qc].

[11] Singal, A. K., *Horizon, homogeneity and flatness problems – do their resolutions really depend upon inflation?* in *Proceedings, National Conference on Current Issues in Cosmology, AstroPhysics and High Energy Physics (CICAHEP): Dibrugarh, India, November 2-5, 2015*, (Dibrugarh, India), pp. 94-99, Dibrugarh Univ., 2016.arXiV:1603.01539.

[12] Veneziano, G. , *A Simple/Short Introduction to Pre-Big Bang Physics/Cosmology* in *Highlights of the subnuclear Physics: 50 years later. Proceedings, 35th Course of the International School of Subnuclear Physics, Erice, Italy, August 26-September 4, 1997*, pp. 364-380, 1997. arXiv: hep-th/9802057.

[13] Langlois, D., *Lectures on inflation and cosmological perturbations*, arXiv: 1001.5259[astro-ph.CO] (2010).

[14] Handley, W. J., Brechet, S. D., Lasenby, A. N. and Hobson, M. P., *Kinetic initial conditions for inflation*, Phys. Rev. **D89** (2014), no. 6 063505, arXiv: 1401.2253[astro-ph.CO] (2018).

[15] Liddle, A., *An Introduction to Modern Cosmolgy, Second Edition*, John Wiley & Sons, 2003.

[16] Hobson, M. P., Efstathiou, G. and Lasenby, A. N., *General Relativity, An Introduction for Physicists*, Cambridge University Press, 2006.

[17] Padmanabhan, T., *Gravitation Foundation and Frontiers*. Cambridge University Press, Cambridge (2010).

[18] Sporea, C. A., *Notes on f(R) Theories of Gravity*, arXiv: 1403.3852.

[19] Martin, J., Ringeval, C., Trotta, R. and Vennin, V., *The Best Inflationary Models After Planck*, JCAP **1403**(2014) 039, arXiv: 1312.3529.

[20] Planck Collaboration (Ade, P.A.R. *et al)*, *Planck 2013 results. XXII. Constraints on inflation* arXiv: 1303.5082 [astro-ph.CO] (2013).

[21] Planck Collaboration (Ade, P.A.R *et al)*, *Planck 2015 results. XIII. Cosmological parameters* arXiv: 1502.01589 (2016).

[22] Planck Collaboration (Aghanim, N. *et al)*, *Planck 2018 results.VI. Cosmological parameters* arXiv: 1807.06209 (2018).

[23] Uzan, J. P., *The big-bang theory: construction, evolution and status*arXiv: 1606.06112 2016.

[24] Heffernan, M. , Banerjee, P. and Walker-Loud, A. , *Quantifying the sensitivity of Big Bang Nucleosynthesis to isospin breaking with input from lattice QCID* arXiV: 1706.04991.

[25] Senatore, L. , *Lectures on Inflation* in *Proceedings, Theoretical Advanced Study Institute in Elementary Particle Physics: New Frontiers in Fields and Strings (TASI 2015): Boulder, CO, USA, June 1-26, 2015* pp. 447-543, 2017. arXiV: 1609.00716.

[26] De la Cruz Dombriz, Á., *Some cosmological and astrophysical aspects of modified gravity theories*(Universidad Complutense de Madrid, 2010).

[27] Astier P., et al., *The Supernova Legacy Survey: Measurement of* Ω_M, Ω_Λ *and* w *from First Year Data Set* (2005). arXiv: astro-phy/0510447.

[28] Eiseinstein, D. J., et al. (SDSS), 2005, Astrophys. J. 633, 560.

[29] Riess, A. G., et al. [Supernova Search Team], 2004, Astrophys. J. 607, 665.

[30] Spergel, D. N., et al., *Wilkinson Microwave Anisotropy Probe (WMAP) Three Year Observations: Implications for Cosmology*, (2007) arXiv: astro-ph/0603449.

[31] Weyl, H. , Annalen Phys. 59, 101 (1919) [Surveys High Energ. Phys. 5, 237(1986)].

[32] Eddington, A. S. , *The Mathematical Theory of Relativity.* Cambridge University Press, Cambridge (1923).

[33] Utiyama, R. and DeWitt, B. S., J. Math. Phys. **3**, 608 (1962).

[34] Hooft, G. 't and Veltman, M. J. G., Annales Poincare Phys. Theor. A **20**, 69 (1974).

[35] Hawking, S. W., *The Theory of Everything: The Origin and Fate of the Universe.* Phoenix Books; Special Anniv. (2005).

[36] Birrell, N. D. and Davies, P. C. W. , *Quantum fields in curved space.* Cambridge Monographs on Mathematical Physics, vol. 7, Cambridge Univ. Press, New York, (1982).

[37] Buchbinder, I. L., Odintsov, S. D. and Shapiro, I. L. , *Bristol, UK: IOP (1992) 413 p.*.

[38] Vilkovisky, G. A. , Class. Quant. Grav. **9**, 895 (1992).

[39] Riess, A. G. et al. [Supernova Search Team Collaboration], *Observational Evidence from Supernovae for an Accelerating Universe and Cosmological Constant*, Astron. J. **116**, 1009 (1998) arXiv: astro-ph/980521.

[40] Busca, N. G. et al., *Baryon Acoustic Oscillations in the Ly-α forest of BOSS quasars*, Astron. AstroPhysics. **552** (2013) A96, arXiv: 1211.2616.

[41] The Dark Energy Survey Collaboration, *The Dark Energy Survey*, arXiv: astro-ph/0510346 (2005).

[42] Perlmutter, S. et al. [Supernova Cosmology Project Collaboration], Astrophys. J. **517**, 565, (1999).

[43] Tonry, J. L. et al. Astrophys. J.**594**, 1 (2003).

[44] Caroll, S. M., De Felice, A., Duvvuri, V., Easson, D.A, Trodden, M. and Turner, M. S., Phys. Rev. D **71**, 063513 (2005).

[45] Nojiri, S. and Odintsov, S. D, Phys. Rev. D, 68 (2003), Article 123512

[46] Nojiri, S. and Odintsov, S. D., , Int. J. Geom. Meth. Mod. Phys. **4**, 115 (2007).

[47] Dobado, A. and Maroto, A. L., Phys. Rev. D **52**, 1895 (1995).

[48] Starobinsky, A. A., , Phys. Lett. **91B**, 99 (1980).

[49] Ganguly, A., Gannouji, R. Goswami, R. and Ray, S., *Neutron stars in Starobinsky model*, arXiv: 1309.3279.

[50] Nojiri, S. and Odintsov, S. D., , Gen. Rel. Grav. **36**, 1765 (2004).

[51] Astashenok, A.V., Capoziello, S. and Odintsov, S. D *Further stable neutron star models from $f(R)$ gravity*, arXiv: 1309.1978 [gr-qc](2013).

[52] Babichev, E. and Langlois, D, *Relativistic stars in $f(R)$ and scalar-tensor theories*, arXiv: 0911.1297 [gr-qc] (2010).

[53] Babichev, E. and Langlois, D, *Relativistic stars in $f(R)$ gravity*, arXiv: 0904.1382 [gr-qc] (2010).

[54] Barrow, J. D. and Ottewill, A. C., J. Phys. A **16**, 2757 (1983).

[55] Cembranos, J. A. R. , Phys. Rev. D **73**, 064029 (2006).

[56] Dvali, G., Gabadadze, G. and M. Porrati , Phys. Lett. **B485**, 208 (2000).

[57] Dobado, A. and Maroto, A. L. , Phys. Lett. B **316**, 250 (1993) [Erratum-ibid. B **321** 435 (1994)].

[58] Beltrán, J. and Maroto, A. L. ,Phys. Rev. D **78**, 063005 (2008); JCAP **0903**, 016 (2009); Phys. Rev. D **80**, 063512 (2009); Int. J. Mod. Phys. D **18**, 2243-2248 (2009).

[59] Siegel, E., *How close are we to a theory of everything?* (2017), URL: `https://www.forbes.com/sites/startswithabang/2017/07/08/ask-ethan-how-close-are-we-to-a-theory-of-everything/$#304a72f65e9c$`.

[60] Capoziello, S. and Faraoni, V., *Beyond Einstein Gravity, A Survey of Gravitational Theories for Cosmology and AstroPhysics*. Springer, Dordrecht, The Netherlands (2010).

[61] Stelle, K. S. , Phys. Rev. D**16**, 953 (1977).

[62] Gregory, C. *Non-linear Lagrangians and the problem of motion* Phys. Rev. **72**(1947).

[63] De la Cruz- Dombriz, Á., Dunsby, P. K. S. and Saez-Gomez, D., *Junction conditions in extended Teleparallel gravities*, (2015) arXiv: 1406.2334 [gr-qc].

[64] Chiba, T. , Phys. Lett. B**575**, 1-3, arXiv:0009008 [gr-qc].

[65] Hu, W. et al. *Models of $f(R)$ Cosmic Acceleration that Evade Solar-System Tests*, Phys. Rev. D**76** (2007) 064004 arXiv: 0705.1158 [astro-ph].

[66] Leach, J. A., *Alternative Theories of Gravity and their Application to Cosmology*, (University of Cape Town, 2008).

[67] Nojiri, S. and Odintsov, S. D., *Modified gravity with negative and positive powers of the curvature: unification of the inflation and of the cosmic acceleration*, arXiv: hep-th/0307288 (2003).

[68] Caroll, S. M., De Felice, A., Duvvuri, V., Easson, D.A, Trodden, M. and Turner, M. S. *Is Cosmic Speed-Up Due to New Gravitational Physics?*, arXiv: astro-ph/0306438 (2003).

[69] Caroll, S. M., De Felice, A., Duvvuri, V., Easson, D. A., Trodden, M. and Turner, M. S. *The Cosmology of Generalized Modified Gravity Models*, arXiv: astro-ph/0410031 (2004).

[70] Olmo, G. J., *Post-Newtonian constraints on $f(R)$ cosmologies in metric formalism*, arXiv: gr-qc/0505135 (2005).

[71] Olmo, G. J., *Post-Newtonian constraints on $f(R)$ cosmologies in Palatini formalism*,arXiv: 0505136 (2005).

[72] Schmidt, H. J. *New exact solutions for power-law inflation Friedmann models*, arXiv: gr-qc/0109004 (2001).

[73] Carloni, S., Dunsby, P. K. S., Capozziello, S. and Troisi, A., *Cosmological dynamics of R^n gravity*, arXiv: gr-qc/0410046 (2004).

[74] Barrow, J. D. and Clifton, T., *Exact cosmological solutions of scale-invariant gravity theories*,arXiv: gr-qc/0509085 (2005).

[75] Clifton, T. and Barrow, J. D., *Further Exact Cosmological Solutions to Higher-Order Gravity Theories*, arXiv: gr-qc/0601118 (2006).

[76] The LIGO Scientific Collaboration, The Virgo Collaboration, *Observation of Gravitational Waves from a Binary Black Hole Merger*, arXiv: 1602.03837[gr-qc] (2016).

[77] The LIGO Scientific Collaboration, The Virgo Collaboration, *GW170817: Observation of Gravitational Waves from a Binary Neutron Star Inspiral*, arXiv: 1710.05832 [gr-qc] (2017).

[78] The LIGO Scientific Collaboration, The Virgo Collaboration, *GW170817: Measurements on Neutron Star Radii and Equation of State*,arXiv: 1805.11581 [gr-qc] (2018).

[79] Seeds, M. A. and Backman, D., *Astronomy: The Solar System and Beyond*. Brooks Cole (2009).

[80] Oppenheimer, J. R. and Volkoff, G. M., *On Massive Neutron Cores*, Phys. Rev. **55**, 374 (1939).

[81] Douchin, F. and Haensel, P. *A unified equation of state of dense matter and neutron star structure*, https://doi.org/10.1051/0004-6361:20011402.

[82] Margalit, B. and Metzger, B. *Constraining the Maximum Mass of Neutron Stars From Multi-Messenger Observations of GW170817*, arXiv: 1710.05938 [astro-ph.HE] (2017).

[83] Pooley, D., Kumar, P., Wheeler, J. C. and Grossan, B. *GW170817 Most Likely Made a Black Hole*, arXiv: 1712.03240 [astro-ph.HE] (2017).

[84] IXO Science Investigations 3, *What is the equation of state of matter in neutron stars?* URL: `https://asd.gsfc.nasa.gov/archive/ixo/science/exampleScience/EquationOfState.pdf`.

[85] Resco, M.A., De la Cruz-Dombriz, Á., Llanes Estrada, F.J. and Castrillo, Z., *On neutron stars in f(R) theories: small radii, large masses and large energy emitted in a merger*, (2016) arXiv:1602.03880.

[86] Clifton, T. , *Spherically Symmetric Solutions to Fourth-Order Theories of Gravity* arXiv: gr-qc/060709v2(2006).

[87] Clifton, T., Ferreira, P. G. , Padilla, A. and Skordis, C. *Modified Gravity and Cosmology*, (2012) arXiv: 1106.2476 [astro-ph.CO].

[88] Clifton, T. and Barrow, J. D., *The Power of General Relativity*, arXiv: gr-qc/0509059.

[89] Capozziello, S., Carloni, S. and Troisi, A., *Quintessence without scalar fields*, arXiv: astro-ph/0303041 (2003).

[90] De la Cruz-Dombriz, Á., Dobado, A. and Maroto, A. L., *Black Holes in $f(R)$ theories*, (2009) arXiv: 0907.3872 [gr-qc].

[91] Kandhai, S. and Dunsby, P. K. S, *Cosmological dynamics of viable $f(R)$ theories of gravity*, (2015) arXiv: 1511.00101 [gr-qc].

[92] Motohashi, H. and Suyama, T., *Third order equations of motion and the Ostrogradsky instability*, (2015) arXiv: 1411.3721 [Physics.class-ph].

[93] Woodard, R. P., *The Theorem of Ostrogradsky* (2015) arXiv: 1506.02210 [hep-th].

[94] Capoziello, S., Lobo, F. S. N. , and Mimoso, J. P. , *Generalized energy conditions in Extended Theories of Gravity*, (2015) arXiv: 1407.7293 [gr-qc].

[95] Capoziello, S., Cardone, V. F., and Troisi, A., *Reconciling Dark Energy models with f(R) theories*, (2005) arXiv: astro-ph/0501426.

[96] Buchdal, H. A. , *Non-linear Lagrangians and cosmological theory.* Monthly Notices of the Royal Astronomical Society, Vol.150 (1970).

[97] Sotiriou, T. P, *The viability of theories with matter coupled to the Ricci scalar*Phys. Lett. B **664**, 225-228 arXiv: 0805.1160 [gr-qc].

[98] Pogosian, L. and Silvestri, A., Phys. Rev. D **77**, 023503 (2008).

[99] Faraoni, V., *Matter instability in modified gravity*, arXiv: astro-ph/0610734.

[100] Woodard, R. P. , *Avoiding Dark Energy with* $\frac{1}{R}$ *Modifications of Gravity* (2006) arXiv: astro-ph/0601672.

[101] Astashenok, A. V. et al. *The realistic models of relativistic stars in* $f(R) = R + \alpha R^2$ *gravity* (2017) arXiv: 1704.08311 [gr-qc].

[102] Dobado, A. and Llanes-Estrada, F. J., *The existence of a two-solar mass neutron star constrains the gravitational constant* G_N *at strong field*, arXiv: 1107.5707 [gr-qc] (2011).

[103] Hebeler, K., Lattimer, J. M., Pethick, C. J. and Schwenk, A., Astrophys. J. 773 (2013) 11, arXiv: 1303.4662 [astro-ph.SR].

[104] *Static and Spherically Symmetric solutions in theories beyond General Relativity. Neutron stars and gravitational waves mergers*, (University of Cape Town, 2016).